Toward Electronic Materials Based on Metal Pincer-Type Complexes

Jeewantha Sampath Hewage
Marquette University

TOWARD ELECTRONIC MATERIALS BASED ON METAL PINCER-TYPE COMPLEXES

by

Jeewantha S. Hewage, B.Sc. (Hons)

A Thesis Submitted to the Faculty of the Graduate School,
Marquette University,
in Partial Fulfillment of the Requirements for
the Degree of Master of Science

Milwaukee, Wisconsin

May 2015

ABSTRACT
TOWARD ELECTRONIC MATERIALS BASED ON METAL
PINCER-TYPE COMPLEXES

Jeewantha S. Hewage, B.Sc. (Hons)

Marquette University, 2015

There is currently a lot of interest in developing electrically conducting or semiconducting metal-organic frameworks (MOF's), highly porous materials constructed by organic ligands bridging metal centers. Typically MOF's are non-conducting and, moreover, they are susceptible to hydrolytic degradation. If hydrolytically stable and electrically conducting MOFs could be realized, then revolutionary new technologies could be envisioned. Currently, organic dicarboxylates are used as bridging organic ligands and one simple strategy to obtain the desired materials is to explore other ligand systems.

Pincer ligands are organic compounds that are uninegative and bind metals in a tridentate, meridional fashion with two five-member chelate rings. There is intense contemporary interest in studying metal complexes of these pincer- or pincer-type ligands (variants with six-membered chelate rings) because they can exhibit remarkable stability and they can often promote unusual chemical transformations depending on the metal and any special properties of the ligand. Another attractive feature of pincer ligands for the purpose of developing conducting MOF's is that certain classes are electrochemically non-innocent, and can readily accept or give away electrons at potentials that depend on the ligand's constituents.

This thesis describes investigations into metal complexes of new ligands that have either two pyrazolyl (pz) or one pz and one diphenylphospine flanking donor(s) attached to diarylamido anchor donors to give pincer-type derivatives with NNN- or NNP- donor sets, respectively. First, the preparation and reaction chemistry of (NNP)rhodium(I) complexes was investigated to determine their potential in catalytic chemistry. It was found by X-ray structural studies, NMR spectroscopic studies and DFT calculations that this ligand was hemilabile with rapid dissociation/association of the pyrazolyl arm. Next, the preparation and properties of $[Ga(NNN)_2](PF_6)$ were thoroughly investigated experimentally and computationally. The complexes are hydrolytically stable. Moreover, electrochemical measurements show that the ligand is an electron donor, undergoing two sequential one-electron oxidations at potentials near 1.0 V vs Ag/AgCl. Spectroscopic studies verified that electronic communication occurs across a diamagnetic metal bridge and that the mono-oxidized species is a Robin-Day class IIA species. These results demonstrate that metal pincer complexes warrant further investigation as candidates for components of electrically conducting MOFs.

ACKNOWLEDGEMENTS

Jeewantha S. Hewage, B.Sc. (Hons)

First and foremost, I would like to thank my esteemed advisor, Dr. James R. Gardinier, for giving me this opportunity to work on exiting projects. His encouragements, advices, support and mentorship were vital to my success. I sincerely thank my committee members, Dr. Chae S. Yi and Dr. Adam Fiedler for their helpful advices and the support. I would like to thank my group members Dr. Sarath Wanniarachchi and Alex Treleven for their support and valuable conversations. In addition, I would like to thank Dr. S. Lindeman for X-ray diffraction analysis.

This thesis would not have been possible without the love and support of my family. I would like to thank my wife Manjula, lovely son Sandila and daughter Sanuli. They are the biggest joy of my life and always filled my heart with happiness and courage. I am grateful to my father and mother; they were with me their love and encouragements.

Finally, I would like to thank the Graduate school and the all of the Marquette University administration.

TABLE OF CONTENTS

LIST OF TABLES

LIST OF FIGURES

LIST OF SCHEMES

CHAPTER 1

INTRODUCTION

Our research group has been interested in metal complexes of non-innocent ligands.[1] Non-innocence can be classified by one or both types of categories: electrochemical or chemical. Thus, a ligand can be regarded as electrochemically (or redox) 'non-innocent' if it does not allow the oxidation state of a metal in a complex to be (easily) defined by simple inspection of its formula.[2] Examples of such behavior occur in metal polypyridyls or metal dithiolenes[3]. For example, (Figure 1.1) the Nickel complex of stilbene-1,2-dithiolate, $[Ni(S_2C_2Ph_2)_2]^{-x}$ (x= 0-2) exists in three oxidation states, however the formal oxidation state is different from the real oxidation state based on the (spectroscopic) metal d-electron configuration. The stilbene-1,2-dithiolate behaves as a redox non-innocent ligand and the oxidation is take place at the ligand rather than the metal.

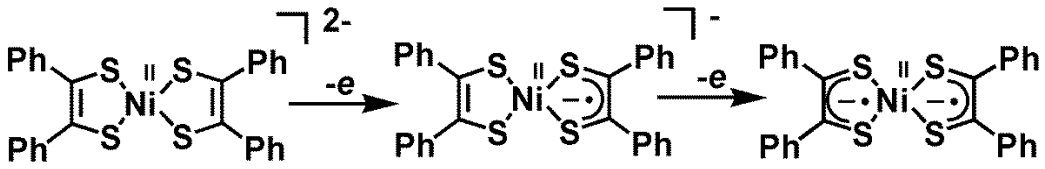

Figure 1.1. Nickel-complex of a redox-active dithiolene ligand.

As a contrast, ligands such as water or ammonia are innocent because the magnitude of their oxidation or reduction potentials is too high (and is accompanied by the loss of protons), so the oxidation number of the metal can be clearly defined. Similarly, a ligand can be regarded as chemically non-innocent if the ligand participates

in ‘two-electron chemistry’ (acts as a Lewis acid or base) and changes its structure during the course of a reaction. Thus, examples of chemically non-innocent behavior include complexes of hemilabile ligands and those that exhibit “metal-ligand cooperativity” (Figure 1.2) in contemporary chemistry vernacular, as well as all examples of structural or constitutional (ionization, Linkage, coordination and hydrate) isomerism in older nomenclature.

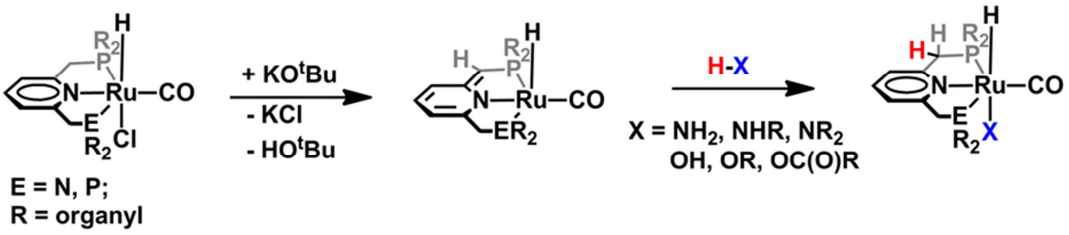

Figure 1.2. Example of a chemically non-innocent ligand.[4]

One main reason for studying metal complexes of redox active ligands is for the discovery of new chemical reactivity. After all, nature uses such complexes to perform some remarkable chemistry such as oxidation of primary alcohols to corresponding aldehyde by the Galactose Oxidase catalyzing reaction (Figure 1.3). In this Galactose Oxidase catalytic cycle Cu(II)-tyrosyl radical unit performs two electron redox chemistry, reducing O_2 to hydrogen peroxide. The active form of this enzyme is with Cu(II)-tyrosyl radical unit and oxidation is occurred through proton-coupled electron transfer to ligand radical as shown in right middle of Figure 1.3. This is an ideal example how nature uses redox active ligands to perform its reactions.

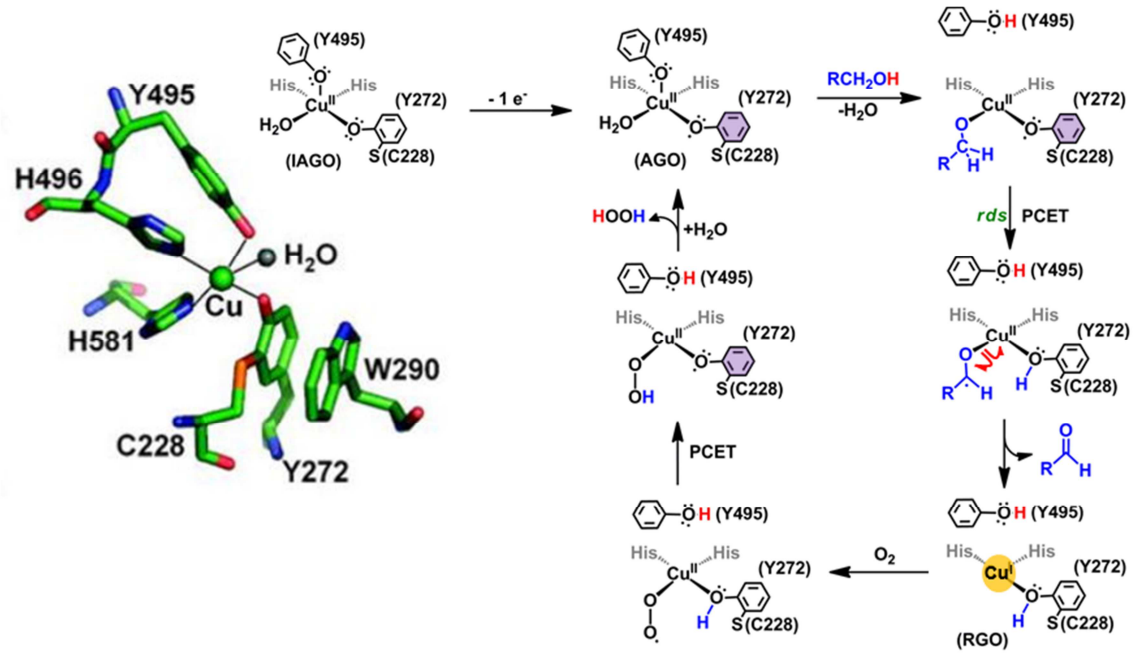

Figure 1.3. Galactose oxidase adapted from refs 5 and 6

A second impetus for studying metal complexes of non-innocent ligands is for the development of new materials for technological applications. One of the most interesting classes of compounds is those that exhibit valence tautomerism. These species can be envisioned as molecular switches (Figure 1.4).

An area of research that is only beginning to be studied is the incorporation of redox active units into metal organic frameworks. Despite being its infancy, Dinca *et al* has recently reported tetrathiafulvalene-tetrabenzoate (H_4TTFTB) assembled MOF with $Zn(NO_3)_2$ (Figure 1.5) exhibits charge mobility commensurate with some of the best organic semiconductors and confirmed by conductivity measurements.[8] These are potentially interesting materials that can be used as new electronic materials for

applications such as photocatalysts, molecular wires, or as alternative porous electrolytic medium in battery applications.

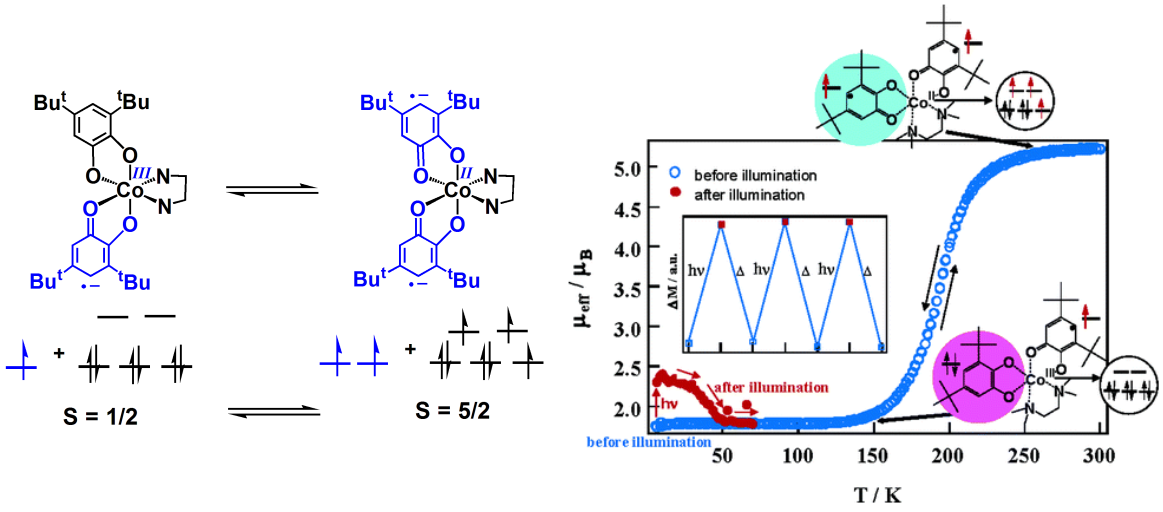

Figure 1.4. Example of valence tautomerism exhibited by cobalt atecholate/semiquinone complexes from ref 7.

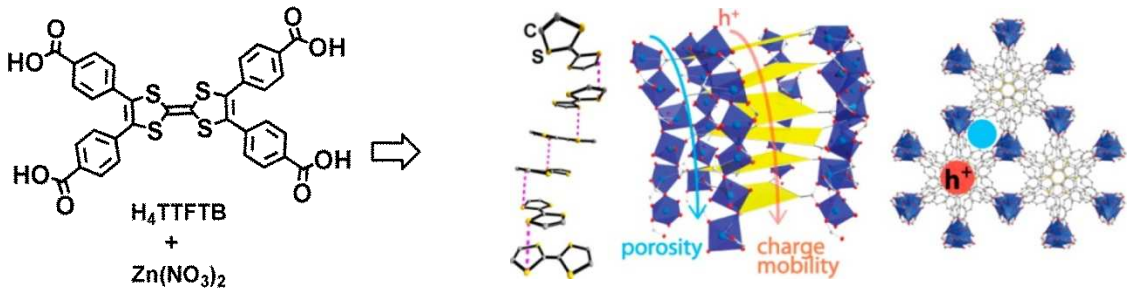

Figure 1.5. Left: Structure of Redox active tetrathiafulvalene-tetrabenzoate ligand, Right: Side view of TTF stack, charge mobility and a view of down the c axis

Advances in any of the above areas of study would benefit from new redox active ligands that are easily prepared and modified to predictably attenuate the electronic properties and chemical reactivity of the resulting complexes. Pincer and pincer type ligands gain much more attention on this field as it can be tuned for remarkable properties on the basis of its different donor capabilities and structurally adaptive nature. A ligand which is uninegative, terdentate and bind metals with five-membered ring is called as a pincer ligand and a ligand which has two of above three properties is called as a pincer type ligand. These type ligands are well suited for the study of redox active systems as tridentate coordination mode prevents ligand dissociation upon the oxidation and the meridional coordination mode helps to maintain a planar geometry allowing redox changes to be delocalized over the entire ligand framework.

In this study, the syntheses of new pincer-type ligands that contain pyrazolyl flanking donors are described. First, the preparation of a derivative with a PNN donor set is examined. The rhodium complexes of the PNN ligand provided an opportunity to study the hemilability. The main thrust of the research, however, is the development of new conductive metal organic frameworks and molecular wires based on metal complexes of redox-active pincer ligands. Thus, chapters 3 describes an initial effort in that direction. First, it was necessary to determine whether electronic communication would occur across metal bridges in L-M-L complexes. The investigation into properties complexes of redox-inactive metals, will facilitate the identification of ligand-centered radicals in transition metal chemistry. The synthesis and characterization of monomeric metal complexes will also facilitate the identification of such motifs in solid-state assemblies or polymers. The syntheses and characterization of metal organic frameworks

and mixed metal organic frameworks is non-trivial. Chapter 4 proposes next logical steps toward such goals and future directions to peruse those objectives and what effect changing metals might have on the strength of electronic communication.

CHAPTER 2

RHODIUM COMPLEXES OF A NEW HEMILABILE AND STRUCTURALLY ADAPTIVE PNN-PINCER TYPE LIGAND

This work was published: Wanniarachchi, S.; Hewage, J. S.; Lindeman, S. V.; Gardinier, J. R. *Organometallics* **2013**, *32*(10), 2885-2888.

2.1 INTRODUCTION

Over the past few decades, there has been intense interest in metal complexes of multidentate 'hemilabile' ligands where one ligating arm readily dissociates or is forcibly displaced by an incoming nucleophile.[1] The identification and study of such hemilabile ligands has been important for the development of both new catalytic reactions and for the discovery of new materials for sensing applications.[2] A majority of hemilabile ligands are bidentate[3] with both 'hard' and 'soft' Lewis donors. Other ligands such as the tris(pyrazolyl)borate or tris(pyrazolyl)methane and related 'scorpionates', which typically bind metals in a facial terdentate manner with six-membered chelate rings, have also been shown to be hemilabile with certain metals.[4] There has been a growing interest in complexes of hemilabile 'pincer' ligands (typically anionic terdentate species that bind metals with five-membered rings) because certain examples have been found to mediate remarkable chemical transformations.[5] The van der Vlugt group recently reported on the hemilabile character of bis(iso-propylisonitrile)rhodium(I) complexes of two PNN-pincer (**A** and **C**, Figure 2.1) and one pincer-type (**B**, Figure 2.1) ligand[6]. The authors provided

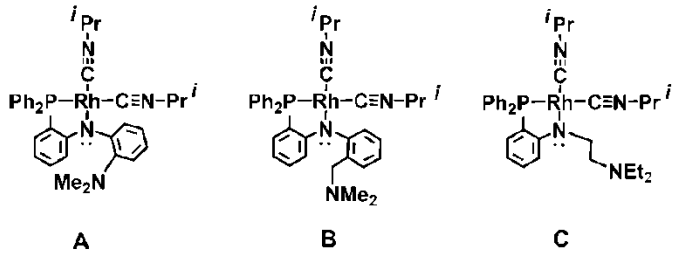

Figure 2.1. Rhodium(I) complexes of hemilabile PNN- ligands reported by the van der Vlugt group.[6]

compelling spectroscopic evidence that various (PNN)Rh(CNR)$_2$ complexes were hemilabile and contained four-coordinate rhodium with κ^2*PN*- ligands but in no case was a complex structurally-authenticated. Instead, computational studies were used tosupport the assertion that one ligand arm was dissociated, since "no minimum (corresponding to a five-coordinate species) could be located on either respective potential energy surface". Given our experience with diarylamido-anchored ligands with six-membered chelate rings similar to complex **B**, we were keenly aware that, although less common than the *mer*- coordination mode, the *fac*- coordination mode is sometimes observed.[7] Such a possibility casts some doubt on the structural nature of the reported (PNN)Rh(CNR)$_2$ complexes. Thus, we set out to exploit the crystallinity of pyrazolyl-containing ligand systems to structurally verify the elusive κ^2*PN*-coordination mode of the (PNN)Rh(CNR)$_2$ complexes. In this chapter, we document a useful coupling reaction to obtain a new pyrazolyl-containing ligand with a PNN- donor set. We also describe the syntheses of various rhodium (I) complexes and the hemilability of one complex. The variability in metal coordinating behavior of the new pincer-type ligand is also illustrated through examination of [(PNN)Rh(Me)(CN^{t}Bu)$_2$](I).

2.2 RESULTS AND DISCUSSION

The synthetic route to the new ligand and its carbonylrhodium(I) complex is outlined in Scheme 2.1. A CuI- catalyzed amination reaction between 2-pyrazolyl-4-toluidine, H(pzAn^{Me}),[8] and diiodobenzene affords 2-iodo-N-(4-methyl-2-(1H-pyrazol-1-yl)phenyl)benzenamine, H(N^{IPh}- pzAn^{Me}), a precursor (top right of Scheme 2.1) that is used in the final step of the ligand construction. A high-yielding Pd^0-catalyzed coupling reaction between H(N^{IPh}-pzAn^{Me}) and diphenylphosphine provides the desired ligand with a PNN donor set (Figure 2.2). The reaction between Rh(CO)$_2$(acac) and H(PNN) in acetone afforded a high yield of (PNN)Rh(CO), **1**. Complex **1** is air-stable in the solid state as well as in solution and no special precautions were required for its handling. Although all attempts to obtain crystals of **1** suitable for X-ray diffraction have been stymied by its propensity to form microcrystalline needles, the NMR spectral data of are in accord with the structural formulation depicted in Scheme 2.1. The C-O stretching

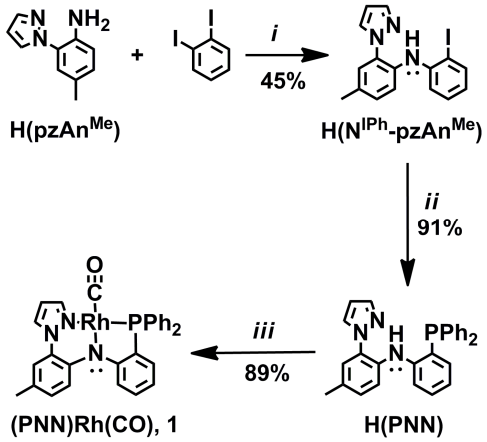

Scheme 2.1. The synthetic route to the new ligand and its carbonylrhodium(I) complex Key: *i*) cat. CuI, 1.2 Cs_2CO_3, *p*-dioxane, Δ 16 h; *ii*) 1.2 $HPPh_2$, 0.5 mol% $Pd_2(dba)_3$, 1 mol % Xantphos, 1.2 NEt_3, *p*-dioxane, Δ, 15 h; *iii*) Rh(CO)$_2$(acac), acetone, Δ, 15 min.

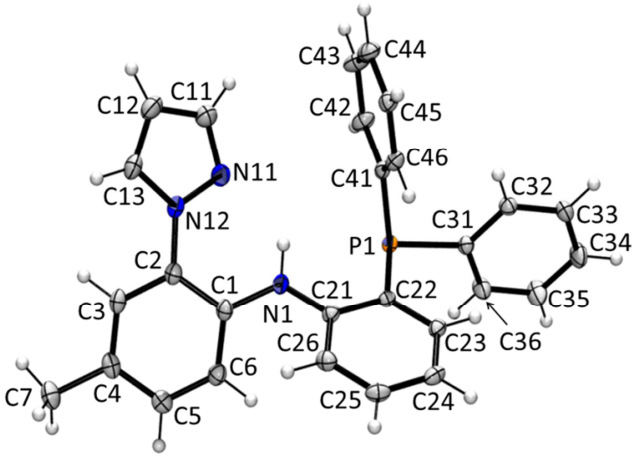

Figure 2.2. Molecular Structure and atom labeling for H(PNN).

frequency, ν_{CO} = 1957 cm^{-1} for **1** is comparable to ν_{CO} = 1960 cm^{-1} reported for the related PNP derivative of Mayer and Kaska with a diarylamido anchor and two PPh_2 flankers.[9] Another related complex, (NNN)Rh(CO), **2**, (NNN has two pyrazolyl flanking donors attached to the same diarylamido backbone as in **1**) has a C-O stretching frequency of ν_{CO} = 1954 cm^{-1},[10] which indicates only a slight increase in backbonding compared to **1**. These comparable results corroborate our previous findings that the *para*-aryl substituents (rather than flanking donors) dictate the electronic properties of the metal complexes of diarylamido-anchored pincer ligands. The ^{13}C NMR spectrum of **1** shows a doublet-of-doublet signal at δ_C = 193 ppm (J_{Rh-C} = 67 Hz and J_{P-C} = 18 Hz) for the rhodium-bound carbonyl; that for **2** showed a doublet resonance at δ_C =193 ppm (J_{Rh-c} = 71 Hz). The similarity of chemical shift and coupling constant between **1** and **2**, suggests that **1** has a square planar coordination geometry about rhodium with *trans*-disposed amido and carbonyl groups like that in structurally-characterized **2**. The ^{31}P

NMR spectrum of **1** shows a doublet resonance at δ_P = 61 ppm ($^1J_{P\text{-}Rh}$ = 167 Hz) which is shifted downfield from the singlet resonance at δ_P = -20 ppm for H(PNN) and the doublet resonance at δ_P = 41.8 ppm ($^1J_{P\text{-}Rh}$ = 135.1 Hz) reported for Mayer and Kaska's PNP derivative.[9]

Complex **1** reacts with excess (4 equiv or more) of CN^{t}Bu to give analytically pure (PNN)Rh(CN^{t}Bu)$_2$ (**3**). As reported for other similar complexes, complex **3** is air sensitive both in the solid state and in solution. Thus, **3** needs to be stored and handled under an inert atmosphere. Single crystals of **3** suitable for X-ray diffraction were grown by extracting the initial product mixture of **1** and excess CN^{t}Bu with pentane and allowing the pentane-soluble portion to stand under nitrogen for several hours. The structure of **3** shown in Figure 2.3 verifies the κ^2*P*,*N* coordination mode of the ligand. The rhodium is in a square-planar geometry, where the sum of angles about the metal is 360°. The isocyanide ligand *trans* to the amido exhibits a shorter Rh–C bond (1.888(2) Å) and a marginally longer unsaturated C–N bond (1.156(8) Å) in comparison with that *trans* to the phosphine arm (Rh–C, 1.983(2) Å; C–N, 1.141(9) Å). The Rh–C bond distances are the ranges found for other charge-neutral rhodium(I) organoisocyanide complexes.[11-15] The Rh–N and Rh–P bonds in **3** are similarly unremarkable.

Dynamic behavior for **3** in solution is evident from an examination of variable-temperature NMR spectral data. The resonances for various nuclei show different temperature-dependent line broadening and changes in chemical shifts depending on the type of resonance. Figure 2.4 shows an overlay of ^{31}P NMR spectra and a representative

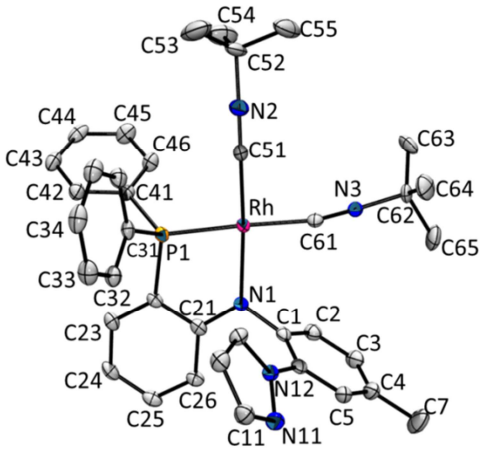

Figure 2.3. Structure of (PNN)Rh(CN^{t}Bu)$_2$ in **3**·0.2(pentane), hydrogen atoms removed for clarity. Thermal ellipsoids are shown at the 50% probability level. Selected bond distances (Å): Rh1–P1, 2.2521(5); Rh1–N1, 2.0728(14); Rh1–C51, 1.8884(18); Rh1–C61, 1.9825(18); C51–N2, 1.156(8); N2–C52, 1.472(8); C61–N3, 1.141(9); N3–C62, 1.457(9); Selected bond angles (deg): P1–Rh1–N1, 82.42(4); P1–Rh1–C51, 93.70(6); C51–Rh1–C61, 88.40(7); N1–Rh1–C61, 95.48(6); N1–Rh1–C51, 176.10(7); P1–Rh1–C61, 177.63(5); C51–N2–C52, 177.3(8); C61–N3–C62, 173.3(17).

portion of the ^{1}H NMR spectra for **3** in acetone-d_6 at various temperatures. At 223 K, the ^{31}P NMR spectrum consists of a doublet at 45.8 ppm with J_{RhP} = 138.5 Hz. When the temperature is raised above 243 K, the doublet resonance shifts slightly downfield and becomes broader until coupling can no longer be detected above 303 K. As can be seen in Figure 2.4, similar behavior occurs for resonances in the ^{1}H NMR spectra, but with notable differences. The resonances for the pyrazolyl, tolyl, and one of the *tert*-butyl group (upfield signal) hydrogens exhibit the greatest line broadening and changes in chemical shifts, followed by resonances for the PC_6H_4N group. The resonances for the hydrogens of the $(C_6H_5)_2P$ group and the other ^{t}Bu group exhibit negligible changes with

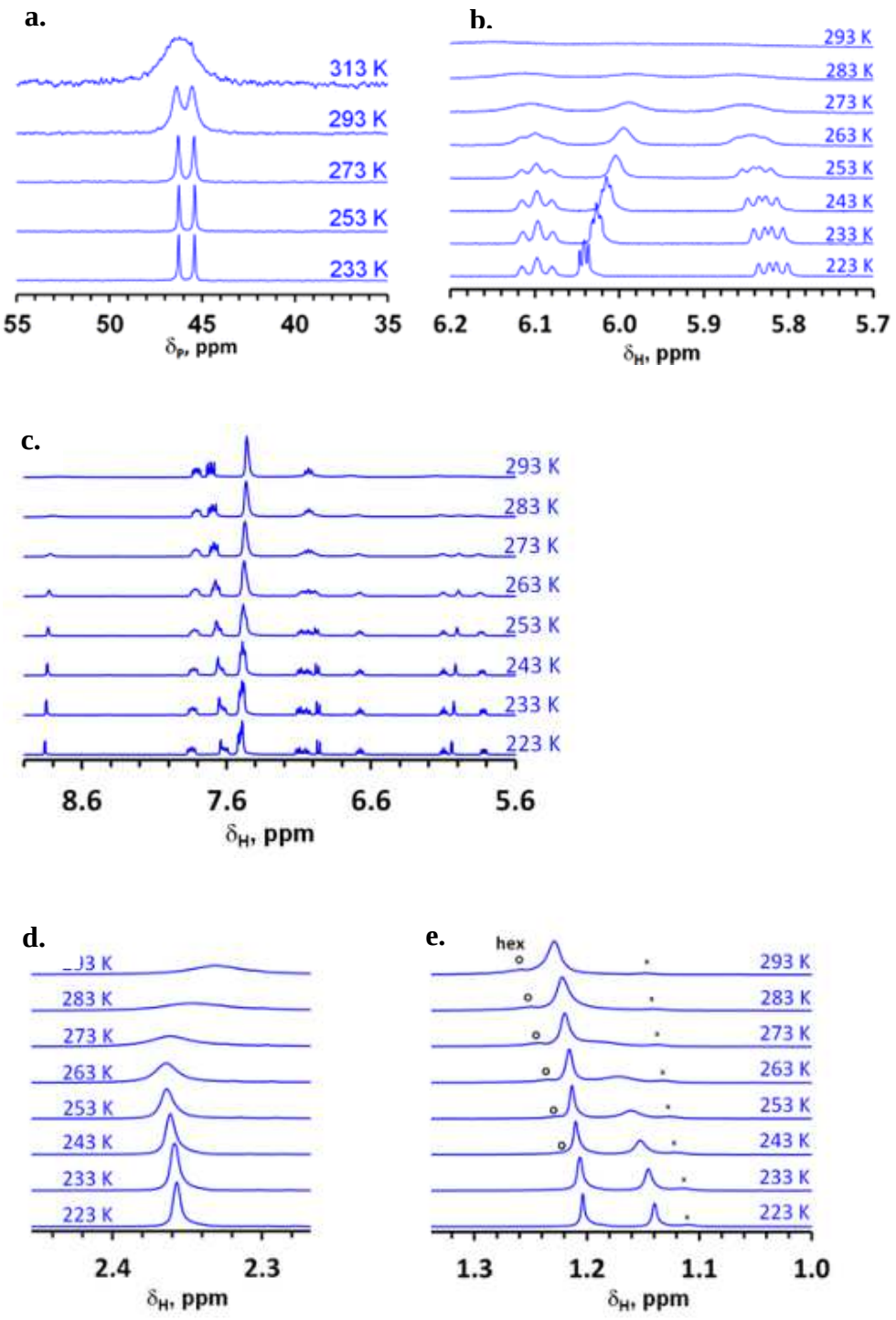

Figure 2.4. Overlay of the ^{31}P NMR spectra (**a**) and representative potions of the ^{1}H NMR (**b, c:** aryl and pz region, **d:** tolyl-CH_3, **e:** ^{t}Bu-CH_3) (400 MHz) of 3 in acetone-d6 obtained at various temperatures.

temperature. The rate constant of the dynamic process can be extracted by measuring $W_{1/2}$, the line broadening in excess of the natural line width, according to the relation $k = \pi W_{1/2}$. As detailed in the Figure 2.5, Eyring analyses of the temperature dependence of the line broadening/rate constant derived from the ^{31}P NMR resonance and the ^{1}H NMR resonances for pyrazolyl, tolyl, and upfield ^{t}Bu hydrogens afforded the following activation parameters: $\Delta G^{\ddagger}$ = 14.3 (±0.1) kcal/mol, $\Delta H^{\ddagger}$ = 9 (±2) kcal/mol, and $\Delta S^{\ddagger}$ = −19(±5) cal/(K mol). The negative value for activation entropy suggests a highly organized transition state. On the basis of experimental observations and theoretical calculations (OP86/Def2-SV(P))[24-29] that show a five-coordinate conformer is only 5.1 kcal higher in energy than a four-coordinate structure (Figure 2.12), we attribute the dynamic process to be a result of reversible coordination of the hemilabile pyrazolyl arm (k_{298} = 229 s^{-1}), as in Scheme 2.2. Such a proposition rationalizes the observed trends in the disparate broadening of resonances and chemical shift changes in the NMR spectra. Also, the possible presence of both four- and five-coordinate isomers of **3** at room temperature provides an explanation for the greater than expected number of CN stretches observed in the IR spectra. Theoretical calculations indicate that two CN stretches are expected at 2164 and 2101 cm^{-1} (in a 0.99 intensity ratio) for four-coordinate **3** and at 2147 and 2075 cm^{-1} (in an intensity ratio of 1.05) for five-coordinate **3**. The experimentally observed CN stretching frequencies for **3** in benzene occur at 2156, 2102, and 2065 cm^{-1} with relative intensities of 1.9:1:1.2. Thus, the relatively high intensity of the high-energy band may be a result of two overlapping bands. It is noted that complexes **A** and **B** (Figure 2.1) each had three CN stretches (near 2157, 2080, and 2040 cm^{-1}); data for **C** were not reported.[6] Finally, the possibility that the solution

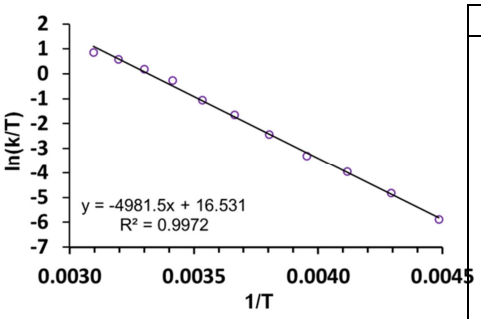

T(K)	δ(ppm)	LWHM (Hz)	$W_{1/2}$ (Hz)	k (s^{-1})	ln(k/T)
223	45.8	153.5	0.2	0.629	-5.87
233	45.8	153.9	0.6	1.886	-4.82
243	45.8	154.8	1.5	4.714	-3.94
253	45.8	156.3	3.0	9.429	-3.29
263	45.8	160.7	7.4	23.257	-2.43
273	45.9	170.3	17.0	53.429	-1.63
283	45.9	185.2	31.9	100.257	-1.04
293	45.9	224.8	71.5	224.714	-0.27
303	45.9	270.0	116.7	366.771	0.19
313	46.2	332.8	179.5	564.143	0.59
323	46.2	396.5	243.2	764.343	0.86

$\Delta G^{\ddagger 293}$ 14.0 kcal/mol $\Delta H^{\ddagger}$ 9.9 kcal/mol $\Delta S^{\ddagger}$ -14.4 cal/(K·mol)

^{1}H NMR H_5pz Resonance:

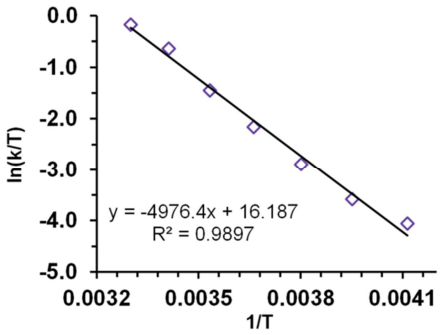

T(K)	δ(ppm)	LWHM (Hz)	$W_{1/2}$ (Hz)	k (s^{-1})	ln(k/T)
223	8.86	3.9	0.6	1.98	-4.72
233	8.85	4.3	1.0	3.14	-4.31
243	8.84	4.6	1.3	4.17	-4.07
253	8.84	5.5	2.2	7.05	-3.58
263	8.83	7.9	4.6	14.56	-2.89
273	8.82	13.2	9.9	31.21	-2.17
283	8.81	24.3	21.0	66.12	-1.45
293	8.76	52. 4	49.1	154.26	-0.64
303	8.70	83.8	80.5	252.97	-0.18

$\Delta G^{\ddagger 293}$ 14.3 kcal/mol $\Delta H^{\ddagger}$ 9.8 kcal/mol $\Delta S^{\ddagger}$ -15.0 cal/(K·mol)

^{1}H NMR upfield ^{t}Bu Resonance:

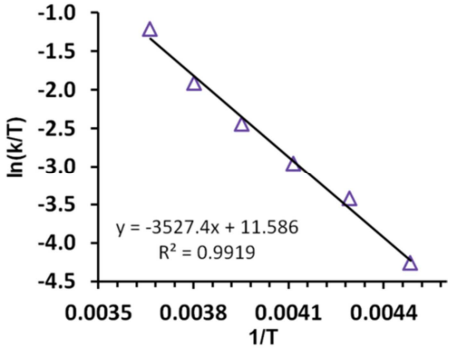

T(K)	δ(ppm)	LWHM (Hz)	$W_{1/2}$ (Hz)	k (s^{-1})	ln(k/T)
223	1.14	1.8	1.0	3.14	-4.26
233	1.15	3.2	2.4	7.56	-3.43
243	1.15	4.8	4.0	12.54	-2.96
253	1.16	7.8	7.0	21.90	-2.45
263	1.17	13.1	12.3	38.75	-1.91
273	1.19	26.5	25.7	80.89	-1.22

$\Delta G^{\ddagger 293}$ 14.1 kcal/mol $\Delta H^{\ddagger}$ 7.0 kcal/mol $\Delta S^{\ddagger}$ -24.2 cal/(K·mol)

Figure 2.5. Representative data for temperature-dependent line-broadening of resonances in the NMR spectra of 3 in acetone-d6 and Eyring Plots .

Calculations of $W_{1/2}$ could only be made for resonances that are resolved (where at least half of the signal is clearly observed). In certain cases resolution is lost on heating, so there are a different number of data points for each resonance. For multiplets, the line-width-at-half-maximum (LWHM) was measured using the outer lines of the multiplet signal (thus, included the coupling constant). To get $W_{1/2}$, the appropriate coupling constant and the appropriate multiple of the natural linewidth were subtracted from the measured LWHM. The slope of Eyring plot = $-\Delta H^{\ddagger}/R$; Intercept = $\Delta S^{\ddagger}/R + 23.759$. R = 1.9872 cal/Kmol.

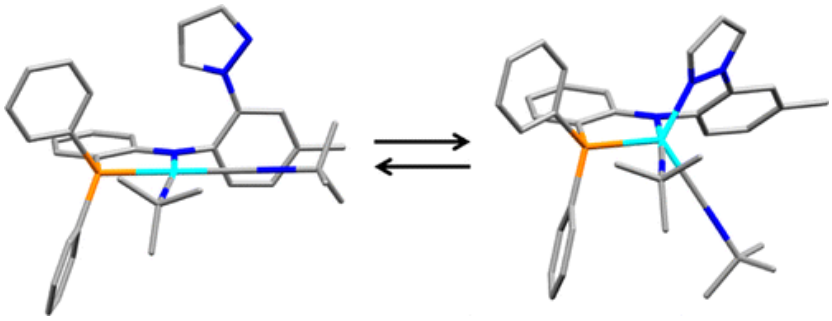

Scheme 2.2. Plausible Process Responsible for Temperature-Dependent NMR Line Broadening in the Spectra of **3**

dynamic process involves dissociation of one CN^tBu is disfavored, owing to the negative value for activation entropy. Furthermore, the NMR resonances for free CN^tBu or for (PNN)Rh(CN^tBu) (***IA***) were not observed. As also described in the experimental section, Figure 2.10 and Scheme 2.4 we have spectroscopically characterized ***IA*** as a synthetic intermediate along the way to **3**. The spectroscopic signatures of ***IA*** and its mixtures with **3** are different from the variable-temperature NMR spectral data.[24-29]

The structural adaptability of the new PNN-pincer type ligand is displayed by rhodium(III) complexes derived from **3**. Thus, as per Scheme 2.3, the reaction between **3** and MeI produced easily separable mixtures of *cis,mer* (hereafter referred to simply as *mer*, since the *trans,mer* isomer has not yet been detected) and *fac* isomers of [(PNN)Rh(Me)($CN^tBu)_2$](I), **4**. The *mer* isomer has some solubility in benzene, in contrast to the *fac* isomer, thereby allowing separation. Figures 2.6 and 2.7 show the structures of the cations in *mer*-**4** and *fac*-**4**, respectively. In these structures, the Rh–N1 distance of 2.068(2) Å (*mer*-**4**) and 2.058(2) Å (*fac*-**4**) are among the longest such bonds

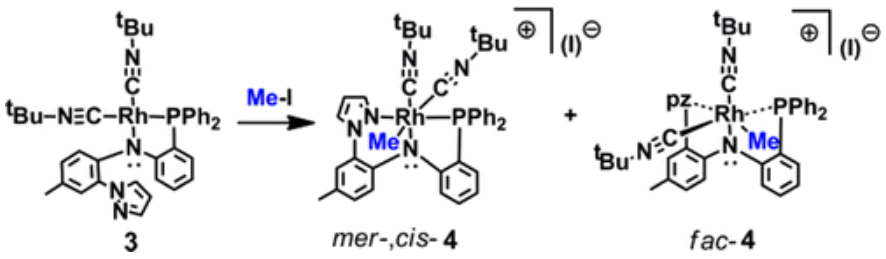

Scheme 2.3. Reaction between MeI and **3** in CH_2Cl_2

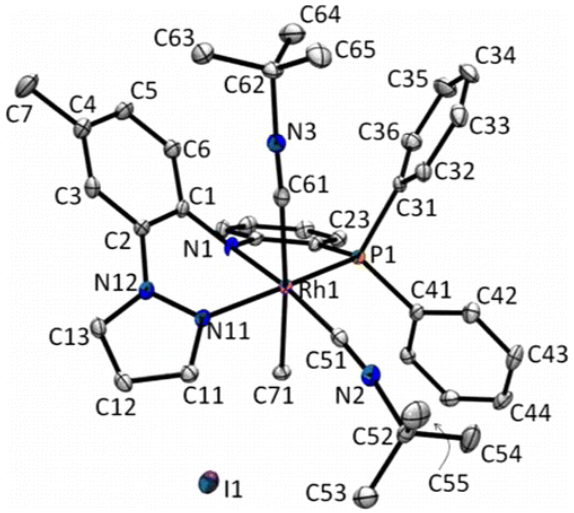

Figure 2.6. Structure of *cis*,*mer*-[(PNN)Rh(Me)($CN^tBu)_2$](I)·C_6H_6, (*mer*-**4**·C_6H_6). Selected bond distances (Å): Rh1–P1, 2.2420(6); Rh1–N1, 2.0684(18); Rh1–N11, 2.0969(19); Rh1–C51, 1.949(2); Rh1–C61, 2.074(2); Rh1–C71, 2.101(2); N2–C51, 1.151(3); N2–C52, 1.466(3); N3–C61, 1.146(3); N3–C62, 1.470(3); Selected bond angles (deg): P1–Rh1–N11, 166.78(5); N1–Rh1–C51, 175.30(9); C61–Rh1–C71, 175.08(9); P1–Rh1–C61, 95.51(6); C71–Rh1–N11, 85.21(8); N1–Rh1–C71, 86.48(9); N11–Rh1–N1, 85.34(7); P1–Rh1–N1, 82.67(6); C51–Rh1–C71, 88.86(9); C51–Rh1–C61, 93.40(9); C61–Rh1–N1, 91.20(8). Hydrogen atoms and benzene molecule have been omitted for clarity.

found in related (pincer)Rh^{III} derivatives,[16] rivaling 2.064(2) Å in *trans*-(NNN)$RhCl_2(PEt_3)$. In fact, the Rh1–N1 distance in *mer*-**4** with a formal rhodium(III) center is close to the 2.0728(14) Å found in **3**, with a rhodium(I) center. For both *fac*- and *mer*-**4**, the CN^tBu *trans* to the amido group has shorter Rh1–C51 and longer C51–N2 bonds versus the analogous bonds in the other CN^tBu group (*trans* to the phosphine). This observation may be indicative of the greater π-donating abilities of the diarylamido versus the triarylphosphine group that increases the metal back-bonding to the *trans*-CN^tBu ligand. This effect is also apparent in **3**. It is also worth noting that the Rh–N_{pz} bond in *fac*-**4** is longer than that in *mer*-**4** or **3**, which might be related to the constrained ligand geometry in this coordination mode and the donating abilities of the ligand *trans* to the pyrazolyl nitrogen.

Interestingly, the ratio of *fac*- to *mer*-**4** obtained from the preparative reactions depends on the solvent and time allotted for reaction, as indicated by NMR spectroscopy (and X-ray crystallography). When the reaction was performed in dichloromethane, a 3:1 *fac*:*mer* ratio was immediately obtained. That is, upon addition of MeI to a CD_2Cl_2 solution of **3**, the original ^{31}P NMR doublet resonance at δ_P 46.0 ppm ($J_{P–Rh}$ = 141 Hz) was immediately replaced by two new doublet resonances at δ_P 57.8 ppm ($J_{P–Rh}$ = 121 Hz) and δ_P 54.3 ppm ($J_{P–Rh}$ = 106 Hz) in a 3:1 ratio. The former resonance with the larger coupling constant is due to *mer*-**4**, while the latter resonance with the smaller coupling constant is due to *fac*-**4**. Over time, the resonance for the *mer* isomer grows at the expense of that for the *fac* isomer. When the reaction between **3** and MeI was performed

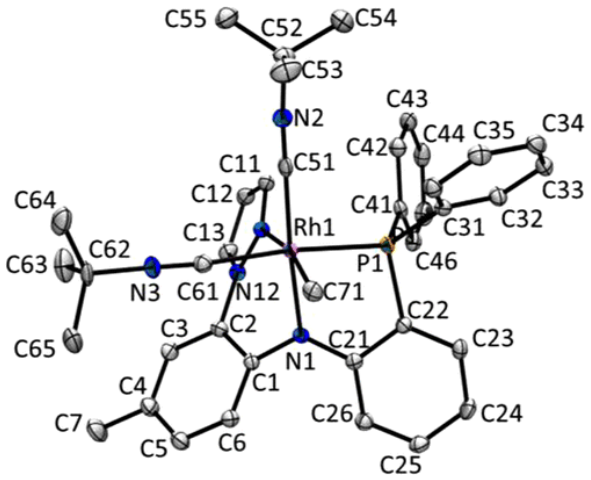

Figure 2.7. Structure of the cation in *fac*-[(PNN)Rh(Me)(CN^{t}Bu)$_2$](I)·H$_2$O (*fac*-**4**·H$_2$O). Selected bond distances (Å): Rh1–P1, 2.2765(6); Rh1–N1, 2.0577(19); Rh1–N11, 2.176(2); Rh1–C51, 1.955(2); Rh1–C61, 2.040(2); Rh1–C71, 2.107(2); N2–C51 1.147(3); N2–C52 1.473(3); N3–C61 1.145(3); N3–C62 1.466(3). Selected bond angles (deg): N1–Rh1–C51, 175.79(9); P1–Rh1–C61, 174.33(7); C71–Rh1–N11, 167.91(8); P1–Rh1–N11, 96.46(5); N1–Rh1–C71, 87.62(9); N11–Rh1–N1, 81.98(7); P1–Rh1–N1, 81.01(6); C51–Rh1–C71, 89.96(10); C51–Rh1–C61, 88.92(9); C61–Rh1–N1, 94.46(9). Hydrogen atoms, the iodide anion, and the water molecule have been omitted for clarity.

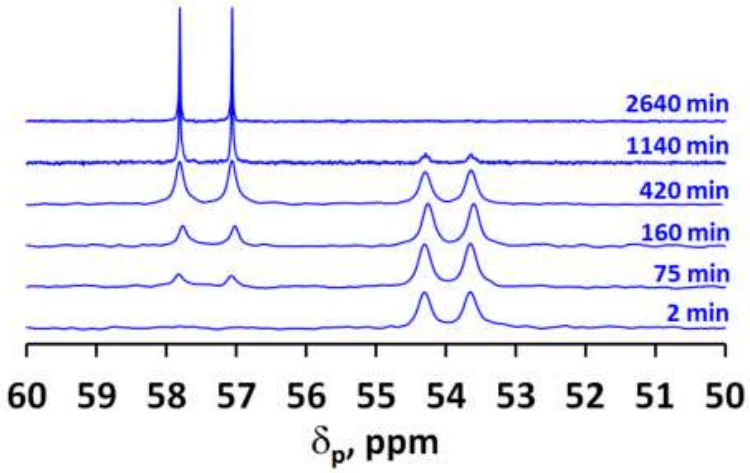

Figure 2.8. ^{31}P NMR spectrum (295 K) of *fac*-4 (δ_P 54 ppm) acquired at various time intervals after dissolving in CD_2Cl_2 showing complete conversion to *mer*-4 (δ_P 57.5 ppm).

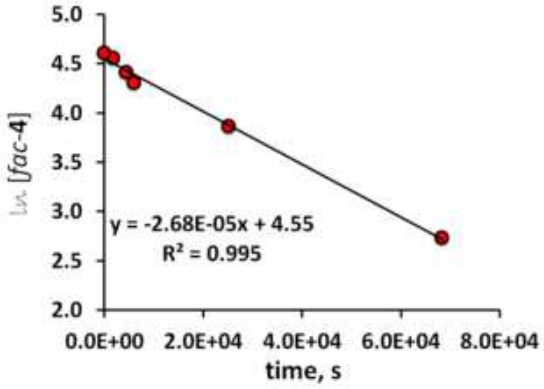

time(s)	[*mer*-**4**]	[*fac*-**4**]	ln[*fac*-**4**]
68400	84.7	15.3	2.73
25200	52.4	47.6	3.86
6000	25.9	74.1	4.31
4500	17.9	82.1	4.41
1800	4.96	95.04	4.55
0	0	100	4.61

Figure 2.9. Plot of ln[*fac*-4] versus time (s) and associated data from an isomerization experiment monitored by ^{31}P NMR spectroscopy showing first-order kinetics.

in a limited amount of benzene, pure *fac*-**4** (59%) immediately precipitated as a yellow solid; the soluble portion contained dark orange *mer*-**4** (40%). The reversal in isomer ratio in C_6D_6 in comparison to the reaction performed in CD_2Cl_2 is kinetic in nature. After the benzene-insoluble product (pure *fac*-**4**) was dissolved in CD_2Cl_2, the ^{31}P NMR spectrum showed complete conversion to *mer*-**4** over the course of 44 h with first-order kinetics ($t_{1/2}$ = 7.2 h; Figures 2.8,2.9). It is noteworthy that theoretical calculations indicate that the *mer* isomer is more stable than the *fac* isomer by about 2 kcal/mol (Figure 2.12).

2.3 CONCLUSION

As the conclusion, a new easily crystallizable pincer-type ligand with a PNN donor set has been prepared. The κ^2*P*,*N* coordination mode in its bis(organoisocyanide)rhodium(I) complex was structurally verified, a mode suggested by the van der Vlugt group for similar complexes. Hemilabile behavior of the pyrazolyl arm

of the ligand to give four- and five-coordinate metal centers in (PNN)Rh(CN^tBu)$_2$ is suggested to be responsible for the dynamic solution behavior detected by NMR spectroscopy. The new PNN ligand was also found to exhibit both *fac* and *mer* coordination modes in its rhodium(III) complexes. The *mer* coordination mode is more stable than the *fac* mode, likely due to the lesser chelate ring strain and greater resonance stabilization associated with the increased planarity of the electroactive diarylamido moiety. The results of DFT calculations suggest that the *fac* mode and five-coordinate (L)Rh(CN^tBu)$_2$ complexes are not unique to the new PNN ligand (Figure 2.12). However, the *fac*- mode is favored for the new ligand over that in related PNN ligands. Perhaps the semirigidity of the new PNN ligand with its finite dihedral angle between mean planes of pyrazolyl and aryl rings helps to minimize the energetic penalties associated with the ligand adopting the *fac* mode (i.e., there is better preorganization in the new ligand versus others). In this manner, the coordination behavior of the new ligand falls somewhere between that of a pincer and a heteroscorpionate. Future investigations will be directed at further examining the stoichiometric reactions and catalytic activity of rhodium(I) and other first-row transition-metal complexes of variants of this new PNN ligand.

2.4 EXPERIMENTAL

Materials. CuI, anhydrous Cs_2CO_3, 1,2-diiodobenzene, NEt_3, $HPPh_2$, CN^tBu, and Li(n-Bu) (1.6 M in hexanes), Xantphos (9,9-dimethyl-4,5-bis(diphenylphosphino)xanthene) were purchased from commercial sources and used without further purification while commercial iodomethane was dried over $CaCl_2$ and

distilled under vacuum before use. The compounds $Pd(PPh_3)_4$,[17] $Rh(CO)_2(acac)$,[18] and $H(pzAn^{Me})$ ($pzAn^{Me}$ = 2-(pyrazolyl)-p-toluidine)[19] were prepared by literature methods. Solvents used in the preparations were dried by conventional methods and were distilled under nitrogen prior to use.

Physical measurements. Midwest MicroLab, LLC, Indianapolis, Indiana 45250, performed all elemental analyses. ^{1}H, ^{13}C and ^{31}P NMR spectra were recorded on a Varian 400 MHz spectrometer. Chemical shifts were referenced to solvent resonances at δ_H 7.26 and δ_C 77.16 for $CDCl_3$, δ_H 5.32 and δ_C 53.84 for CD_2Cl_2, δ_H 2.05 and δ_C 29.84 for acetone-d_6. ^{31}P NMR chemical shifts were referenced against an external standard, 85% H_3PO_4 (aq), with a resonance at δ_P = 0.00 ppm. Infrared spectra were recorded on samples as either KBr pellets or as acetone solutions with cells having KBr windows using a Nicolet Magna-IR 560 spectrometer. Melting point determinations were made on samples contained in glass capillaries using an Electrothermal 9100 apparatus and are uncorrected.

Ligand Syntheses.

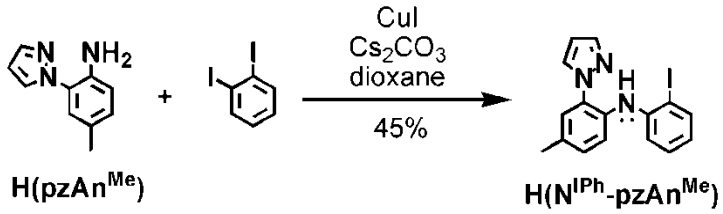

N-(2-iodophenyl)-4-methyl-2-(1H-pyrazol-1-yl)benzenamine, **$H(N^{IPh}$-$pzAn^{Me})$.**

In an argon-filled drybox, a Schlenk flask was charged with 5.32 g (30.7 mmol) $H(pzAn^{Me})$, 12.00 g (36.8 mmol, 1.2 eq) Cs_2CO_3, and 1.17 g (6.14 mmol, 20 mol %) CuI.

The Schlenk flask was removed from the drybox and an argon-sparged (20 min) solution of 11.14 g (33.8 mmol, 1.1 eq) 1,2-diiodobenzene in 30 mL of dry deoxygenated dioxane was added via cannula transfer. After the reaction mixture had been heated at reflux 15h under argon and had been allowed to cool to room temperature, 25 mL each of H_2O and ethyl acetate was added with stirring. The resulting unidentified pale yellow-orange solid was separated from the dark green organic and blue aqueous fractions by filtration. The organic and aqueous layers were separated and the aqueous layer was extracted with three 25 mL portions ethyl acetate. The combined organic fractions were washed with 25 mL water, dried over $MgSO_4$, filtered and solvent was removed by vacuum distillation. The product mixture was separated by column chromatography on silica gel. First, elution with hexanes removed unreacted $I_2C_6H_4$ (R_f = 0.7). Then, elution with 8:1 hexane: ethyl acetate afforded 5.230 g (45 %) of the desired product (R_f = 0.55) as a colorless solid after removing of solvents. Mp: 218-221 ^oC. ^1H NMR ($CDCl_3$): δ_H 8.01 (s, 1 H), 7.79 (d, *J* = 2 Hz, 1 H), 7.75 (m, 2 H), 7.33 (d, *J* = 8 Hz, 1H), 7.19 (m, 1 H), 7.16 (m, 2 H), 7.09 (dd, *J* = 8.3, 1.6 Hz, 1 H), 6.59 (m, 1 H), 6.44 (t, *J* = 2.1 Hz, 1 H), 2.36 (s, 3 H) ppm. ^{13} C NMR ($CDCl_3$): δ_C 144.2, 140.9, 139.8, 133.8, 131.6, 130.4, 129.8, 128.84, 128.76, 125.1, 122.2, 120.2, 116.4, 106.8, 89.6, 20.8 ppm. The product can be recrystallized by cooling a saturated Et_2O solution to -20^{o}C for several hours.

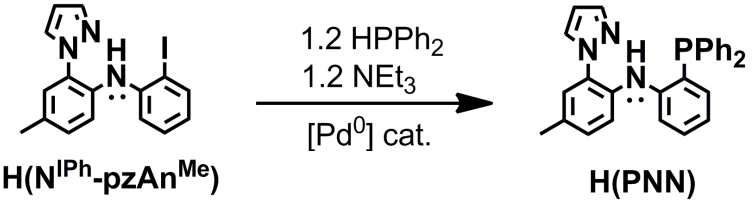

Method A. 0.5 mol% $Pd_2(dba)_3$, 1 mol % XANTPHOS, dioxane, Δ 15 h, **91%**

Method B. 0.5 mol% $Pd(PPh_3)_4$, toluene, Δ 40 h, **72%**

4-methyl-N-(2-(diphenylphosphino)phenyl)-2-(1H-pyrazol-1-yl)benzenamine, **H(PNN).**

Method A. In an argon-filled drybox, a Schlenk flask was charged with 1.13 g (3.00 mmol) $H(N^{IPh}\text{-}pzAn^{Me})$, 0.0137 g (15.0 µmol, 0.5 mol %) $Pd_2(dba)_3$, 0.0174 g (3.00 mmol, 1 mol%) Xantphos, and 0.65 mL (0.70 g, 3.74 mmol) $HPPh_2$. The flask was removed from the drybox and connected to a Schlenk line where 20 mL dry, deoxygenated (20 min argon purge) dioxane and 0.50 mL (0.37 g, 3.6 mmol, 1.2 eq) Et_3N (also deoxygenated with a 20 min argon purge) were added sequentially. After the mixture had been heated at reflux for 15 h under argon, it was cooled to room temperature, and volatiles were removed by vacuum distillation. The resulting solid residue was dissolved in a biphasic mixture of 25 mL each ethyl acetate and water, then the organic and aqueous phases were separated. The aqueous layer was extracted with two 10 mL portions ethyl acetate. The combined organic layers were washed with 10 mL H_2O, dried over $MgSO_4$, and filtered. The product mixture was adsorbed onto silica gel by adding ca. 5 g silica gel to the dried, filtered organic fraction and then removing solvent by rotary evaporation. The resulting solid was loaded onto a fresh column of silica gel. The column was eluted with 8:1 hexane:ethyl acetate where excess diphenylphosphine elutes first (R_f = 0.8, Stench!) followed by the desired product (R_f = 0.45). Removal of solvents from the second band gives 1.18 g (91% yield) of H(PNN) as

a colorless solid. Mp: 141-143 ^{o}C. Anal. Calcd. (found) for $C_{28}H_{24}N_3P$: C, 77.27 (77.09), H, 5.56 (5.69), N, 9.66 (9.63). ^{1}H NMR (acetone-d_6): δ_H 8.55 (s, 1H), 7.97 (m, 1H), 7.39 (m, 6 H), 7.27 (m, 9 H), 7.04 (m, 1 H), 6.86 (m, 1 H), 6.77 (m, 1 H), 6.34 (m, 1 H), 2.30 (s, 3 H) ppm. ^{13}C NMR (acetone-d_6): δ_C 147.1 (d, J = 20.8 Hz), 147.0 (d, J = 20.7 Hz), 140.74, 140.73, 137.1 (d, J = 10.4 Hz), 135.4 (d, J = 1 Hz), 135.3 (d, J = 11 Hz), 134.8, 134.82, 134.7 (d, J = 20.0 Hz), 131.07, 131.05, 130.6, 130.3, 130.2, 129.8, 129.5 (d, J = 7.0 Hz), 129.0, 128.1 (d, J = 11.2 Hz), 128.0 (d, J =11.3 Hz), 124.92, 124.91, 122.5 (d, J = 0.9 Hz), 119.8, 119.34 (d, J = 2.5 Hz), 119.28, 107.1, 20.5 ppm. ^{31}P NMR (acetone-d_6): δ_P -18.3 ppm. ^{1}H NMR (CD_2Cl_2): δ_H 8.04 (d, 1 H, J = 3.5 Hz, N-H), 7.67 (dd, 1 H, J = 2.5, 0.6 Hz), 7.40 – 7.25 (m, 11 H), 7.21 (m,3 H), 7.12 (d, 1 H, J = 2 Hz), 7.02 (m, 1 H), 6.84 (m, 1 H), 6.77 (m, 1 H), 6.28 (dd, 1 H, J = 2.5, 1.9 Hz), 2.31 (s, 3 H) ppm. ^{31}P NMR (CD_2Cl_2): δ_P -20.4 ppm.

Method B. In an argon-filled drybox, a Schlenk flask was charged with 4.29 g (11.4 mmol) H(N^{IPh}-pzAn^{Me}), 0.067 g (0.058 mmol, 0.5 mol %) $Pd(PPh_3)_4$, and 2.00 mL (11.4 mmol) $HPPh_2$. The flask was removed from the drybox and connected to a Schlenk line where 40 mL dry, deoxygenated (30 min Ar-purge) toluene and 1.75 mL (12.6 mmol, 1.1 eq) Et_3N (also deoxygenated with a 30 min Ar-purge) were added sequentially. After the mixture had been heated at reflux for 40 h under inert atmosphere, it was cooled to room temperature, and toluene and other volatiles were removed by vacuum distillation. The solid product mixture was extracted with three 25 mL portions dichloromethane. The combined organic fractions were washed with water then dried over $MgSO_4$, filtered, and volatiles were removed by vacuum distillation to afford an oily residue that was further

purified by column chromatography on silica gel. First elution with 18:1 hexane: ethyl acetate permitted separation of excess $HPPh_2$, followed by unreacted $H(N^{IPh}\text{-}pzAn^{Me})$, then trace hydrolyzed species, $H(N^{Ph}\text{-}pzAn^{Me})$. Finally elution with 6:1 hexane: ethyl acetate afforded the desired product in the next band ($R_f = 0.6$). Removal of solvents by rotary evaporation afforded 3.56 g, (72 %) H(PNN) as a white solid whose characterization data match those above in Method A.

It is noted that the sequence of reactions to the PNN- ligand in Scheme 2.1 (and shown here above) was the only successful method of several that were attempted. For instance, the reactions between Li(n-Bu) and $H(N^{IPh}\text{-}pzAn^{Me})$ or its bromophenyl counterpart $H(N^{BrPh}\text{-}pzAn^{Me})$, and subsequent addition of PPh_2Cl gave diphenylphosphine substitution exclusively at the 5-pyrazolyl carbon rather than at the expected aryl position. The 'unexpected' substitution of acidic hydrogens of pyrazolyl via alkyllithium reagents is not unique to this ligand system.[20] Also, attempts to reverse the sequence of coupling steps (i.e., introducing the diphenylphosphine before the pyrazolyl flanker) were unsuccessful despite trying a variety of different amination catalysts or reaction conditions.

Metal Complex Syntheses.

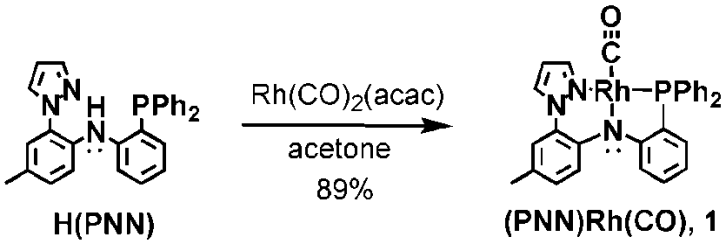

H(PNN) (PNN)Rh(CO), 1

(PNN)Rh(CO), **1**. A mixture of 1.04 g (2.41 mmol) H(PNN) and 0.621 g (2.41 mmol) $Rh(CO)_2(acac)$ in 20 mL acetone was heated at reflux for 15 minutes. After cooling to room temperature, volatiles were removed under vacuum to leave 1.21 g (89 %) of pure1 as a yellow crystalline solid. Mp: 161-71 ^{o}C (dec.). Anal. Calcd. (found) for $C_{29}H_{23}N_3OPRh$: C, 61.82 (61.52), H, 4.11 (4.52), N, 7.46 (6.94). IR (ν_{CO}, cm^{-1}): 1957 (KBr pellet), 1961 (acetone). ^{1}H NMR (acetone-d_6): δ_H 8.45 (m, 1 H), 8.12 (d, J = 1.7 Hz, 1 H), 7.76 (m, 2 H), 7.69 (m, 2 H), 7.49 (m, 6 H), 7.37 (d, J = 8.4 Hz, 1 H), 7.14 (m, 4 H), 6.86 (dd, J = 8.4, 1.5 Hz, 1 H,), 6.76 (t, J = 2.1 Hz, 1 H), 6.61 (m, 1 H), 2.21 (s, 3H) ppm. ^{13}C NMR (acetone-d_6): δ_C 193.2 (dd, $J_{Rh\text{-}C}$ = 67.1, $J_{P\text{-}C}$ =18.3 Hz, Rh-CO), 164.1 (dd, J = 26.1, 2.6 Hz), 146.3 (d, J = 1.4 Hz), 144.0, 135.4, 134.9, 134.5 (d, J = 1.8 Hz), 134.1, 134.0, 133.8, 133.6, 133.5, 132.5 (d, J = 1.3 Hz), 131.5 (d, J = 1.9 Hz), 131.2 (d, J = 1.8 Hz), 130.8, 130.4, 129.9, 129.6 (d, J = 10.4 Hz), 129.4 (d, J = 10.9 Hz), 127.8, 125.8, 124.7, 124.2, 120.3, 120.2, 118.8 (d, J = 7.3 Hz), 108.4, 20.3 ppm. ^{31}P NMR (acetone-d_6): δ_P 60.7 (d, J = 167 Hz) ppm.

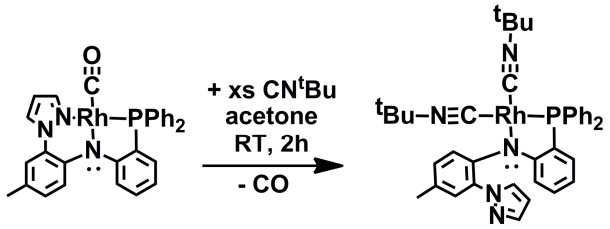

1 **3**

κ^2PN-(PNN)Rh(CN^tBu)$_2$, **3**. Under an argon atmosphere, 121 µL (1.07 mmol) aliquot of CN^tBu was added via syringe to a solution of 0.150 g (0.266 mmol) **1** in 20 mL dry acetone. After the solution had been stirred 2 h, solvent was removed by vacuum distillation. The yellow orange residue was washed with 15 mL pentane and was dried

under vacuum to leave 0.163 g (87 %) **3** as a yellow-orange solid. Mp: 165-71 ^{o}C (dec.). Anal. Calcd. (found) for $C_{38}H_{41}N_5PRh$: C, 65.05 (65.42), H, 5.89 (5.62), N, 9.98 (9.90). IR (ν_{CN}, cm^{-1}, KBr pellet): 2200 (vw), 2158 (m), 2095 (w), 2063 (w). IR (ν_{CN}, cm^{-1}, C_6H_6): 2156 (m), 2102 (w), 2065 (w). ^{1}H NMR (acetone-d_6, 293 K): δ_H 8.78 (m, 1H), 7.83 (m, 2H), 7.72 (m, 3H), 7.47 (m, 7H), 7.04 (m, 3H) 6.72 (s, 1H), 6.02 (m, 3H), 2.21 (s, 3H), 0.88 (s, 9H), 0.83 (s, 9H) ppm. ^{1}H NMR (acetone-d_6, 223 K): δ_H 8.86 (d, J = 2.3 Hz, 1H, H5pz), 7.85 (m, 2H), 7.68 (d, J = 1.5 Hz, 1H, H3pz), 7.64 (m, 2H), 7.45 (m, 7H), 7.08 (m, 2H), 6.97 (d, J = 8.0 Hz, 1H), 6.69 (ps t, Japp = 7.7 Hz, 1H) 6.11 (t, J = 6.9 Hz, 1H), 6.04 (dd, J = 2.3, 1.5 Hz, 1H, H4pz), 5.84 (dd, J = 8.3, 5.1 Hz, 1H), 2.37 (s, 3H), 1.20 (s, 9H), 1.15 (s, 9H) ppm. ^{13}C NMR (acetone-d_6, 293 K): δ_C 137.25 (d, J =1.9 Hz), 136.79 (d, J =1.7 Hz), 135.34, 134.35, 134.21, 134.02, 133.90, 132.99, 132.96, 132.91, 132.82, 132.51, 132.16, 130.71 (broad), 130.49 (d, J =2.26 Hz), 129.81, 129.59, 129.48, 129.20, 129.12, 129.10, 129.02, 128.63, 105.90, 34.86, 23.02, 20.90, 14.36 ppm. ^{31}P NMR (acetone-d_6, 293 K): δ_P 46.0 (d, J = 141 Hz) ppm. ^{31}P NMR (acetone-d_6, 223 K): δ_P 45.8 (d, J = 139 Hz) ppm. X-ray quality crystals of **3**·0.2pentane were deposited after allowing the filtrate from the pentane washing to sit under a N_2 atmosphere overnight. Lower quality crystals can be grown by preparing a saturated hexane solution, filtering, and storing the solution at -30^{o}C for two days.

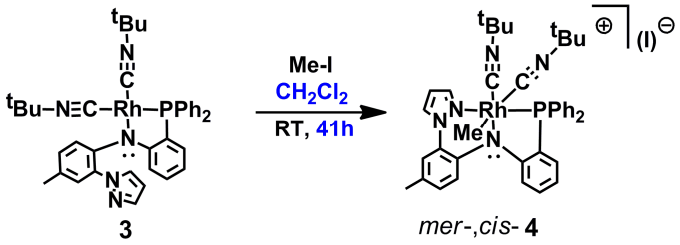

3 *mer-,cis-* **4**

[*mer*-(PNN)Rh(Me)($CN^tBu)_2$](I), ***mer*-4.** A 150 µL (2.41 mmol) aliquot of MeI was added via syringe to a solution of 0.1585 g (0.226 mmol) 3 in 10 mL CH_2Cl_2. After the resulting red-orange solution had been stirred 30 min, CH_2Cl_2 and excess MeI were removed by vacuum distillation to leave a mixture of *fac*- and *mer*-4 (determined from the ^{31}P NMR spectrum). The mixture was dissolved in 20 mL of CH_2Cl_2 and was stirred an additional 40 h. Solvent was then removed under vacuum to leave 0.183 g (96 %) pure *mer*-4 as a red orange solid. Anal. Calcd. (found) for $C_{39}H_{44}N_5IPRh$: C, 55.53 (55.76), H, 5.26 (5.32), N, 8.30 (7.98). IR (ν_{CN}, cm^{-1}, KBr pellet): 2206, 2190. IR (ν_{CN}, cm^{-1}, CH_2Cl_2): 2205, 2186. ^1H NMR (CD_2Cl_2): δ_H 8.22 (m, 1 H), 7.65 (d, J = 2.2 Hz, 1H), 7.62 (m, 1 H), 7.59 (d, J = 1.6 Hz, 1 H), 7.53 (m, 4 H), 7.49 (m, 2 H), 7.44 (m, 1 H), 7.34 (m, 3 H), 7.26 (m, 2 H), 7.08 (d, J = 1.8 Hz, 1 H), 6.93 (dd, J = 8.5, 2.0 Hz, 1 H), 6.80 (m, 2 H), 2.26 (s, 3 H), 1.58 (s, 9 H), 0.69 (s, 9 H) 0.53 (dd, J = 3.35, 1.6 Hz) ppm. ^{13}C NMR (CD_2Cl_2): δ_C 162.1 (d, J = 19.9 Hz), 147.1, 144.0, 136.4, 135.9, 134.1 (d, J = 9.2 Hz), 133.9, 132.6 (d, J = 1.9 Hz), 132.2 (br s), 132.1, 131.6, 131.6 (d, J = 2.8 Hz), 131.1 (d, J = 2.6 Hz), 129.8, 129.6, 129.5, 129.4, 129.1, 129.0, 128.6, 127.3 (d, J = 1.9 Hz), 126.7 (d, J = 1.8 Hz), 125.3, 122.55 (d, J = 13.1 Hz), 121.0, 118.7 (d, J = 8.9 Hz), 109.74 (d, J = 2.5 Hz), 60.4, 59.9, 57.6, 30.57, 29.2, 20.3, 6.9 (dd, J = 15.9, 7.1 Hz) ppm. ^{31}P NMR (CD_2Cl_2): δ_P 57.8 (d, J = 121 Hz) ppm.

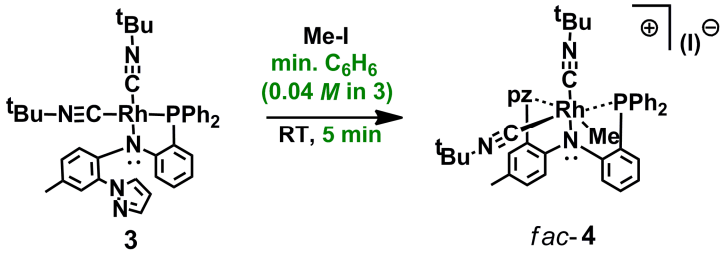

[*fac*-(PNN)Rh(Me)($CN^tBu)_2$](I), ***fac*-4**. A 110 µL (1.77 mmol) aliquot of MeI was added via syringe to a solution of 0.125 g (0.178 mmol) **3** in 5 mL C_6H_6 and a precipitate formed immediately. After the resulting suspension had been stirred 30 min, the insoluble portion was collected by filtration, was washed with 2 mL hexane, and was dried under vacuum to give 0.0886 g (59 %) of pure *fac*-4 as a light yellow solid. Anal.Calcd. (found) for $C_{39}H_{44}N_5IPRh$: C, 55.53 (55.28), H, 5.26 (5.57), N, 8.30 (8.49). IR (ν_{CN}, cm^{-1}, KBr pellet): 2215 (sh), 2210, 2187. IR (ν_{CN}, cm^{-1}, CH_2Cl_2): 2215, 2186. ^1H NMR (CD_2Cl_2): δ_H 7.92 (d, *J* = 2 Hz, 1H), 7.90 (m, 2 H), 7.68 (m, 1H), 7.62 (dd, *J* = 8, 2Hz, 2 H), 7.57 (d, *J* = 8.1 Hz, 1H), 7.41 (ps t, *J*app = 6.9 Hz, 1 H), 7.25 (m, 3 H), 7.12 (m, 2 H), 7.03 (m, 1 H), 6.91 (dd, *J* = 11.5, 11.0 Hz, 2 H), 6.49 (d, *J* = 7.5 Hz, 1 H), 6.47 (d, *J* = 1 Hz, 1H), 6.10 (dd, *J* = 2, 1 Hz, 1 H, H_4pz), 2.43 (s, 3 H, $ArCH_3$), 1.59 (s, 9 H), 1.18 (s, 9 H), 0.73 (dd, $^2J_{RhH}$ = 5 Hz, $^3J_{PH}$ = 1.9 Hz, 3H, $RhCH_3$) ppm. ^{31}P NMR (CD_2Cl_2): δ_P 54.3 (d, *J* = 106 Hz) ppm. The orange, benzene soluble fraction (0.060 g, 40 %) was *mer*-4.

A mixture of X-ray quality crystals of *fac*- and *mer*- 4 can be grown by dissolving the benzene insoluble precipitate from a preparative reaction of *fac*-4 in CH_2Cl_2, layering the resultant solution with pentane and allowing solvents to diffuse. This produces both large and small yellow prism crystals of *mer*-4 (major component) and *fac*-4 (minor component), respectively.

Identification of Reaction Intermediates.

When **1** was reacted with three equivalents or less of CN^tBu, an intermediate species, (PNN)Rh(CN^tBu), ***IA***, could be identified by NMR spectroscopy (and by chemical

reactivity with MeI, Xray structure Figure 2.10). Intermediate ***IA*** could not be isolated in pure form due to an apparent equilibrium according to Scheme 2.4 favoring the formation of **3**. Of the various NMR-active nuclei, the chemical shift and the associated coupling constants of ^{31}P NMR resonances are the simplest diagnostic tools for the various species present in the mixture. Thus, the doublet resonance for complex ***IA*** has a very similar ^{31}P NMR chemical shift as that for unreacted **1** but is slightly upfield at δ_P = 60.1 ppm and has a larger coupling constant, $J_{P\text{-}Rh}$ = 180 Hz, which makes this signal distinguishable from that of the starting material. Relative to the resonance for either **1** or ***IA***, that for **3** is found further upfield at δ_P = 46 ppm and has a smaller coupling constant, $J_{P\text{-}Rh}$ = 141Hz. The reaction with MeI was explored in order to give (PNN)Rh(Me)(CN^{t}Bu)(I), **5**, (Figure 2.10) which would further support the identity of ***IA***.

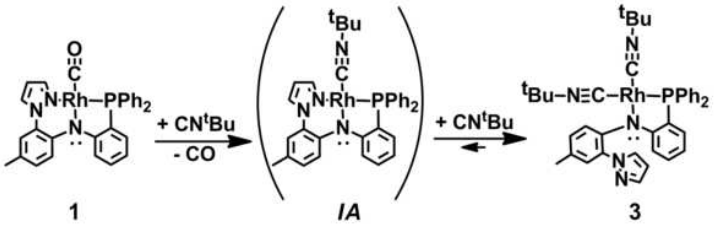

Scheme 2.4. Reaction of **1** with CN^{t}Bu.

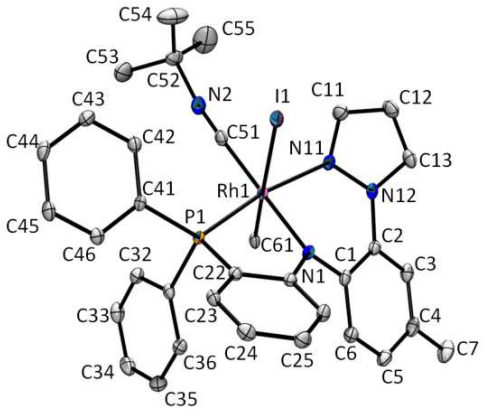

Figure 2.10. Molecular Structure and atom labeling for (PNN)Rh(Me)(CN^{t}Bu)(I)·C_6H_6, **5**·C_6H_6. Thermal ellipsoids drawn at the 50% probability level. Hydrogen atoms and solvent molecule removed for clarity.

Attempt to prepare (PNN)Rh(CN^{t}Bu), ***IA***.

Under an argon atmosphere, 29.0 µL (0.256mmol) aliquot of CN^{t}Bu was added via syringe to a solution of 0.142 g (0.252 mmol) **1** in 20 mL acetone. After the solution had been stirred 2 h at room temperature, solvent was removed by vacuum distillation to leave 0.156 g (99% yield based on Rh) of a mixture that was 75% ***IA***, 16% **3**, and 9% starting material **1**, based on ^{31}P NMR integration and deconvolution, see spectrum in Figure 2.11. The following characterization data are only for the main component of the mixture which we attribute to ***IA***. IR (ν_{CN}, cm^{-1}, KBr pellet): 2088 (w), 2052 (w). ^{1}H NMR (acetone-d_6): δ_H 8.34 (br s, 1 H, pz), 7.99 (br s, 1 H, pz), 7.81 (m, 2 H), 7.57 (m, 1 H), 7.43 (br m, 8 H), 7.20 (m, 1 H), 7.06 (m, 2 H), 6.99 (ps t, J = 7.4 Hz, 1 H), 6.79 (m, 1 H), 6.64 (br s, 1H, pz) 6.47 (ps t, J = 7.4 Hz, 1 H), 2.19 (s, 3 H, CH_3-tolyl), 2.21 (s, 9 H, ^{t}Bu-CH_3) ppm. ^{31}P NMR (acetone-d_6): δ_P 60.1 (d, J = 180 Hz) ppm.

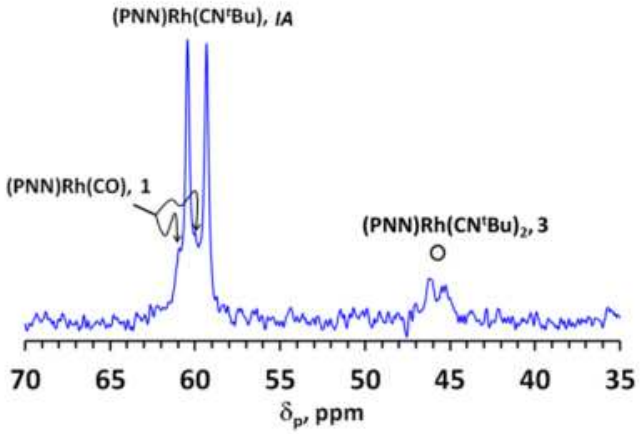

Figure 2.11. ^{31}P NMR spectrum of mixture obtained from the reaction between (PNN)Rh(CO) and one equivalent of CN^{t}Bu in acetone.

Reaction between ***IA*** and MeI to give (PNN)Rh(Me)(CN^{t}Bu)(I), **5**.

A 110 µL (1.77 mmol) aliquot of iodomethane was added by syringe to a yellow solution of 0.1143 g (0.182 mmol) of the 75:16:9 mixture of ***IA*:3:1** (from the above attempted preparation of ***IA***) in 5 mL C_6H_6. After the resulting turbid red-orange solution had been stirred 30 min at room temperature, and filtered to remove [(PNN)Rh(Me)(CN^{t}Bu)$_2$](I), **4**, the volatile components of the soluble portion were removed by vacuum distillation to leave 0.103 g of a mixture of mainly (PNN)Rh(Me)(CN^{t}Bu)(I), **5**, with a trace of (PNN)Rh(Me)(CO)(I) as a mixture of isomers [IR(ν_{CO}, cm^{-1}): 2046 (KBr pellet); ^{31}P NMR (CD_2Cl_2): δP 59.7 (d, *J* = 121.4 Hz, major isomer), 59.0 (d, *J* = 121.4 Hz, minor isomer) ppm]. X-ray quality crystals of **5**·C_6H_6 were deposited after slow evaporation of a benzene solution of the above product

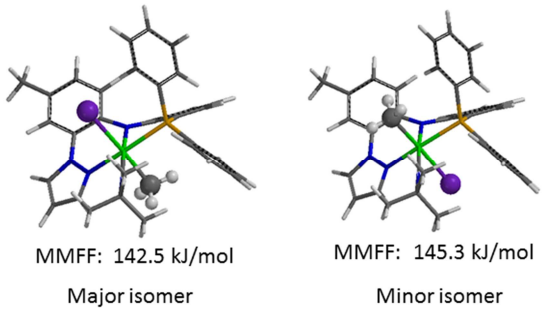

mixture (Figure 2.10). The following data are attributed to **5** based on data collected from X-ray quality crystals. Anal. Calcd. (found) for $C_{34}H_{35}N_4IPRh$: C, 53.70 (54.01), H, 4.64 (4.78), N, 7.37 (7.13). IR (ν_{CN}, KBr, cm^{-1}); 2174. ^{31}P NMR (acetone-d_6): δ_P 58.1 (d, J = 130 Hz, major isomer), 57.2 (d, J = 129 Hz, minor isomer) ppm.

2.5 SINGLE CRYSTAL X-RAY DIFFRACTION

X-ray intensity data from a colorless prism of H(PNN), a yellow plate of **3**·0.2 pentane, a yellow plate of ***mer*-5**·C_6H_6, an orange block of ***mer*-4**·$3C_6H_6$, a yellow prism of ***mer*-4**·C_6H_6, a yellow prism of ***mer*-4**·$2CH_2Cl_2$, and a yellow prism of ***fac*-4**·$0.25H_2O$ were measured with an Oxford Diffraction Ltd. Supernova diffractometer equipped with a 135 mm Atlas CCD detector using Cu(K_α) radiation for ***fac*-4**·$0.25H_2O$ and Mo(K_α) radiation for the remaining experiments. Raw data frame integration and Lp corrections were performed with CrysAlis Pro (Oxford Diffraction, Ltd.).[21] Final unit cell parameters were determined by least-squares refinement of 31802, 16522, 16801, 11073, 17967, 11276, and 12681 reflections from the data sets of H(PNN), **3**·0.2 pentane, ***mer*-5**·C_6H_6, ***mer*-4**·$3C_6H_6$, ***mer*-4**·C_6H_6, ***mer*-4**·$2CH_2Cl_2$, and ***fac*-4**·$0.25H_2O$, respectively, with $I>2\sigma(I)$ for each. Analysis of the data showed negligible crystal decay during collection in each case. Direct methods structure solutions, difference Fourier calculations and fullmatrix least-squares refinements against F^2 were performed with OLEX2. [22] Empirical absorption corrections were applied to the data of H(PNN) using spherical harmonics implemented in the SCALE3 ABSPACK multi-scan method.[23] Numerical absorption corrections based on gaussian integration over a multifaceted crystal model were applied to the data of the remaining complexes. All non-hydrogen atoms were

refined with anisotropic displacement parameters. Hydrogen atoms were placed in geometrically idealized positions and included as riding atoms. The X-ray crystallographic parameters and further details of data collection and structure refinements are presented in Tables 2.1 and 2.2.

Table 2.1. Crystallographic Data Collection and Structure Refinement for **H(PNN)**, **3**·0.2 pentane, *mer*-**5**·C_6H_6, and *mer*-**4**·$3C_6H_6$.

Compound	**H(PNN)**	**3**·0.2 pentane	*mer*-**5**·C_6H_6	*mer*-**4**·$3C_6H_6$
Formula	$C_{28}H_{24}N_3P$	$C_{39}H_{43.4}N_5PRh$	$C_{40}H_{41}IN_4PRh$	$C_{48}H_{53}IN_5PRh$
Formula weight	433.47	716.09	838.55	960.73
Crystal system	triclinic	triclinic	triclinic	triclinic
Space group	P -1	P -1	P -1	P -1
Temp. [K]	100.6	100.0(1)	100.0(1)	100.0(1)
a [Å]	9.8762(3)	11.5283(4)	9.8201(3)	11.1383(4)
b [Å]	10.5856(3)	13.2391(5)	13.4080(4)	13.5899(6)
c [Å]	12.9701(4)	14.1743(5)	15.6990(6)	15.4823(5)
α[°]	72.002(3)	63.183(4)	76.809(3)	81.434(3)
β[°]	69.415(3)	89.650(3)	77.066(3)	77.878(3)
γ [°]	64.541(3)	74.920(3)	69.199(3)	87.488(3)
V [Å^3]	1125.96(6)	1848.59(11)	1858.05(11)	2265.52(15)
Z	2	2	2	2
$D_{calcd.}$ [gcm^{-3}]	1.279	1.286	1.499	1.408
λ[Å] (Mo Kα)	0.7107	0.7107	0.7107	0.7107
μ.[mm^{-1}]	0.143	0.538	1.366	1.131
Abs. Correction	multi-scan	numerical	numerical	numerical
F(000)	456	745	844	978
2θ range [°]	6.74 to 58.92	6.74 to 59.16	6.70 to 59.22	6.98 to 54.00
Reflections collected	63636	41908	42012	27954
Independent reflections	6000[R(int) = 0.0271]	9464 [R(int) = 0.0378]	9487[R(int) = 0.0378]	11056[R(int) = 0.0335]
T_min/max	0.85229/1.00000	0.895/0.970	0.745/0.930	0.819/0.901
Data/restraints/ parameters	6000/0/294	9464/100/537	9487/0/429	11056/0/513
Goodness-of-fit on F^2	1.069	1.071	1.055	1.066
*R*1/*wR*2[$I>2\sigma(I)$][a]	0.0354/0.0866	0.0300/0.0609	0.0268/0.0528	0.0300/0.0602
*R*1/*wR*2 (all data)[a]	0.0391/0.0894	0.0398/0.0667	0.0359/0.0582	0.0415/0.0679
Largest diff. peak/hole / e Å^{-3}	0.405/-0.294	0.867/-0.362	1.046/-0.686	0.698/-0.730

[a] $R = \sum||F_o|-||F_c||/\sum|F_o|$. [d] $wR = [\sum w(|F_o^2|-|F_c^2|)^2/\sum w|F_o^2|^2]^{1/2}$

Table 2.2. Crystallographic Data Collection and Structure Refinement for *mer*-**4**·C_6H_6, *mer*-**4**·$2CH_2Cl_2$, and *fac*-**4**·$0.25H_2O$.

Compound	***mer*-4·C_6H_6**	***mer*-4·$2CH_2Cl_2$**	***fac*-4·$0.25H_2O$**
Formula	$C_{45}H_{50}IN_5PRh$	$C_{41}H_{48}Cl_4IN_5PRh$	$C_{39}H_{44}IN_5O_{0.25}PRh$
Formula weight	921.68	1013.42	847.63
Crystal system	triclinic	triclinic	triclinic
Space group	P -1	P -1	P -1
Temp. [K]	100.0(1)	100.0(1)	100.0(1)
a [Å]	10.7444(3)	10.9887(5)	10.6257(4)
b [Å]	14.5778(4)	13.7160(6)	13.1378(5)
c [Å]	15.3318(4)	16.4225(7)	15.8308(6)
α[°]	100.965(2)	106.957(4)	97.659(3)
β[°]	104.590(3)	95.347(4)	107.384(3)
γ [°]	103.059(3)	104.978(4)	111.238(4)
V [Å^3]	2184.72(11)	2248.81(17)	1891.93(12)
Z	2	2	2
$D_{calcd.}$ [gcm^{-3}]	1.401	1.497	1.488
λ[Å] (Mo or Cu Kα)	0.7107	0.7107	1.5418
μ.[mm^{-1}]	1.170	1.373	10.715
Abs. Correction	numerical	numerical	numerical
F(000)	936	1020	856
2θ range [°]	6.66 to 56.00	6.90 to 59.14	7.50 to 147.80
Reflections collected	49262	32086	27026
Independent reflections	11169 [R(int) = 0.0390]	11112 [R(int) = 0.0370]	7522 [R(int) = 0.0332]
T_min/max	0.760/0.931	0.687/0.918	0.438/0.679
Data/restraints/ parameters	11169/0/486	11112/0/486	7522/0/442
Goodness-of-fit on F^2	1.070	1.060	1.031
*R*1/*wR*2[*I*>2σ(*I*)][a]	0.0308/0.0638	0.0321/0.0630	0.0255/0.0616
*R*1/*wR*2 (all data)[a]	0.0443/0.0716	0.0479/0.0718	0.0297/0.0641
Largest diff. peak/hole / e Å^{-3}	1.001/-0.755	0.833/-0.753	0.525/-1.044

[a]$R = \sum||F_o|-||F_c||/\sum|F_o|$. [d]$wR = [\sum w(|F_o^2|-|F_c^2|)^2/\sum w|F_o^2|^2]^{1/2}$

2.6. COMPUTATIONAL DETAILS

Methodology. DFT calculations were performed with Perdew's gradient corrected local correlation functional[24] modified by Handy's optimized exchange[25] ,OP86, using the def2-SV(P) double-zeta basis set.[26] Solvent (DCM) effects were accounted for by using the polarizable continuum model IEFPCM,[27] as implemented in Gaussian 09.[28] This computational model was chosen since it was found to be a reliable and computationally inexpensive alternative to the OP86/Lanl2-[6s4p4d2f] (Rh), aug-cc-pVTZ (Cl), cc-PVTZ (C,N,H) model (referred to as BS2 in reference 29 and henceforth) known to give highly accurate calculations for complexes of this metal. Such an evaluation was made by comparing the experimentally known and theoretically calculated enthalpy of reaction R1, [29] the metrical parameters and the vibrational frequencies of carbonyl stretches from the associated rhodium-containing structures.

$$[(CO)_2Rh(\mu\text{-}Cl)]_2 + 2\ py \longrightarrow 2\ Rh(CO)_2Clpy\ (in\ benzene) \qquad (R1)$$

Discussion of Computational Results

Given the conformational adaptability of the new PNN ligand we sought to make a comparison of the "flexidentate" character of PNN ligands. Similar to the approach by the van der Vlugt group for related rhodium complexes we evaluated results of DFT calculations but we used a reliable and computationally inexpensive OP86/def2-SV(P) model in CH_2Cl_2 (PCM). Rhodium(I) complexes of the four ligands in the top of Fig.2.12 were interrogated. It was found that (κ^2PN-L)Rh($CN^tBu)_2$ and (κ^3-L)Rh(CN^tBu) (and free CN^tBu) were nearly isoergonic (±4 kcal/mol) which correctly predicts the

experimentally observed equilibrium between these species. A five-coordinate intermediate was also located as a minimum of the potential energy surface for three of the four complexes. All attempts to locate a five-coordinate minima using various starting geometries for (κ^3-L3)Rh(CN^tBu)$_2$ resulted in convergence to (κ^2PN-L3)Rh(CN^tBu)$_2$. Of the various three coordinate species, (κ^2PN-L)Rh(CN^tBu) with the isocyanide bound trans- to the amido was lowest in energy. The five coordinate intermediates of L1 and LG were lower energy than their three coordinate counterparts (and free CN^tBu) but the opposite was true for L2 and L3, suggesting that the conversion between (κ^2PN-L)Rh(CN^tBu)$_2$ and (κ^3-L)Rh(CN^tBu) (and free CN^tBu) may occur by different pathways depending on the ligand backbone. That is, the conversion between (κ^2PN-L)Rh(CN^tBu)$_2$ and (κ3-L)Rh(CN^tBu) likely occurs by a dissociative route for L3 and L2 but mainly an associative pathway for LG. However, the similar energies of the three- and five-coordinate intermediates of L1 probably ensure that both associative and dissociative pathways are thermally accessible.

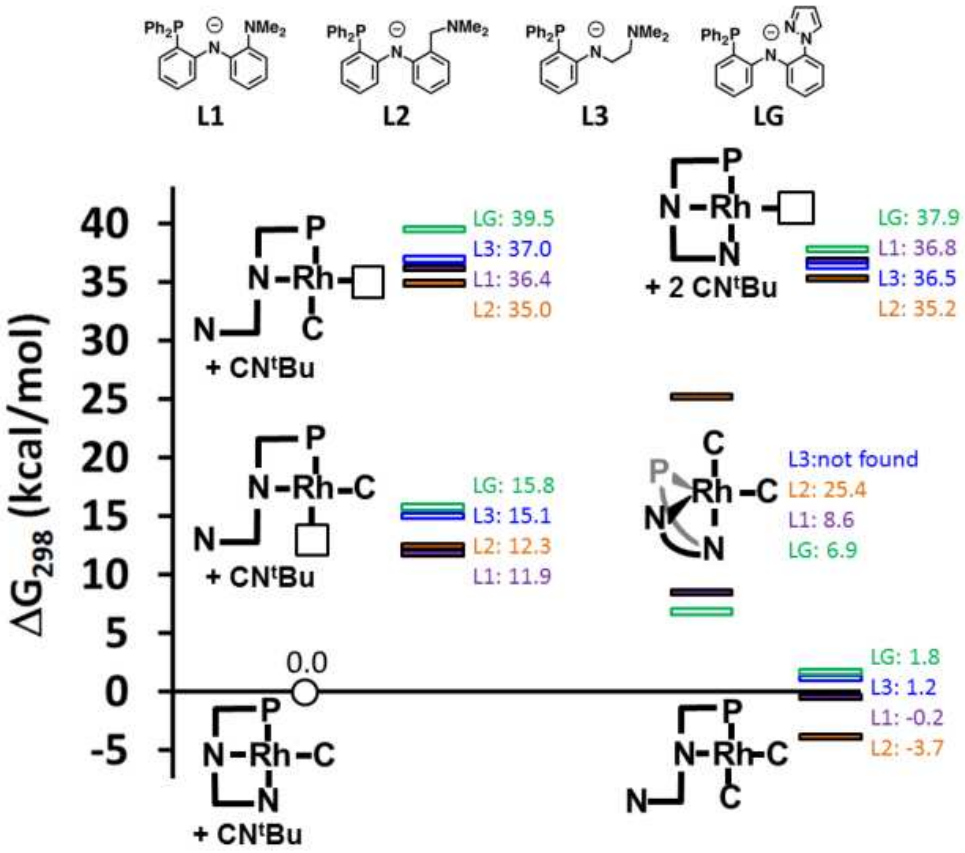

Figure 2.12. Free energy scale (298 K) of various (L)Rh(CN^{t}Bu)(2-x) + x CN^{t}Bu ("C" indrawings of complexes) (x = 1-2) relative to (L)Rh(CN^{t}Bu) and 1 equiv. free CN^{t}Bu (ΔG = 0 kcal/mol) from DFT calculations (OP86/def2-SV(P)).

CHAPTER 3

ELECTRONIC COMMUNICATION ACROSS DIAMAGNETIC METAL BRIDGES: A HOMOLEPTIC GALLIUM(III) COMPLEX OF A REDOX-ACTIVE DIARYLAMIDO BASED LIGAND AND ITS OXIDIZED DERIVATIVES

This work was published: Liddle, B. J.; Wanniarachchi, S.; Hewage, J. S.; Lindeman, S. V.; Bennett, B.; Gardinier, J. R. *Inorg. Chem.* **2012**, *51*(23), 12720-12728.

3.1 INTRODUCTION

Over the past few decades, the study of mixed-valence (MV) compounds has been pivotal for advancing comprehension of long-range electron transfer of importance to both basic biological functions and, potentially, to future molecular electronics applications.[1] A majority[2] of the MV complexes studied have been of the type M^{n+}-(bridge)-$M^{(n-1)+}$ where the bridge is an organic group such as in the Creutz-Taube ion, $[(NH_3)_5Ru^{II}(\mu\text{-pyrazine})Ru^{III}(NH_3)_5]^{5+}$.[3] There has also been a great deal of interest in purely organic systems of the type D-OB-$D^{+\cdot}$, where OB is an organic bridge and $D/D^{+\cdot}$ are the one-electron redox partners of an organic donor.[4] A popular class of such organic derivatives is those with diarylamine donors that flank an organic bridge, Figure 3.1.[5−8] Electronic communication between donor ends of such molecules can vary dramatically by changing: (i) the groups, X, along the diarylamine donor;[5c,h−j] (ii) the type of bridge;[7a,8,9] (iii) the bridge length or (iv) the geometric disposition of donors about the bridge,[5i,j,9] including the dihedral angle between bridging phenylene groups (that also affect the dihedral angle of orbitals containing the nitrogen lone pair).[10]

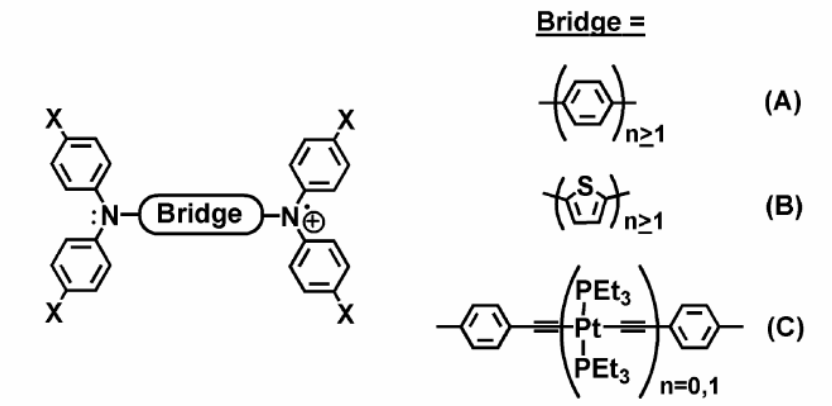

Figure 3.1. (A-C) Diarylamine-based mixed valent compounds.

In cases such as A and B in Figure 3.1, electronic communication can occur via tunneling, superexchange, or a "hopping" mechanism whereby the bridge becomes an active participant. The latter is important for longer, more highly conjugated and electron-rich bridges. Both through-bond and through-space superexchange interactions become important for short bridges such as found in the tetraanisyl-o-phenyl-enediamine cation radical.[9]

An important class of MV complexes is one like Figure 3.1C (n= 1)[8] that contains organic donors separated by a metal bridge.[11] One-electron oxidized or reduced forms of metal dioxolenes,[12] dithiolenes,[13] diimines,[14–17] o-semiquinones,[18] o-iminosemiquinones,[19] polypyridyls,[20] and tridentate catecholates[21] can all fall into this category. Some important aspects of the chemistry of these and related metal complexes of redox-active ligands were the subjects of a recent special issue of Inorganic Chemistry[22] and of several reviews.[23] With relation to the organic derivatives mentioned above, the interjection of the $Pt(PEt_3)_2$ bridge between (di/tri)arylamine donors, Figure 3.1C (n = 1), permitted

weak electronic coupling (H_{ab}= 350 cm^{-1}) between donor ends, but this coupling was weaker than that found for derivatives where a phenylene (H_{ab}= 440 cm^{-1})[5c] or a p- dimethoxyphenylene group (H_{ab}= 520 cm^{-1})[7a] replaces the metal bridge. Thus, despite the former possessing fewer number of sigma bonds separating donor ends (and a shorter $D\cdots D^{+\cdot}$ separation) than in the pure organic cases, the energetic mismatch between donor and the metal bridge has a small detrimental influence on the electron transfer.

We were interested in further examining how effectively electronic communication could be mediated by using only a single atom bridge between two diarylamido groups. In particular, we recently prepared a series of diarylamines that have a pyrazolyl group situated at an ortho-position of each aryl (Figure 3.2).

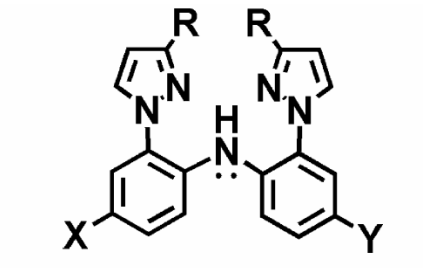

Figure 3.2. Di(2-3R-pyrazolyl)-p-arylamines, $H(XY^R)$.

The coordination chemistry of tricarbonylrhenium(I)[24] and rhodium[25] complexes showed that these pincer-type ligands are electrochemically active and chemically noninnocent. The electronic properties and reactivity of the complexes could be predictably fine-tuned by substituting at the pyrazolyl, at the para-aryl positions, or even

at the metal center. In those studies, only one ligand was bound to a metal center. We envisioned constructing molecular wires by assembling strings of $M(L = XYR)_2$ complexes together to give species such as LM-$[(L\text{-}L)M(L\text{-}L)]_n$-ML (n = 0, 1, 2...). Therefore, it became of interest to examine potential electronic interactions between two ligands across a single metal ion bridge to inform future wire designs. Our investigations began with simple model complexes of redox-silent gallium(III) with the added purpose of obtaining structural and spectroscopic markers for ligand-based radicals that should also be of use in future studies that incorporate transition metals. Herein, we report on the preparation and properties of the complete valence series of $[Ga(L)_2]^{n+}$ complexes (n = 1−3).

3.2 RESULTS AND DISCUSSION

The reaction between 2 mol equivalents of "Li(L)" (formed insitu from Li(n-Bu) and H(L) in THF at −20 °C) and 1 molequivalent GaI_3 gives blue-luminescent $[Ga(L)_2](I)$, rather surprisingly, as the insoluble product and LiI as the soluble product, a mixture that can be easily separated by filtration. As the signal for iodide oxidation interferes with the ligand oxidation wave in voltammetry experiments (Figure 3.3), an ensuing metathetical reaction between$[Ga(L)_2](I)$, (**1**)(I), and $TlPF_6$ afforded $[Ga(L)_2](PF_6)$, (**1**)(PF_6), in high yield.

Single crystals of (**1**)$(PF_6)\cdot 1.75\ CH_2Cl_2$ suitable for X-ray diffraction were grown by layering hexanes on a CH_2Cl_2 solution and allowing solvents to diffuse. The

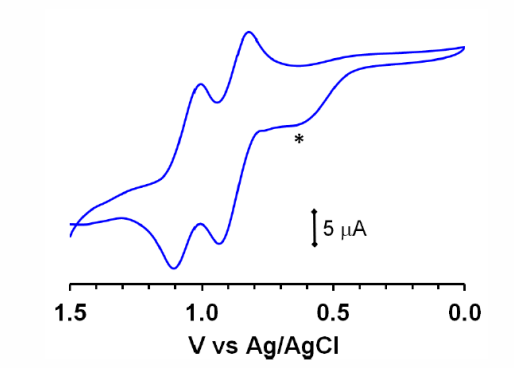

Figure 3.3. Cyclic Voltagram of $[Ga(L)_2](I)$, (**1**)(I), in CH_2Cl_2 (200 mV/s, NBu_4PF_6 supporting electrolyte). The asterisk demarcates the wave of the I^-/I_2 couple.

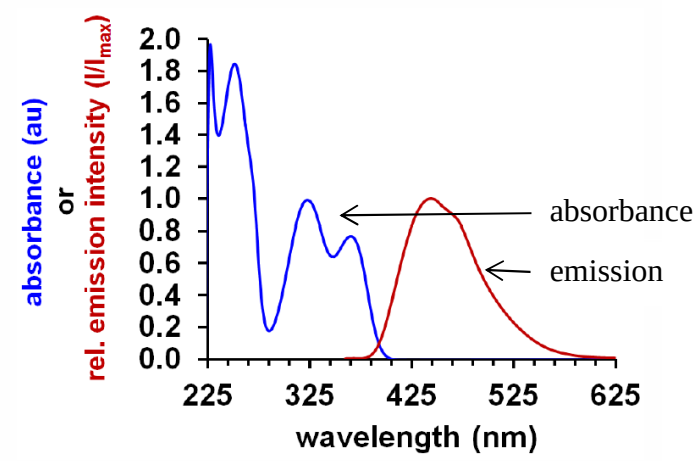

Figure 3.4. Overlay of absorption and emission spectrum of $[Ga(L^-)_2]^+$,$(1)^+$ in CH_2Cl_2 at 295 K.

compound crystallizes with two crystallographically independent (**1**)(PF_6) units. Views of the structure of one of the cations are shown in Figure 3.5. The gallium center in each

resides in a compressed octahedral GaN_6 environment as a result of the disparate distances associated with the two types of Ga−N bonds. Those bonds associated with the diarylamido portion of the ligand, $Ga-N_{Ar}$, average 1.949(6) Å which is shorter than found in two independent structure determinations of a related hexacoordinate gallium(III) ONO- pincer complex Ga(dbqdi = 3,5-di-tert-butyl-1,2-quinone-1-(2-hydroxy-3,5-ditert-butyl-phenyl)imine)$_2$ (avg. 2.020(3) Å[21]dand avg. 2.027(3) Å[21e]). As expected, the $Ga-N_{Ar}$ bonds in the current six-coordinate complex are longer than those in three- or four-coordinate diphenylamidogallium(III) complexes which range from 1.85 to 1.91 Å.[26] The gallium−nitrogen bonds in (**1**)$^+$ associated with pyrazolyl groups, $Ga-N_{pz}$, range from 2.085(2) Å to 2.141(3) Å and average 2.101 Å. These values are in good agreement with sixcoordinate tris(pyrazolyl)borate complexes of gallium(III).[27] Notably, in (**1**)$^+$ the amido nitrogen atoms are planar with the sum of angles around each of 360°. The six-membered chelate rings (avg. Npz−Ga−Npz bite angle, 88(1)^o) are nonplanar such as to allow the diarylamido NC_2- moieties to be nearly coplanar across the gallium bridge. That is, there is a small dihedral angle of 16.6(8)^o between the mean plane containing C1−N1−C31 and that containing C41−N41−C71 (Figure 3.5, right). Thus, the nitrogen p-orbitals containing the lone-pair electrons are expected to be roughly parallel with each other but are separated by 3.897(3) Å (avg. N···N distance) This geometry is in contrast to the case of the ONO-pincer complex, Ga(dbqdi)$_2$ whose five-member (planar) chelate rings force the two ligands to be orthogonal, with the dihedral angle of 87.05° between mean planes containing the C−N−C atoms.[21d,e]

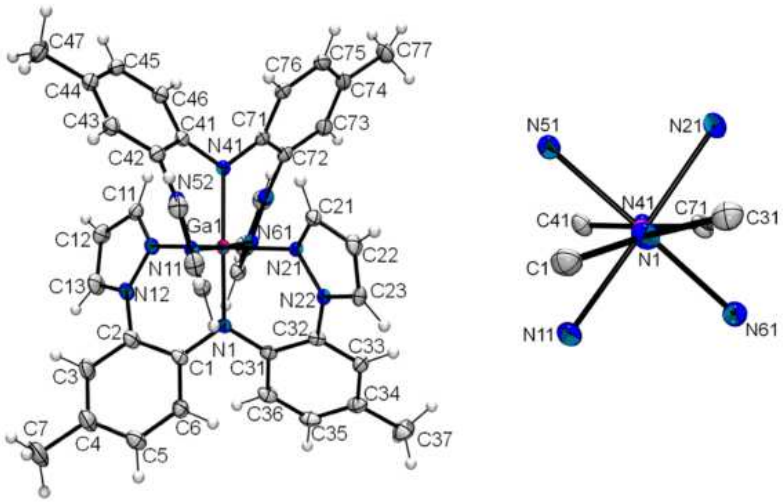

Figure 3.5. Views of one of the two crystallographically independent cations $[Ga(L)_2]^+$, $(\mathbf{1})^+$, in the crystal of $(1)(PF_6)\cdot 1.5CH_2Cl_2$(left) with a view approximately down the N1−Ga1−N41 vector showing the small dihedral angle between C1−N1−C31 and C41−N41−C71 planes. Selected bond distances (Å): Ga1−N1, 1.947(2); Ga1−N41, 1.953(2); Ga1−N11, 2.099(2); Ga1−N21, 2.094(2); Ga1−N51, 2.101(2); Ga1−N61, 2.085(2). Selected bond angles (o): N1−Ga1−N41, 179.05(11); N11−Ga1−N21, 178.60(9); N51−Ga1−N61, 177.85(9); N1−Ga1−N11, 90.00(10); N1−Ga1−N21, 89.34(9); N41−Ga1−N51, 89.08(10); N41−Ga1−N61, 88.85(10); N11− Ga1−N51, 92.93(9); N11−Ga1−N61, 86.49(10); N21−Ga1−N51, 85.85(9); N21−Ga1−N61, 94.75(9).

Representative cyclic voltammograms of the free ligand, H(L), and of (**1**)(PF_6) in CH_2Cl_2 are given in Figure 3.6, while a summary of electrochemical data of (**1**)(PF_6) in three different solvents is provided in Table 3.1. The voltammogram of H(L) in CH_2Cl_2 shows a single irreversible oxidation wave with an anodic peak at ca. 1.2 V versus Ag/AgCl ($i_a/i_c > 1$), whereas that of $[Ga^{III}(L^-)_2](PF_6)$ in this solvent shows two overlapping, reversible, one-electron oxidation waves at 0.94 and 1.17 V versus Ag/AgCl. Since gallium(III) cannot be oxidized to gallium(IV), the oxidation waves are

unequivocally identified as ligand-based affording $[Ga^{III}(L^{-})(L^{0})]^{2+}$, $(\mathbf{2})^{2+}$, and $[Ga^{III}(L^{0})_2]^{3+}$, $(\mathbf{3})^{3+}$, respectively. The close proximity of the two ligands connected by a one-atom spacer can give rise to two oxidation waves by simple Coulombic means and/or by electronic communication via superexchange or hopping mechanisms. Coulombic interactions do not have a spectroscopic marker, whereas electronic communication (via super-exchange or hopping) leaves a signature in the form of an intravalence charge transfer (IVCT) band which is indeed observed in the current case, vide infra. The equilibrium constant for comproportionation according to eqs 1 and 2 is on the order of 10^2 to 10^3 (determined from the electrochemical data in various solvents, Table 3.1), which indicates a small but significant degree of electronic communication in mono-oxidized $(\mathbf{2})^{2+}$.The relatively small value of $K_{com} \sim 10^3$ is one indicator that $(\mathbf{2})^{2+}$is a Robin-Day class II mixed valent species.[3c,28]

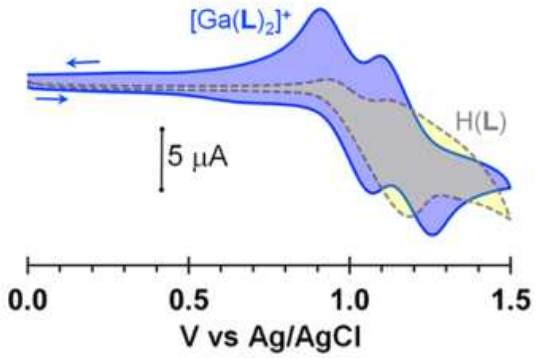

Figure 3.6. Overlay of cyclic voltammograms of H(L) and $(\mathbf{1})(PF_6)$ in CH_2Cl_2 obtained at a scan rate of 200 mV/s.

Table 3.1. Electrochemical Data for (**1**)(PF_6) in Various Solvents

Solvent	$E_{1/2}(1)$, V[a,b]	$E_{1/2}(2)$, V[a,b]	ΔE, V[c]	K_{com}[d]
CH_2Cl_2	0.989(3)	1.173(4)	0.184	1.39×10^3
PC[e]	0.838(2)	0.994(5)	0.156	4.62×10^2
CH_3CN	0.888(1)	1.065(1)	0.177	1.06×10^3

[a] average values obtained for scan rates of 50, 100, 200, and 400 mV/s with 0.1 M $NBu_4(PF_6)$ as supporting electrolyte; [b] V versus Ag/AgCl; [c] $\Delta E = E_{1/2}(1) - E_{1/2}(2)$; [d] $K_{com} = e^{(\Delta E \cdot F/RT)}$, T = 295 K; [e] propylene carbonate

$$[Ga^{III}(L^-)_2]^+ + [Ga^{III}(L^0)_2]^{3+} \longleftrightarrow 2[Ga^{III}(L^-)(L^0)]^{2+} \quad (1)$$

$$K_{com} = [(\mathbf{2})^{2+}]^2 / [(\mathbf{1})^+][(\mathbf{3})^{3+}] \quad (2)$$

3.3. THEORETICAL STUDIES

In order to gain further insight into the nature of the two oxidation waves and to help rationalize the other experimental properties of the oxidized species, the cations $(\mathbf{1})^+$, $(\mathbf{2})^{2+}$, and $(\mathbf{3})^{3+}$ were studied by density functional theory. Four models were examined (M06 or B3LYP functionals with either the LANL2DZ or Def2-SV(P) basis sets), each also accounted for solvation in dichloromethane by employing the polarizable continuum model (PCM). While all gave qualitatively similar trends, the combination (U)M06/ Def2-SV(P) gave most satisfactory correlation to experimental data (bond distances and spectroscopic parameters) as summarized in the Table 3.2. The major findings of these

studies are summarized below. First, despite missing solvated anions in the theoretical study, a 625 mV difference between first and second oxidation potentials was obtained which parallels the experimental finding of two separate oxidation waves. Second, for the doubly oxidized $(\mathbf{3})^{3+}$, the singlet diradical state was found to be 21.7 cm^{-1} lower energy than the triplet state. Third, the major structural changes along the valence series occur for Ga−N bonds (despite a lack of participating orbitals on the metal center). Thus, upon successive oxidation, the Ga−N bonds associated with the diarylamido, $Ga-N_{Ar}$, lengthen while those associated with the pyrazolyls, $Ga-N_{pz}$, shorten. The unoxidized and dioxidized complexes are more symmetric about gallium(III). However, the bond distances associated with each ligand of the mono-oxidized species $(\mathbf{2})^{2+}$ are distinct. One ligand has a longer $Ga-N_{Ar}$ bond and a shorter average $Ga-N_{pz}$ distance than the other ligand. In $(\mathbf{2})^{2+}$, the longer $Ga-N_{Ar}$ bond distance 2.081 Å resembles the average distance 2.043 Å calculated for the doubly oxidized complex $(\mathbf{3})^{3+}$, while the shorter $Ga-N_{Ar}$ distance of 1.937 Å resembles the average distance of 1.966 Å calculated for the unoxidized complex $(\mathbf{1})^{+}$. The intraligand C−C bond distances also show a similar disparity, but the differences between each ligand in $(\mathbf{2})^{2+}$ are much less pronounced than those distances involving gallium. Therefore, examination of the Ga−N bond distances allows one to most easily discern which ligand is oxidized. Electronically, the paramagnetic species are ligand-centered radicals with negligible spin density on the gallium center. Finally, time-dependent DFT revealed that in the paramagnetic derivatives, a set of pi-radical bands for β-HOMO(-N = 2−7) to SOMO (β-LUMO) transitions should be observed in the 590−830 nm range. For the mono-oxidized complex $(\mathbf{2})^{2+}$, an additional weak (oscillator strength, f, $\sim 10^{-3}$), low-energy intervalence charge

transfer (IVCT) band for a β-HOMO-SOMO (β-LUMO, see Figure 3.7) transition was predicted to be found in the NIR region. Moreover, the IVCT band was predicted to show a small solvent dependence, shifting (473 cm^{-1}) from 4237 cm^{-1}(2657 nm, f = 6.3×10^{-3}) in CH_2Cl_2 to 3764 cm^{-1} (2360 nm, f = 5.3×10^{-3}) in CH_3CN, in line with behavior expected for a Class II mixed valence species.

By careful choice of organic oxidants, it was possible to characterize and isolate either the one- or the two-electron oxidation products, $(\mathbf{2})^{2+}$ and $(\mathbf{3})^{3+}$, respectively, as mixed $SbCl_6^-/PF_6^-$ salts. For example, spectrophotometric titration of $(CRET^+)(SbCl_6^-)$[29] ($E_{1/2}$= 1.09 V versus Ag/AgCl, top of Figure 3.8) with substoichiometric amounts of (**1**)(PF_6) in CH_2Cl_2 showed the disappearance of the signature bands for the organic oxidant at 486 and 518 nm concomitant with the growth of new bands near 590 and 855 nm for pi-radical transitions of $(\mathbf{2})^{2+}$ [β-HOMO to SOMO]. The reaction was complete after an equimolar ratio of starting materials was achieved verifying the one-electron nature of oxidation of $(\mathbf{1})^+$. The shape and energies of these pi-radical bands are nearly identical to those found in the rhenium(I) or rhodium(III) complexes of this oxidized ligand.[24,25]

Table 3.2. Summary of bond distances versus cation valence in experiment versus in silico. For bond labeling see Figure 3.14

		(**1**)$^{+}$					(**2**)$^{2+}$					(**3**)$^{3+}$			
	Exper.	Calcd.				Exper.	Calcd.				Exper.	Calcd.			
	Avg	**MO6/ LANL2DZ**	**MO6/ DEF2-SVP**	**B3LYP/ LANL2DZ**	**B3LYP/ DEF2-SVP**	Avg	**MO6/ LANL2DZ**	**MO6/ DEF2-SVP**	**B3LYP/ LANL2DZ**	**B3LYP/ DEF2-SVP**	Avg	**MO6/ LANL2DZ**	**MO6/ DEF2-SVP**	**B3LYP / LANL2 DZ**	**B3LYP/ DEF2-SVP**
Ga-N_{Ar}	1.947(3)	1.96	1.966	1.975	1.99	1.994(2)	1.996	2.009	2.011	2.033	2.023(5)	2.027	2.043	2.05	2.07
Ga-N_{pz}	2.102(3)	2.06	2.105	2.084	2.128	2.066(2)	2.038	2.068	2.063	2.101	2.039(5)	2.022	2.049	2.046	2.08
All GaN avg	2.050(3)	2.027	2.059	2.048	2.082	2.042(2)	2.024	2.048	2.046	2.078	2.034(5)	2.024	2.047	2.047	2.077
A	1.402(6)	1.408	1.392	1.419	1.399	1.380(4)	1.402	1.384	1.413	1.392	1.398(7)	1.395	1.374	1.406	1.383
B	1.405(4)	1.418	1.411	1.424	1.417	1.420(4)	1.421	1.414	1.426	1.42	1.413(8)	1.424	1.419	1.43	1.424
C	1.380(4)	1.392	1.385	1.397	1.389	1.369(4)	1.389	1.382	1.395	1.386	1.364(8)	1.386	1.378	1.391	1.383
D	1.394(4)	1.411	1.404	1.418	1.408	1.387(5)	1.412	1.405	1.419	1.409	1.405(9)	1.414	1.407	1.42	1.411
E	1.385(7)	1.396	1.391	1.402	1.395	1.389(4)	1.401	1.395	1.409	1.399	1.404(8)	1.407	1.401	1.412	1.405
F	1.394(4)	1.407	1.4	1.414	1.406	1.381(4)	1.402	1.396	1.405	1.402	1.379(8)	1.395	1.389	1.402	1.395
G	1.403(6)	1.416	1.41	1.421	1.416	1.414(4)	1.422	1.419	1.431	1.422	1.414(8)	1.429	1.427	1.433	1.429
H	1.508(5)	1.506	1.498	1.517	1.51	1.503(4)	1.503	1.494	1.514	1.507	1.504(8)	1.499	1.49	1.509	1.502
I	1.425(4)	1.432	1.424	1.436	1.428	1.414(4)	1.429	1.421	1.433	1.424	1.428(7)	1.426	1.418	1.43	1.421
A’	1.404(6)	1.409	1.393	1.419	1.399	1.387(4)	1.402	1.382	1.413	1.391	1.380(7)	1.394	1.373	1.405	1.384
B’	1.405(4)	1.417	1.411	1.424	1.417	1.411(4)	1.42	1.415	1.426	1.42	1.405(8)	1.424	1.419	1.43	1.424
C’	1.378(4)	1.392	1.385	1.397	1.389	1.381(4)	1.389	1.381	1.395	1.386	1.376(9)	1.386	1.378	1.391	1.383
D’	1.397(4)	1.412	1.403	1.418	1.408	1.387(5)	1.413	1.404	1.419	1.41	1.396(9)	1.414	1.407	1.419	1.411
E’	1.382(5)	1.396	1.391	1.402	1.395	1.394(5)	1.401	1.395	1.409	1.399	1.378(9)	1.402	1.401	1.412	1.405
F’	1.397(7)	1.407	1.4	1.414	1.406	1.381(4)	1.401	1.396	1.405	1.402	1.403(8)	1.395	1.389	1.402	1.395
G’	1.401(6)	1.415	1.41	1.421	1.416	1.418(4)	1.422	1.42	1.431	1.423	1.422(8)	1.429	1.428	1.433	1.43
H’	1.509(4)	1.506	1.498	1.517	1.51	1.497(5)	1.503	1.495	1.514	1.506	1.497(9)	1.499	1.49	1.509	1.502
I’	1.427(4)	1.431	1.424	1.436	1.428	1.416(4)	1.428	1.421	1.433	1.424	1.414(7)	1.426	1.418	1.43	1.421

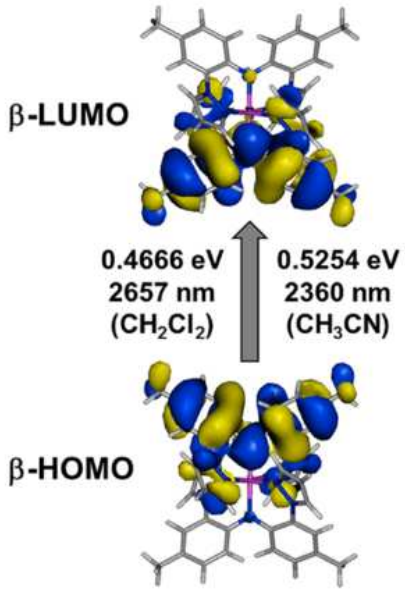

Figure 3.7. β-Frontier orbitals for $(\mathbf{2})^{2+}$ from TD-DFT calculations.

As indicated by the theoretical calculations, an IVCT band was predicted to be found in the NIR spectrum. For a weakly coupled Robin-Day Class II mixed valent species, the IVCT band is expected to have a Gaussian shape, be of weak intensity, and have an energy that is solvent dependent.[1c,3c,30] All of these expectations were met for the IVCT band of (**2**)(PF_6)($SbCl_6$). A representative spectrum for (**2**)(PF_6)($SbCl_6$) dissolved in CH_2Cl_2 is shown in Figure 3.9, while a summary of data obtained from multiple analyses using Gaussian fits of bands in three solvents (CH_2Cl_2, PC = propylene carbonate, CH_3CN) is given in Table 3.3. That is, the NIR spectra obtained for bulk samples of (**2**)(PF_6)($SbCl_6$) dissolved in various solvents revealed the presence of a very broad (full-width-at-half-maximum, $\Delta\tilde{\nu}_{1/2}$, ca. 5000 cm^{-1}), weak-intensity (ε_{max}~ 40−80 $M^{-1}cm^{-1}$) IVCT band in the range of 6390−6925 cm^{-1}(dark band in Figure 3.9).

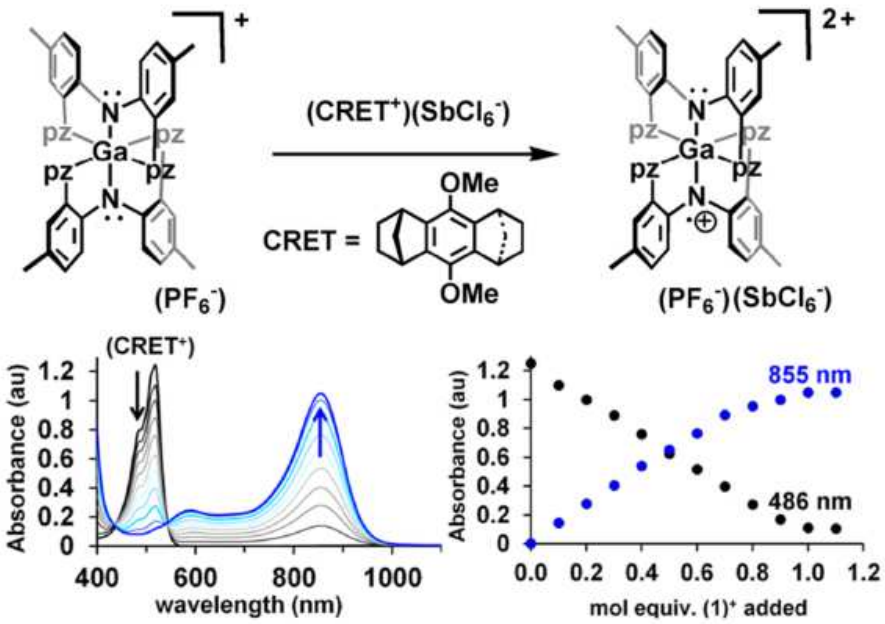

Figure 3.8. Preparation of (**2**)(PF6)(SbCl6) and spectrophotometric titration using organic oxidant $(CRET^{+})(SbCl_6^{-})$.

It is noteworthy that such a band is absent in the NIR spectra of the doubly oxidized derivative $(\mathbf{3})^{3+}$ and of all $(L^{\cdot +})MXYZ$ complexes (M = Re^{I}, Rh^{III})[24,25] that contain only one singly oxidized ligand. It is also worthwhile to note that among the numerous reports on gallium(III) complexes of the type $[Ga(L^{R})(L^{R\cdot})]^{n+}$ where L^{R}= a redox active ligand such as N,N-diazabutadiene = DAB[15] variants, di-tert-butyl semiquinone =DBSQ[18] or dbqdi,[21] an IVCT band has not been observed. Perhaps, the broadness and weak intensity of the IVCT band hinders its identification in these other systems. For (**2**)$(PF_6)(SbCl_6)$, the Gaussian shape of the IVCT band and the indication of a Robin-Day Class II species

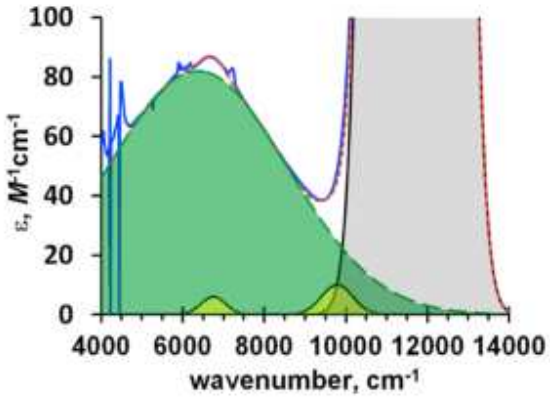

Figure 3.9 NIR spectrum (blue line) of (**2**)(PF_6)($SbCl_6$) in CH_2Cl_2 showing the IVCT band (green), the lowest energy pi-radical band (gray), and unidentified bands (yellow), and the sum of all Gaussianbands used to fit the spectra (red dotted line).

from the analysis of K_{com} suggest that the Hush relations[31](eqs 3 and 4) can be used to estimate the strength of the electronic interaction.

$$E_{OP} = \lambda \qquad (3)$$

$$H_{ab}\ (cm^{-1}) = [(4.2 \times 10^{-4})\varepsilon_{max}\Delta\tilde{\nu}_{1/2}E_{OP}]^{1/2} / d \qquad (4)$$

Here, E_{OP} is the energy of the absorption maximum, λ is the Marcus reorganization energy, H_{ab} is the electronic coupling element, ε_{max} is the molar extinction coefficient, $\Delta\tilde{\nu}_{1/2}$ is the full-width-at-half-maximum, and d is the separation between redox centers in Å. The value d = 3.9735 was used as this represents the distance between amido nitrogen centers obtained by taking into account an average of all crystallographic data for unoxidized, mono-oxidized, and dioxidized species in an effort to minimize potential errors of a single point structural determination. The following three observations further support that (**2**)(PF_6)($SbCl_6$) is a Robin-Day Class II(A) mixed valent species. First, from

the Gaussian fits of the IVCT band, the experimental $\Delta\tilde{\nu}_{1/2}$ was larger than the theoretical value $\Delta\tilde{\nu}_{1/2}$ (HTL) = $[16 \ln(2) k_B T \lambda]^{1/2}$.[3c,30] Second, as predicted by dielectric continuum theory, the energy of the IVCT band showed a linear correlation with the solventparameter,[32] $\gamma = 1/\varepsilon_s - 1/n^2$ where ε_s is the static dielectric constant and n is the refractive index of the solvent (Figure 3.10). Third, the values of H_{ab}(ca. 200cm^{-1}) and λ (6390−6925) cm^{-1} fall within the accepted limits of $0 < H_{ab} < \lambda/2$ or $0 < 2H_{ab}/\lambda < (1 - [\Delta\tilde{\nu}Z_{1/2}(\text{HTL})]/2\lambda)$ for Class II or Class IIA species, respectively.[30] The thermal energy barrier to electron transfer, ΔG^*, calculated from classical Marcus Theory[33] (eq 5) is 1344−1515 cm^{-1}. The corresponding rate constant for electron transfer k_{et} is found to be on the order of $(0.76-2.9) \times 10^{10}$ s^{-1} from eq 6, where Planck's constant, h = 3.336 × 10^{-11} cm$^{-1}\cdot$s, and the gas constant R = 0.695 cm^{-1}K^{-1}.

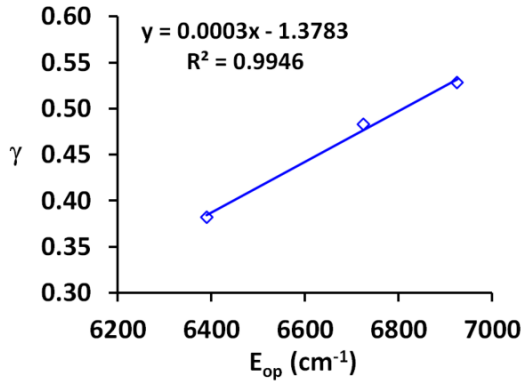

γ: CH_2Cl_2 = 0.382; PC = 0.483; CH3CN = 0.582

Figure 3.10. Solvent dependence of IVCT band

Table 3.3. Summary of IVCT Band Shape Fitting and ET Parameters of (**2**)$(PF_6)(SbCl_6)$ in Three Different Solvents

	CH_2Cl_2	PC	CH_3CN
E_{OP} = λ (cm^{-1})	6390 (±20)	6725 (±25)	6925 (±25)
ε_{max}($M^{-1}cm^{-1}$)	79 (±3)	44 (±3)	55 (±5)
$\Delta\tilde{\nu}Z_{1/2}$(cm^{-1})	5192 (±17)	4900 (±100)	4900 (±300)
oscillator strength[a] ,f_{obs} (f_{calc})	1.9 x 10^{-3} (603 x 10^{-3})	9.9 x 10^{-4} (n.d.)	1.2 x 10^{-3} (5.3 x 10^{-3})
H_{ab}(cm^{-1}), see eq 4	264	196	223
$\Delta\tilde{\nu}Z_{1/2}$(HTL)[b]	3812	3910	3968
θ = $\Delta\tilde{\nu}_{1/2}/\Delta\tilde{\nu}Z_{1/2}$ (HTL)	1.36	1.25	1.23
α = H_{ab}/λ	0.0413	0.0291	0.0322
ΔG^* (cm^{-1}), see eq 5	1344	1491	1515
k_{et}(s^{-1}), see eq 6	2.9 x 10^{10}	7.6 x 10^9	8.6 x 10^9
γ = $1/\varepsilon_s - 1/n^2$	0.382	0.480	0.582

[a]f_{obs} = $(4.6 \times 10^{-9})\varepsilon max\Delta\tilde{\nu}Z_{1/2}$, f_{calc} from DFT calculations. [b]$\Delta\tilde{\nu}Z_{1/2}$(HTL) = [16 ln(2)k_BTλ]$^{1/2}$ where k_B= 0.695 $cm^{-1}K^{-1}$and T = 295 K.

$$\Delta G^* = (\lambda - 2H_{ab})2 / 4\lambda \text{ cm}^{-1} \quad (5)$$

$$k_{et} = (2H_{ab}^2 / h)[\pi^3 / \lambda RT]^{1/2} \exp-(\Delta G^*/RT) \quad (6)$$

These k_{et} values are comparable to those organic cation radicals with diarylamido groups linked by unsaturated 12- to 16-atom (phenylethynyl-) spacers but are of approximately 1−2 orders of magnitude smaller than found for shorter conjugated spacers such as in Figure 3.1A and their related N,N′-diphenyl-1,4-phenylenediamine cation radical counterparts.[34]

Figure 3.11 shows that the titration of $(OMN^{+})(SbCl_6^{-})$[35] ($E_{1/2}$ = 1.39 V versus Ag/AgCl) was complete after 1/2 equiv of gallium complex was added to the oxidant verifying the two electron nature of oxidation. In (**3**)$(PF_6)(SbCl_6)_2$, the pi-radical bands persisted in the electronic spectrum indicating a diradical species. The effective magnetic moment of the isolated powder, μ_{eff}= 2.4 μB (295 K), was lower than the expected spin-only value of 2.83 μB, which suggests that the triplet state is probably not wholly thermally populated. Although we do not have access to a magnetometer capable of variable (low) temperature magnetic measurements that would permit elucidation of the ground state properties, the theoretical calculations of $(\mathbf{3})^{3+}$ suggest that the singlet diradical lies 21.7 cm^{-1} lower than the triplet. This value is on par with the 23cm^{-1} singlet−triplet energy difference in a tin(IV) complex of the aforementioned ONO-pincer radical ion, $Sn^{IV}(dbqdi)_2$,[21] for the 64.6 cm^{-1} difference in Zn(tmeda)(3,6-DBSQ)(3,6-DBCat).[18b] The presence of a 'half-field' signal for a ΔM_s= 2 transition in the EPR spectra of solid (**3**)$(PF_6)(SbCl_6)_2$ acquired at 5 K in both normal and parallel-modes (Figure 3.12) verified that the triplet state is thermally populated even at this low temperature. It is noted that the EPR spectrum of an isolated sample of (**2**)$(PF_6)(SbCl_6)$ only showed an isotropic signal at g = 2.006, a g-value expected for a ligand-based radical (Figure 3.13).

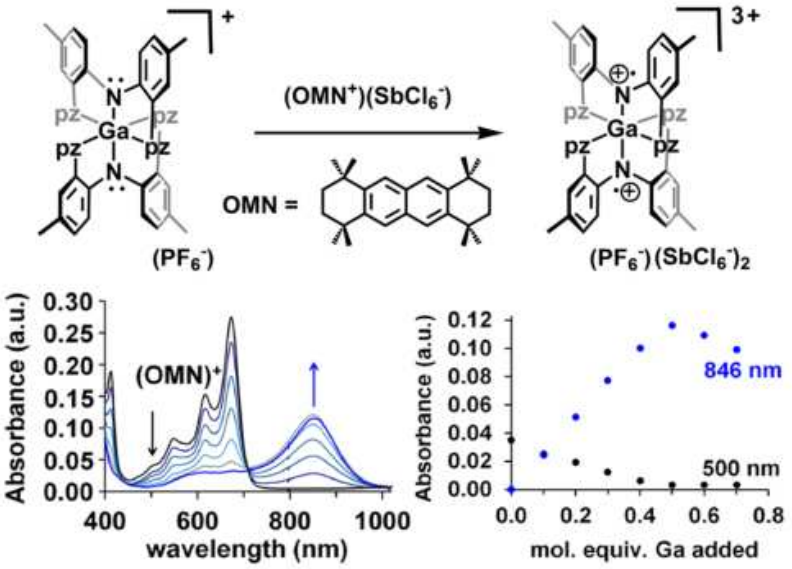

Figure 3.11. Spectrophotometric titration of (**3**)$(PF_6)(SbCl_6)_2$ and the organic oxidant $(OMN^+)(SbCl_6^-)$.

It was possible to obtain X-ray quality, blue single crystals of the dioxidized complex (**3**)$(PF_6)_2(SbCl_6)\cdot 2.33CH_2Cl_2\cdot$toluene after mixing (**1**)(PF_6) with 2 equiv of $(NO)(SbCl_6)$ in CH_2Cl_2, layering with toluene, and allowing solvents to diffuse (Crystallographic data is found in Table 3.7). Obviously, solubility issues dictated the unexpected ratio of P- versus Sb-centered anions. After numerous attempts, X- ray quality violet crystals of "$[Ga(L)_2](PF_6)1.5\cdot 1.05$ toluene$\cdot 0.65CH_2Cl_2\cdot 0.17H_2O$" were obtained from an equimolar mixture of (**1**)(PF_6) with (CRET)$(SbCl_6)$ in CH_2Cl_2 layered with toluene, as above. After careful scrutiny of the various bond distances (vide infra), this latter structure is best described as the solvate of $[Ga(L^-)_2](PF_6)/[Ga(L^-)(L^0)](PF_6)_2$ (Table 3.6). An overlay of cation structures of $(\mathbf{1})^+$, $(\mathbf{2})^{2+}$, $(\mathbf{3})^{3+}$ and an intraligand bond labeling diagram are found in Figure 3.14.

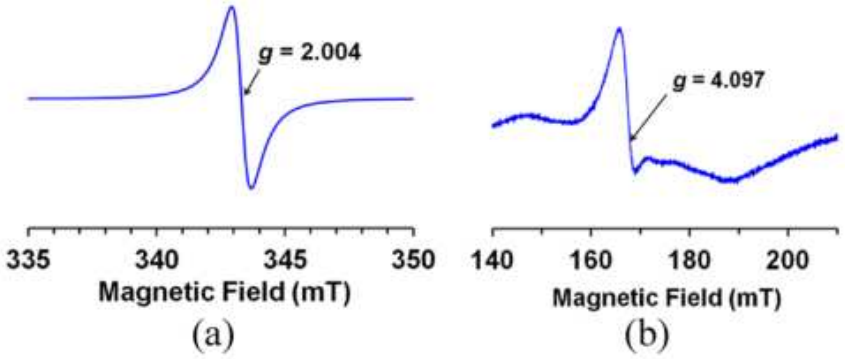

Figure 3.12. (a) X-band (9.63 GHz, 295 K) EPR spectrum of a powder sample of (**3**)$(PF_6)(SbCl_6)_2$, (b) 'half-field' spectrum acquired at 5 K (100 mW) in parallel-mode.

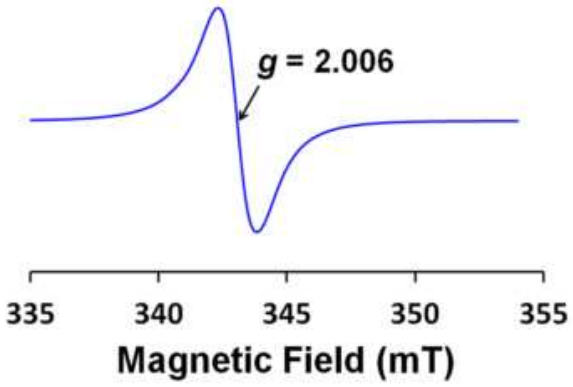

Figure 3.13. X-band (9.63 GHz) EPR spectrum of $[Ga^{III}(L^{-})(L^{0})](PF_6)(SbCl_6)$ at 20K in CH_3CN:toluene glass

Complete structural data are found in the crystallography section. As suggested by calculations, the most significant structural changes along the valence series involved the Ga−N bond distances, which serve as oxidation number markers for the ligand. The average gallium-amido nitrogen Ga−N_{Ar} bond distance increased linearly from 1.947(3) Å in $[Ga^{III}(L^{-})_2]^{+}$ to 2.023(5) Å in $[Ga^{III}(L^{0})_2]^{3+}$ (0.074 Å change), while the average

Ga−N_{pz} distance (dative bonds from the pyrazolyls) decreased from 2.102(3) Å in $[Ga^{III}(L^{-})_2]^+$ to 2.039(5) Å in $[Ga^{III}(L_0)_2]^{3+}$(0.063 Å change). As described earlier, each of these distances fall within ranges reported for other gallium(III)diphenylamido[26] or pyrazolyl[27] complexes. The bond length changes within the ligand backbone are much less pronounced, and are at the borderline of statistical significance. The most significant change occurs for bond-type G (right of Figure 13) between ipso- carbons which on average increases from 1.402(7) Å in $[Ga^{III}(L^{-})_2]^+$to 1.418(8) Å in $[Ga^{III}(L^{0})_2]^{3+}$ (0.016 Å change). Such a change would imply a bonding interaction between these atoms in $(\mathbf{1})^+$, an interaction that is supported by computational studies.

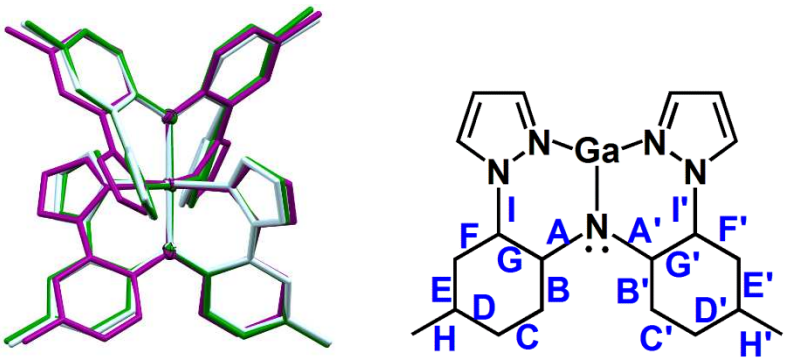

Figure 3.14. Left: Overlay of cation structures from X-ray diffraction. Key: pale blue, $(\mathbf{1})^+$; green, $(\mathbf{2})^{2+}$; purple, $(\mathbf{3})^{3+}$; right: Labeling diagram for bonds within the ligand.

3.4 CONCLUSION

The homoleptic complex $[Ga(L^{\bullet-})_2](PF_6)$ and its mono- and dioxidized derivatives have been prepared and characterized in solution and in the solid state. The triplet state of the dioxidized species was found to be thermally populated even at 5 K. For the paramagnetic, mono-oxidized species (**2**)$(PF_6)(SbCl_6)$, electrochemical and spectroscopic data established that weak electronic communication occurs between electroactive ligands across the gallium(III) bridge. The electronic communication across the diamagnetic metal ion bridge may occur either by direct tunneling,[33,36] by nonresonant charge transfer using the empty, high-energy 4p orbitals on gallium as a coupling medium (McConnell superexchange[37]), or by a thermally activated "hopping" mechanism.[38] Given the previous magnetic studies of diamagnetic metal complexes of organic diradicals that can promote either ferromagnetic or antiferromagnetic interactions with *J* values of different magnitude depending on the metal,[18b] the superexchange mechanism seems to be the most probable pathway for electronic communication. Clearly further experimental and theoretical investigations of other $[M(L)_2]^{n+}$ complexes of redox silent d^{10} or d^0 metal ions and their oxidized counterparts would be needed to elucidate the mechanism. Nevertheless, if oligomeric assemblies of the type LM-[(L-L)M(L-L)]$_n$-ML (n = 0, 1, 2...) can be prepared then wire-like behavior is anticipated even for diamagnetic bridging ions. Stronger electronic communication is expected for transition metal analogues with available d-orbitals that can engage in dπ−pπ interactions with the ligand. Details regarding such monomeric main group and transition metal complexes and their oligomeric assemblies will be reported in due course.

3.5 EXPERIMENTAL

General Considerations.

The compounds Li(n-Bu) 1.6 M in hexanes, GaI_3, $TlPF_6$, $(NO)(SbCl_6)$ were purchased commercially and used as received. The compounds H(L),[24] $(CRET^+)(SbCl_6^-)$,[29] $(OMN^+)(SbCl_6^-)$[35] were prepared according to literature procedures. Solvents were dried by conventional means and distilled under nitrogen prior to use.

Physical Measurements.

Midwest MicroLab, LLC, Indianapolis, Indiana 45250, performed all elemental analyses. Melting point determinations were made on samples contained in glass capillaries using an Electrothermal 9100 apparatus and are uncorrected. ^1H,^{13}C, ^{19}F, and ^{31}P NMR spectra were recorded on a Varian 400 MHz spectrometer. Chemical shifts were referenced to solvent resonances at δ_H 5.33, δ_C 53.84 for CD_2Cl_2 or δ_H1.94, δ_C118.9 for CD_3CN and δ_H 2.05, δ_C 29.84 for acetone-d_6, while those for ^{19}F and ^{31}P NMR spectra were referenced against external standards of $CFCl_3$(δ_F 0.00 ppm) and 85% H_3PO_4(aq) (δ_P 0.00 ppm), respectively. Abbreviations for NMR and UV−vis br (broad), sh (shoulder), m (multiplet), ps (pseudo-), s (singlet), d (doublet), t (triplet), q (quartet), p (pentet), sept (septet). Electrochemical measurements were collected under a nitrogen atmosphere for samples as 0.1 mM solutions in CH_3CN and in CH_2Cl_2, each with 0.1 M NBu_4PF_6as the supporting electrolyte. A three-electrode cell comprised of an Ag/AgCl electrode (separated from the reaction medium with a semipermeable polymer membrane filter), a platinum working electrode, and a glassy carbon counter electrode were used for

the voltammetric measurements. Data were collected at scan rates of 50, 100, 200, 300, 400, and 500 mV/s. With this set up, the ferrocene/ferrocenium couple had an $E_{1/2}$ value of +0.53 V in CH_3CN and +0.41 V in CH_2Cl_2 at a scan rate of 200 mV/s, consistent with the literature values.[39] Solid state magnetic susceptibility measurements were performed using a Johnson-Matthey MSB-MK1 instrument. Electronic absorption (UV−vis/NIR) measurements were made on a Cary 5000 instrument. Emission spectra were recorded on a JASCO FP-6500 spectrofluorometer. EPR spectra were obtained on both solid powder samples and as solutions ~0.2 mM in 1:1 CH_2Cl_2/toluene mixtures using a Bruker ELEXYS E600 equipped with an ER4116DM cavity resonating at 9.63 GHz, an Oxford instruments ITC503 temperature controller and a ESR-900 helium flow cryostat. The spectra were recorded using 100 kHz field modulation unless otherwise specified.

Syntheses.

[Ga(L)2](I), (**1**)(I).

A 3.45 mL aliquot of 1.6 M Li(n-Bu) in hexanes (5.52 mmol) was slowly added via syringe to a solution of 1.814 g (5.51 mmol) of H(L) in 15 mL of THF maintained at −78 °C. The resulting bright yellow solution was stirred 15 min, and then a solution of 1.241 g (2.76 mmol) of GaI_3 in 5 mL of THF was added by cannula transfer under nitrogen. The mixture was maintained at −78 °C for 2 h, and then the cold bath was removed and the mixture was allowed to warm naturally with stirring 12 h. The colorless precipitate (which exhibited bright blue luminescence upon irradiation with 354 nm light) was collected by vacuum filtration and was further dried under a vacuum 4 h to leave 2.026 g (86%) of (**1**)(I) as a colorless powder. Anal. Calcd (obs.) for $C_{40}H_{36}N_{10}GaI$: C, 56.30

(56.22); H, 4.25 (4.27); N, 16.41 (16.19). ^{1}H NMR (acetone-d6) δ_H: 8.40 (d, *J* = 2.6 Hz, 1H, H5-pz), 7.28 (s, 1H, H3−Ar), 7.22 (part of AB, 1H, Ar), 7.21 (d, *J* = 2.5 Hz, 1H, H3pz), 7.09 (part of AB, 1H, Ar), 6.39 (ps t, J_{app}= 2.5 Hz, 1H, H4pz), 2.25 (s, 3H, CH3). ^{13}C NMR (acetone-d_6) δ_C: 143.8, 140.3. 132.9, 130.9, 130.7, 130.2, 127.2, 123.5, 108.3, 20.3. UV−vis (CH_2C_{l2}): nm (ε, $M^{-1}cm^{-1}$) 249 (57,800), 267sh (32,300), 322 (24,700), 365 (19,300). Very fine needle crystals were grown by layering a CH_2Cl_2 solution with hexanes and then allowing solvents to slowly diffuse. A sample that was exposed to the atmosphere for a few hours analyzed as (**1**)(I)·H_2O. Anal. Calcd (obs.) for $C_{40}H_{38}IGaN_{10}O$: C, 55.13 (55.62); H, 4.40 (4.27); N, 16.07 (15.56).

[Ga(L)$_2$](PF$_6$), (**1**)(PF_6).

A 0.618 g (1.77 mmol) sample of $TlPF_6$ was added as a solid to a solution of 1.510 g (1.77 mmol) (**1**)(I) in 20 mL of dichloromethane. After the mixture had been stirred magnetically 1h, the colorless solution was separated from the pale yellow precipitate of TlI by filtration through a pad of Celite. The CH_2Cl_2 was removed under vacuum to give 1.52 g (99%) (**1**)(PF_6) as a pale yellow powder. Mp: 280 °C dec Anal. Calcd (obs.) for $C_{40}H_{36}N_{10}F_6GaP$: C, 54.97 (55.37); H, 4.15 (4.25); N, 16.03 (15.82). ^{1}H NMR (acetone-d6) δ_H: 8.34 (d, *J* = 2.6 Hz, 1H, H5-pz), 7.25 (s, 1H, H3−Ar), 7.22 (part of AB, 1H, Ar), 7.21 (d, *J* = 2.4 Hz, 1H, H3pz), 7.09 (part of AB, 1H, Ar), 6.39 (ps t, J_{app}= 2.5 Hz, 1H, H4pz), 2.24 (s, 3H, CH3). ^{13}C NMR (acetone-d6) δ_C: 143.8, 140.3, 132.8, 130.9, 130.7, 130.2, 127.3, 123.4, 108.4, 20.3. ^{19}F NMR (acetone-d6): δ_F:−72.6 (d, J_{FP} = 707 Hz). ^{31}P NMR (acetone-d6): δ_P:−144.3 (sept, J_{P-F} = 707 Hz) ppm. UV−vis (CH2Cl2): nm (ε, $M^{-1}cm^{-1}$) 251 (47,500), 269 sh (29,500), 323 (25,500), 366 (19,800). Single crystals of

(**1**)(PF_6)· 1.75CH_2Cl_2 used for X-ray diffraction were grown by layering a dichloromethane solution with hexanes and allowing solvents to slowly diffuse overnight.

Oxidation Reactions.

[Ga(L)$_2$](PF$_6$)(SbCl$_6$), (**2**)(PF_6)($SbCl_6$).

A colorless solution of 0.1055 g (0.121 mmol) of (**1**)(PF_6) in 10 mL of CH_2Cl_2 was added to a red solution of 0.0732 g (0.121 mmol) of (CRET)($SbCl_6$) in 25 mL of CH_2Cl_2. The flask originally containing (**1**)(PF_6) was washed with another 10 mL of CH_2Cl_2 to ensure quantitative transfer to the reaction mixture. After the resulting royal blue solution had been stirred 15 min, solvent was removed under a vacuum. The resulting blue residue was washed with three 10 mL portions of hexanes to remove the organic byproduct and then was dried under a vacuum for several hours to leave 0.132 g (90%) of (**2**)(PF_6)($SbCl_6$) as a blue powder. μ_{eff}(solid, 295 K): 1.8 ± 0.1 μB. UV−vis (CH_2Cl_2): nm (ε, $M^{-1}cm^{-1}$) 250 (59,200), 321 (25,600), 362 (21,600), 596 (1,100), 857 (5,500), 1490 (90). Violet needle crystals of [Ga(L)$_2$](PF_6)$_{1.5}$· 1.05 toluene· 0.65CH_2Cl_2· 0.17H_2O were grown by layering an equimolar mixture of (**1**)(PF_6) and (CRET)($SbCl_6$) in CH_2Cl_2 with toluene and allowing solvents to diffuse in a −20 °C freezer.

[Ga(L)$_2$](PF$_6$)(SbCl$_6$)$_2$, (**3**)(PF_6)($SbCl_6$)$_2$.

A colorless solution of 0.1382 g (0.159 mmol) of (**1**)(PF_6) in 20 mL of CH_2Cl_2 was added to a colorless solution of 0.1156 g (0.317 mmol) of (NO)($SbCl_6$) in 30 mL of CH_2Cl_2. After the resulting royal blue solution had been stirred 15 min, solvent was removed under a vacuum and the blue residue was dried under a vacuum to leave 0.213 g (87%) of

(**3**)$(PF_6)(SbCl_6)_2$ as a blue powder. $\mu_{eff\ (}$solid, 295 K): 2.4 ± 0.1 μB. UV−vis (CH_2Cl_2): nm (ε, $M^{-1}cm^{-1}$) 605 (1,300), 849 (6,200). Blue crystals of (**3**)$(PF_6)_2(SbCl_6)\cdot 2.33CH_2Cl_2\cdot$toluene were obtained from by mixing 15 mg (17 μmol) of (**1**)(PF6), 13 mg (34μmol) of (NO)$(SbCl_6)$ in 5 mL of CH_2Cl_2, layering with 15 mL of toluene, and allowing solvents to diffuse.

3.6 COMPUTATIONAL STUDIES

DFT calculations were performed with the M06 meta-hybrid GGA functional[40] using the def2-SV(P) double-ζ basis set.[41] Solvent (DCM) effects were accounted for by using the polarizable continuum model IEFPCM,[42]as implemented in Gaussian 09.[43] The chosen model proved superior over other combinations of functionals (M06 or B3LYP44) and basis sets (def2-SV(P) or 6311-G*/LANL2DZ45) for reproducing bond distances and spectroscopic data, as summarized in the Table 3.2, 3.8, 3.9, 3.10. Gas phase structures of the metal complexes were optimized using the initial geometry from X-ray structural studies. Analytical vibrational frequency calculations were also carried out to verify that the optimized geometries were stationary points. Time-dependent DFT methodology was used for excitation energy calculations.[46]

1.7 CRSTALLOGRAPHY

X-ray intensity data from a colorless prism of (**1**)$(PF_6)\cdot 1.75CH_2Cl_2$ and a dark blue plate of (**3**)$(PF_6)_2(SbCl_6)\cdot 2.33CH_2Cl_2\cdot$toluene were collected at 100(2) K with a Bruker AXS 3-circle diffractometer equipped with a SMART2[47] CCD detector (Cu Kα radiation, λ = 1.54178 Å). X-ray intensity data from a violet needle of (**2**)$(PF_6)1.5\cdot 1.05$

toluene·0.65CH_2Cl_2·0.17H_2O, were collected at 100(2) K with an Oxford Diffraction Ltd. Supernova equipped with a 135 mm Atlas CCD detector, by using Cu Kα radiation, λ = 1.54178 Å. Raw data frame integration and Lp corrections were performed with AINT+[47]for the data collected from the Bruker instrument but with CrysAlisPro[48] for that from the Oxford instrument. Final unit cell parameters were determined by least-squares refinement of 9343 reflections from the data set of (**1**)(PF_6)·1.75CH_2Cl_2, 19744 reflections from the data set of (**2**)(PF_6)1.5·1.05·toluene·0.65CH_2Cl_2·0.17H_2O, and 5460 reflections from data set of (**3**)(PF_6)$_2$($SbCl_6$)·2.33CH_2Cl_2·toluene, with I > 2σ(I) for all cases. Analysis of the data showed negligible crystal decay during collection in each case. Direct methods structure solutions, difference Fourier calculations and full-matrix least-squares refinements against F2were performed with SHELXTL.[49] Numerical absorption corrections based on the real shapes of the crystals for (**1**)(PF_6)·1.75CH_2Cl_2, and (**3**)(PF_6)$_2$($SbCl_6$)·2.33CH_2Cl_2·toluene were applied using SADABS,[47]while an empirical absorption correction using spherical harmonics implemented in the SCALE3 ABSPACK scaling algorithm was used for (**2**)(PF_6)1.5·1.05·toluene·0.65CH_2Cl_2·0.17H_2O. The carbon atoms of the highly disordered solvent molecules in each structure were refined with isotropic displacement parameters. The remaining non-hydrogen atoms were refined with anisotropic displacement parameters. Hydrogen atoms were placed in geometrically idealized positions and included as riding atoms. The X-ray crystallographic parameters and further details of data collection and structure refinements are presented in Table 3.4. The crystallographic data for other complexes are given in Table 3.5-7.

Table 3.4. Crystallographic data collection and structure refinement for (**1**)$(PF_6)\cdot 1.75CH_2Cl_2$, (**2**)$(PF_6)1.5\cdot 1.05$ toluene$\cdot 0.65CH_2Cl_2\cdot 0.17H_2O$, and (**3**)$(PF_6)_2(SbCl_6)\cdot 2.33CH_2Cl_2\cdot$toluene

Compound	**(1)(PF_6)**$\cdot 1.75CH_2Cl_2$	**(2)$(PF_6)_{1.5}$**$\cdot 1.05$ toluene$\cdot 0.65CH_2Cl_2\cdot 0.17H_2O$	**(3)$(PF_6)_2(SbCl_6)$**$\cdot 2.33CH_2Cl_2\cdot$toluene
Formula	$C_{41.75}H_{39.50}Cl_{3.50}F_6GaN_{10}$	$C_{47.99}H_{45.68}Cl_{1.3}F_9GaN_{10}O_{0.17}P_{1.5}$	$C_{49.33}H_{48.66}Cl_{10.66}F_{12}GaN_{10}P_2Sb$
Formula weight	1020.1	1098.43	1640.8
Crystal system	triclinic	monoclinic	orthorhombic
Space group	P -1	P 2_1/c	Pbca
Temp. [K]	100(2)	100(2)	100(2)
a [Å]	12.9440(3)	17.6021(3)	17.5543(5)
b [Å]	17.4584(4)	24.6732(3)	24.9500(6)
c [Å]	20.9702(5)	23.2482(4)	29.1682(8)
a [°]	73.149(2)	90	90
b [°]	85.8230(10)	108.0987(18)	90
g [°]	79.4170(10)	90	90
V [Å^3]	4457.29(18)	9597.2(3)	12775.1(6)
Z	4	8	8
D_{calcd}. [gcm^{-3}]	1.52	1.52	1.706
l [Å] (Mo or Cu Ka)	1.54178	1.54178	1.54178
μ.[mm^{-1}]	3.716	2.644	9.151
Abs. Correction	numerical	numerical	numerical
F(000)	2078	4492	6526
θ range [°]	3.47 to 67.37	3.30 to 71.02	3.03 to 68.05
Reflections collected	37225	53008	107137
Independent reflections	14703 (R_{int} 0.0203)	18009 (R_{int} 0.0384)	11388 (R_{int} 0.0813)
T_min/max	0.4226 / 0.6243	0.68/0.963	0.2619/0.7110
Data/restraints/ parameters	14703/63/1231	18009 /48/1285	11388/15/790
Goodness-of-fit on F^2	0.982	0.914	1.062
$R1/wR2[I>2\sigma(I)]$[a]	0.0484/0.1257	0.0433/0.1067	0.0646/0.1433
$R1/wR2$ (all data)[a]	0.0536/0.1294	0.0731/0.1163	0.0853/0.1528
Largest diff. peak/hole / e Å^{-3}	1.763/-0.730	0.84/-0.57	1.79/-1.28

[a] $R1 = \Sigma||F_o| - |F_c||/\Sigma|F_o|$ $wR^2 = [\Sigma w(|F_o| - |F_c|)^2/\Sigma w|F_o|^2]^{1/2}$.

Table 3.5. Selected Bond Distances in $[Ga(L)_2](PF_6)\cdot 1.5CH_2Cl_2$, **1**$\cdot(PF_6)\cdot 1.5CH_2Cl_2$

Bond label[a]	Atom label (x-ray)l	Distance (Å)	Bond label	Atom label (x-ray)l	Distance (Å)
Cation A			Cation B		
Ga-N_{Ar}	Ga1-N1	1.947(2)	Ga- N_{Ar}	Ga2-N1A	1.954(3)
	Ga1-N41	1.953(2)		Ga2-N41A	1.941(3)
Ga-N_{pz}	Ga1-N11	2.099(2)	Ga-N_{pz}	Ga2-N11A	2.081(2)
	Ga1-N21	2.094(2)		Ga2-N21A	2.118(3)
	Ga1-N51	2.101(2)		Ga2-N51Aa	2.141(3)
	Ga1-N61	2.085(2)		Ga2-N61A	2.088(2)
A	N1-C1	1.406(4)	A''	N1A-C1A	1.396(4)
B	C1-C6	1.403(4)	B''	C1A-C6A	1.409(4)
C	C6-C5	1.379(4)	C''	C6A-C5A	1.379(5)
D	C5-C4	1.394(5)	D''	C5A-C4A	1.393(5)
E	C4-C3	1.380(5)	E''	C4A-C3A	1.392(4)
F	C3-C2	1.393(4)	F''	C3A-C2A	1.394(4)
G	C2-C1	1.402(4)	G''	C2A-C1A	1.409(4)
H	C4-C7	1.513(5)	H''	C4A-C7A	1.505(4)
I	C2-N12	1.427(4)	I''	C2A-N12A	1.426(4)
A'	N1-C31	1.400(4)	A'''	N1A-C31A	1.412(4)
B'	C31-C36	1.409(4)	B'''	C31A-C36A	1.405(5)
C'	C36-C35	1.378(5)	C'''	C36A-C35A	1.375(5)
D'	C35-C34	1.393(5)	D'''	C35A-C34A	1.398(5)
E'	C34-C33	1.385(4)	E'''	C34A-C33A	1.386(5)
F'	C33-C32	1.389(4)	F'''	C33A-C32A	1.404(5)
G'	C32-C31	1.402(4)	G'''	C32A-C31A	1.395(5)
H'	C34-C37	1.510(5)	H'''	C34A-C37A	1.511(5)
I'	C32-N22	1.429(4)	I'''	C32A-N22A	1.428(4)
For bond labeling see Figure 3.14					

Table 3.6. Selected Bond Distances in $[Ga(L)_2](PF_6)\cdot[Ga(L^-)(L^0)](PF_6)_2\ 1.5CH_2Cl_2$, $\mathbf{1\cdot 2}\cdot(PF_6)_3\cdot 1.5CH_2Cl_2$

Bond label[a]	Atom label (x-ray)l	Distance (Å)	Bond label	Atom label (x-ray)l	Distance (Å)
Cation A			Cation B		
Ga-N_{Ar}	Ga1-N1	1.941(2)	Ga-N_{Ar}	Ga2-N1A	2.062(2)
	Ga1-N41	1.947(2)		Ga2-N41A	1.926(2)
Ga-N_{pz}	Ga1-N11	2.098(2)	Ga-N_{pz}	Ga2-N11A	2.066(2)
	Ga1-N21	2.126(2)		Ga2-N21A	2.077(2)
	Ga1-N51	2.093(2)		Ga2-N51Aa	2.054(2)
	Ga1-N61	2.105(2)		Ga2-N61A	2.067(2)
A	N1-C1	1.405(3)	A''	N1A-C1A	1.380(4)
B	C1-C6	1.402(4)	B''	C1A-C6A	1.420(4)
C	C6-C5	1.381(4)	C''	C6A-C5A	1.369(4)
D	C5-C4	1.394(4)	D''	C5A-C4A	1.387(5)
E	C4-C3	1.384(4)	E''	C4A-C3A	1.389(4)
F	C3-C2	1.396(4)	F''	C3A-C2A	1.381(4)
G	C2-C1	1.398(4)	G''	C2A-C1A	1.414(4)
H	C4-C7	1.506(4)	H''	C4A-C7A	1.503(4)
I	C2-N12	1.421(4)	I''	C2A-N12A	1.414(4)
A'	N1-C31	1.400(3)	A'''	N1A-C31A	1.387(4)
B'	C31-C36	1.401(4)	B'''	C31A-C36A	1.411(4)
C'	C36-C35	1.380(4)	C'''	C36A-C35A	1.381(4)
D'	C35-C34	1.400(4)	D'''	C35A-C34A	1.387(5)
E'	C34-C33	1.376(4)	E'''	C34A-C33A	1.394(5)
F'	C33-C32	1.398(4)	F'''	C33A-C32A	1.381(4)
G'	C32-C31	1.405(4)	G'''	C32A-C31A	1.418(4)
H'	C34-C37	1.505(4)	H'''	C34A-C37A	1.497(5)
I'	C32-N22	1.423(4)	I'''	C32A-N22A	1.416(4)

[a]For bond labeling see Figure 3.14

Table 3.7. Selected Bond Distances in $[Ga(L^0)_2](PF_6)_2(SbCl_6)$ $2.33CH_2Cl_2 \cdot C_7H_8$, **3**$\cdot(PF_6)_2(SbCl_6)$ $2.33CH_2Cl_2 \cdot C_7H_8$

Experimental				Summary Experimental		
$Ga\text{-}N_{Ar}$	Ga1-N1	2.032(5)		Non-ox	mono	Di
	Ga1-N41	2.013(5)		Avg	Avg	Avg
$Ga\text{-}N_{pz}$	Ga1-N11	2.043(5)	$Ga\text{-}N_{Ar}$	1.947(3)	1.994(2)	2.023(5)
	Ga1-N21	2.034(5)	$Ga\text{-}N_{pz}$	2.102(3)	2.066(2)	2.039(5)
	Ga1-N51	2.038(5)				
	Ga1-N61	2.040(5)	avg			
A	N1-C1	1.398(7)	A	1.403(4)	1.384(4)	1.402(8)
B	C1-C6	1.413(8)	B	1.405(4)	1.416(4)	1.409(8)
C	C6-C5	1.364(8)	C	1.379(5)	1.375(4)	1.370(9)
D	C5-C4	1.405(9)	D	1.396(5)	1.387(5)	1.401(9)
E	C4-C3	1.404(8)	E	1.384(5)	1.392(5)	1.391(9)
F	C3-C2	1.379(8)	F	1.396(5)	1.381(4)	1.391(8)
G	C2-C1	1.414(8)	G	1.402(7)	1.416(4)	1.418(8)
H	C4-C7	1.504(8)	H	1.508(5)	1.500(4)	1.501(9)
I	C2-N12	1.428(7)	I	1.426(5)	1.415(4)	1.421(7)
A’	N1-C31	1.380(7)				
B’	C31-C36	1.405(8)				
C’	C36-C35	1.376(9)				
D’	C35-C34	1.396(9)				
E’	C34-C33	1.378(9)				
F’	C33-C32	1.403(8)				
G’	C32-C31	1.422(8)				
H’	C34-C37	1.497(9)				
I’	C32-N22	1.414(7)				

[a] For bond labeling see Figure 3.14

Table 3.8. TDDFT/TDA Excitation Energies and Transitions of $[Ga(L^-)_2]^+$, $(\mathbf{1})^+$

Excited State	Total Energy (hartrees)	Excitation energy (eV)	Oscillator Strength	Origin	Amplitude	Transition moment X	Y	Z	Strength (AU)
1	-4014.727923	3.4043	0.1243	D(187)→V(190)	-0.25	1.1442	-0.1287	0.4061	1.4907
				D(188)→V(189)	0.6541				
2	-4014.72655	3.4416	0.3522	D(187)→V(190)	0.57212	0.0279	2.0269	0.2595	4.1766
				D(188)→V(189)	-0.40127				
3	-4014.719104	3.6442	0.001	D(187)→V(189)	0.40231	0.004	-0.1045	-0.005	0.011
				D(188)→V(190)	0.56601				
4	-4014.717693	3.6826	0.0226	D(187)→V(190)	0.64415	-0.4737	0.0144	-0.162	0.2507
				D(188)→V(189)	0.24824				
				D(188)→V(193)	-0.10938				
5	-4014.716175	3.7239	0.0001	D(187)→V(192)	0.14415	-0.0123	-0.0118	0.0168	0.0006
				D(188)→V(191)	0.68431				
6	-4014.713235	3.8039	0.1274	D(187)→V(191)	0.67053	0.402	0.1087	-1.093	1.3672
				D(188)→V(192)	0.19065				
7	-4014.704445	4.0431	0.0011	D(187)→V(194)	0.41889	0.0785	0.0092	0.0707	0.0112
				D(188)→V(193)	0.53691				
8	-4014.70389	4.0582	0.2798	D(187)→V(193)	0.47136	-0.0118	1.6656	0.1993	2.8141
				D(188)→V(194)	0.49495				
9	-4014.70314	4.0786	0.0214	D(187)→V(191)	0.19498	0.1662	0.1048	-0.419	0.214
				D(188)→V(192)	0.669				
10	-4014.701093	4.1343	0.0002	D(187)→V(192)	0.6794	0.1662	0.1048	-0.419	0.214
				D(188)→V(191)	-0.14896				
11	-4014.687341	4.5085	0.035	D(187)→V(193)	0.44653	0.1662	0.1048	-0.419	0.214
				D(187)→V(194)	-0.20414				
				D(187)→V(195)	0.12351				
				D(188)→V(193)	-0.19058				
				D(188)→V(194)	0.43313				
12	-4014.687139	4.514	0.0084	D(187)→V(193)	0.20198	0.1662	0.1048	-0.419	0.214
				D(187)→V(194)	0.48483				
				D(188)→V(193)	0.36734				
				D(188)→V(194)	0.19746				
				D(188)→V(195)	0.17768				

Key: D(188) = HOMO, D(187) = HOMO(-1) , etc.; V(189) = LUMO, V(190) = LUMO(=1), etc.

Table 3.9. TDDFT/TDA Excitation Energies For Transitions of $[Ga(L^{-})(L^{0})]^{2+}$, $(\mathbf{2})^{2+}$

Excited State	Total Energy (hartrees)	Excitation energy (eV)	Oscillator Strength	Origin	Amplitude	Transition moment X	Transition moment Y	Transition moment Z	Strength (AU)
1	-4014.62941063	0.4666	0.0063	(187 β)→ (188 β)	0.99890	0.2563	0.0802	-0.6934	0.5530
			<S**2>=0.784						
2	-4014.59183481	1.4891	0.1351	(183 β)→ (188 β)	-0.15346	-0.1701	-1.8982	-0.2679	3.7038
			<S**2>=0.779	(184 β)→ (188 β)	0.92495				
				(185 β)→ (188 β)	0.18115				
				(186 β)→ (188 β)	0.24226				
3	-4014.58607243	1.6459	0.0008	(184 β)→ (188 β)	-0.22418	-0.0394	0.1376	0.0166	0.0208
			<S**2>=0.785	(186 β)→ (188 β)	0.96257				
4	-4014.5769107	1.8952	0.0127	(182 β)→ (188 β)	0.98220	0.1939	0.0319	-0.4852	0.2740
			<S**2>=0.798						
5	-4014.57380166	1.9798	0.0003	(184 β)→ (188 β)	-0.18672	0.0187	0.0477	-0.0643	0.0068
			<S**2>=0.785	(185 β)→ (188 β)	0.97783				
6	-4014.56946885	2.0977	0.0358	(181 β)→ (188 β)	0.94144	-0.3880	0.7350	-0.0699	0.6956
			<S**2>=0.797	(183 β)→ (188 β)	-0.25385				
7	-4014.56572772	2.1995	0.0097	(181 β)→ (188 β)	0.24492	-0.0199	0.4208	0.0441	0.1794
			<S**2>=0.786	(183 β)→ (188 β)	0.94874				
				(184 β)→ (188 β)	0.17215				
8	-4014.54713597	2.7054	0.0045	(177 β)→ (188 β)	-0.18824	0.0153	-0.2535	-0.0556	0.0676
			<S**2>=0.809	(180 β)→ (188 β)	0.97088				
9	-4014.54376969	2.7971	0.0042	(174 β)→ (188 β)	0.20285	0.0883	0.0431	-0.2262	0.0608
			<S**2>=0.789	(178 β)→ (188 β)	-0.25853				
				(179 β)→ (188 β)	0.93163				
10	-4014.54231072	2.8367	0.0002	(186 α)→ (193 α)	-0.13117	-0.0073	-0.0486	-0.0060	0.0024
			<S**2>=2.757	(186 α)→ (200 α)	-0.12402				
				(188 α)→ (189 α)	-0.15830				
				(188 α)→ (191 α)	0.47282				
				(188 α)→ (192 α)	0.32875				
				(188 α)→ (195 α)	0.18231				
				(188 α)→ (196 α)	0.13700				
				(188 α)→ (198 α)	0.11818				
				(185 β)→ (191 β)	-0.11908				
				(186 β)→ (193 β)	0.12663				
				(186 β)→ (200 β)	-0.11643				
				(187 β)→ (189 β)	-0.15141				
				(187 β)→ (191 β)	0.56286				
				(187 β)→ (194 β)	-0.20417				
				(187 β)→ (195 β)	-0.10683				
				(187 β)→ (198 β)	-0.11198				

Key: 187 β = β-HOMO, (186 β) = β–HOMO(-1) , 188 α = α-HOMO, etc.; (188 β) = β-LUMO, (189 β) = β-LUMO(+1), etc.

Table 3.10. TDDFT/TDA Excitation Energies For Transitions of $[Ga(L^0)_2]^{3+}$, $(\mathbf{3})^{3+}$

Excited State	Total Energy (hartrees)	Excitation energy (eV)	Oscillator Strength	Origin	Amplitude	Transition moment X	Transition moment Y	Transition moment Z	Strength (AU)
1	-4014.37250818	1.4309	0.0008	(185 β)→ (188 β)	-0.60218	-0.1199	-0.0531	-0.0654	0.0215
			<S**2>=2.05	(186 β)→ (187 β)	0.78113				
2	-4014.36977079	1.5054	0.2921	(185 β)→ (187 β)	0.70778	-0.0074	2.7979	0.3007	7.9185
			<S**2>=2.05	(186 β)→ (188 β)	-0.68026				
3	-4014.35745224	1.8409	0.0162	(183 β)→ (187 β)	-0.38691	0.2375	-0.0792	-0.5455	0.3602
			<S**2>=2.07	(183 β)→ (188 β)	-0.48734				
				(184 β)→ (187 β)	0.64051				
				(184 β)→ (188 β)	0.39997				
4	-4014.35726849	1.8456	0.0078	(183 β)→ (187 β)	0.59377	0.0902	-0.0402	-0.4028	0.1720
			<S**2>=2.07	(183 β)→ (188 β)	-0.37102				
				(184 β)→ (187 β)	0.40730				
				(184 β)→ (188 β)	-0.54022				
5	-4014.3544314	1.9228	0.0127	(181 β)→ (187 β)	-0.27926	0.0332	0.5187	0.0086	0.2702
			<S**2>=2.05	(182 β)→ (188 β)	0.32253				
				(185 β)→ (187 β)	0.62261				
				(186 β)→ (188 β)	0.62942				
6	-4014.35411168	1.9315	0.0055	(181 β)→ (188 β)	-0.23571	-0.3189	0.0430	-0.1115	0.1160
			<S**2>=2.05	(182 β)→ (187 β)	0.35906				
				(185 β)→ (188 β)	0.70435				
				(186 β)→ (187 β)	0.53649				
7	-4014.3492019	2.0651	0.0628	(181 β)→ (187 β)	0.67739	-0.0064	-1.1085	-0.1085	1.2406
			<S**2>=2.06	(182 β)→ (188 β)	-0.55609				
				(185 β)→ (187 β)	0.27453				
				(186 β)→ (188 β)	0.35007				
8	-4014.34882337	2.0754	0.0128	(181 β)→ (188 β)	-0.59422	-0.4710	0.0321	-0.1721	0.2525
			<S**2>=2.06	(182 β)→ (187 β)	0.64295				
				(185 β)→ (188 β)	-0.33024				
				(186 β)→ (187 β)	-0.29769				
9	-4014.33647175	2.4115	0.0000	(183 β)→ (187 β)	0.67387	-0.0083	-0.0115	-0.0054	0.0002
			<S**2>=2.05	(184 β)→ (187 β)	-0.10342				
				(184 β)→ (188 β)	0.72116				
10	-4014.33624758	2.4176	0.0000	(183 β)→ (187 β)	0.11714	-0.0027	-0.0039	0.0086	0.0001
			<S**2>=2.05	(183 β)→ (188 β)	0.76469				
				(184 β)→ (187 β)	0.62270				
11	-4014.32973918	2.5947	0.0015	(181 β)→ (187 β)	0.45396	0.0361	0.1466	0.0105	0.0229
			<S**2>=2.05	(181 β)→ (188 β)	0.54197				
				(182 β)→ (187 β)	0.47975				
				(182 β)→ (188 β)	0.50659				
12	-4014.32969508	2.5959	0.0017	(181 β)→ (187 β)	0.47235	-0.0267	0.1599	-0.0023	0.0017
			<S**2>=2.05	(181 β)→ (188 β)	-0.50928				
				(182 β)→ (187 β)	-0.44974				
				(182 β)→ (188 β)	0.54952				

Key: 186 β = β-HOMO, (185 β) = β–HOMO(-1), etc.; (187 β) = β-LUMO, (188 β) = β-LUMO(+1), etc.

CHAPTER 4

FUTURE DIRECTIONS

We have documented the synthesis of two pincer-type ligands and their Rhodium and Gallium complexes in this thesis. Chapter 2 was consisted of easily crystallizable PNN pincer-type ligand and its Rhodium complex. We have shown that this pincer type ligand is a structurally adaptive ligand in the rhodium(I) complex and κ^2 *P,N*-coordination mode was structurally authenticated by its (PNN)Rh(CN^tBu)$_2$ complex. The ability to isolate this complex is likely do to the "soft" nature of the of the low valent metal center that prefers the excellent donor properties of the "soft" isocyanide ligand over the "intermediate-to-hard" pyrazolyl donor with which it is in competition. In fact, dynamic behavior of this complex in solution was discovered by NMR spectral data. We attributed this process to be a result of reversible coordination of the isocyanide and the hemilabile pyrazole arm to give either four- or five- coordinate metal centers. Theoretical calculations supported that these two structures are energetically similar and the five-coordinated structure is only 5.1 kcal higher in energy than the four coordinated structure. A variety of rhodium(III) complexes were obtained by oxidative addition reactions. In these complexes, structural adaptability of this ligand was demonstrated. The reaction of (PNN)Rh(CN^tBu)$_2$ complex with MeI produced easily separable *mer* and *fac* coorinadated [(PNN)Rh(Me)(CN^tBu)$_2$](I). The *mer* coordinated complex was found to be more stable than *fac* coordinated complex. The pure *fac*- coordinated compound was converted slowly in CD_2Cl_2 to *mer* coordinated compound over the course of 44 h with first order kinetics. Given the ease of the preparation of (PNN)Rh(CO) complexes,

one could envision constructing metal organic frameworks using suitably derivatized PNN derivatives. The incorporation of low valent rhodium(I) centers may also bestow interesting catalytic properties into future MOF's that show selective gas uptake. As such, future studies will center on preparing and characterizing such MOFs and on exploring the catalytic properties of the molecular (PNN)Rh derivatives as potential homogeneous catalysts and the MOF as heterogeneous counterparts.

For studies on the viability of metal pincer complexes to act as electroactive centers in MOFs, a model complex was first prepared using a redox silent metal. The study of this complex will benefit future studies where it is desirable to identify ligand radicals and presumably to give the lower boundary for electron communication if any, across the N-M-N junction. The gallium complex [Ga(Me,Me)](PF_6) was prepared, found to be hydrolytically stable and, most importantly, was found to undergo two reversible one-electron oxidations near 1.0 V versus Ag/AgCl. This observation is an indicator that significant electronic communication occurs across the metal center. Full analysis of electrochemical and spectroscopic properties showed that the mono-oxidized homoleptic gallium(III) complex of the NNN pincer-type ligand can be categorized as the Robin-Day Class II mixed valance species. The weak electronic communication may occur either by direct tunneling, by nonresonant charge transfer using empty, high-energy 4p orbitals on gallium as a coupling medium, or by thermally activated hopping mechanism. This result suggests that if MOFs could be prepared, one could consider using diamagnetic main group transition metals in the framework and electronic communication would still be possible.

Obviously replacing the gallium(III) with a transition metal should greatly strengthen the electronic communication. The d orbitals should be energetically accessible and allow for dπ-pπ interactions with the magnetic orbitals on the ligand. Future studies in this area will focus on homoleptic transition metal complexes (Figure 4.1 left). Particular attention will be paid to earth-abundant first-row transition metals, but other metals should be studied. For instance, to gain a deeper understanding of trends in electronic structure, it may be desirable to examine the properties across a group such as either Fe, Ru, Os or group 9 (Co, Rh, Ir), and or, the earlier transition metals (such as Cr, Mo, W).

In addition to changing metals, it would also be interested in determining whether changing the electronic properties of the redox active pincer ligands would provides a

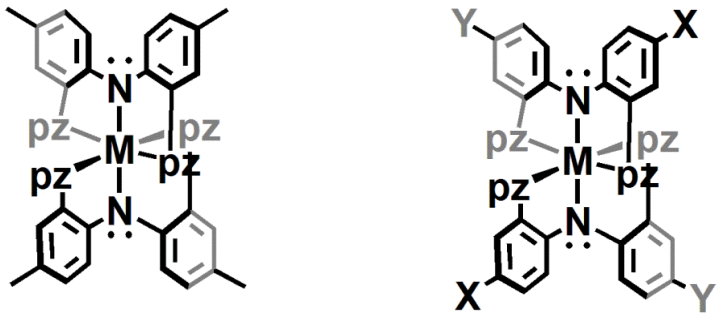

Figure 4.1. Proposed homoleptic transition metal complexes

means to alter the strength of electronic communication. It has been already shown that changing para-aryl substituents can affect electronic properties in rhodium chemistry, but it is unclear whether this translated to first-row transition metals. Therefore as an

extension of this project, it would be interested to synthesis series of metal complexes for a first-row transition metal with varying X and Y groups (Figure 4.1 right). If the transition metals facilitate the electronic communication over main group metal gallium it will be great invention for future electronic materials.

In order to create a MOF one needs a ligand that is either homoditopic (two identical binding pockets), heteroditopic (with two different binding sites) or both, in a divergent binding geometry. For this purpose it would be of interest to prepare homoditopic pincer ligands such as that in Figure 4.2. The linker would ideally be an aromatic ring such as phenyl groups, alkene, or an alkyne to allow electronic communication. As our group has previously characterized tricarbonylrhenium(I) pincer complexes that are very stable and display rich spectroscopic handles for characterization, the $Re(CO)_3$ unit may be an ideal candidate for studying electronic communication in the homoditopic ligands.

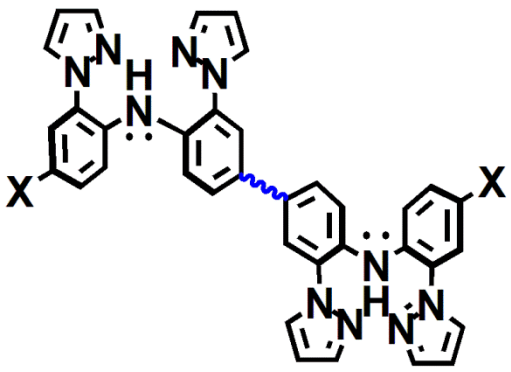

Figure 4.2 Covalently linked homoditopic multi-pincer ligand

Heteroditopic pincer ligands could be synthesized either by substituting donor atoms at the *para* aryl position (Figure 4.3, left) or by attaching exo-donor groups to the para aryl positions (Figure 4.3, right). An inspection of experimental and calculated structure of $[Ga(CH_3,CH_3)_2](PF_6)$ reveals that these compounds may provide ideal platforms for the construction of three dimensional solids (Figure 4.4).

Figure 4.3 Heteroditopic pincer ligands. D is a donor group

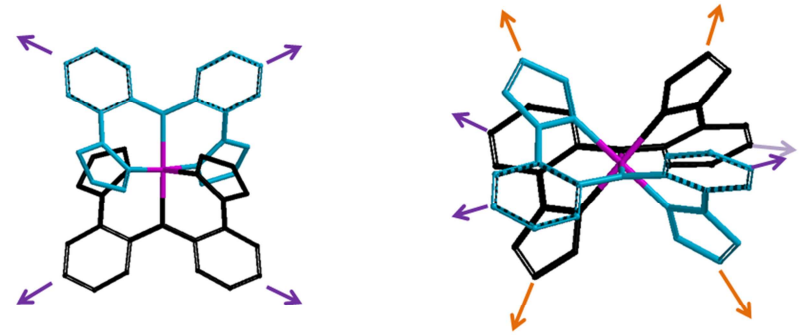

Figure 4.4. View of a model $M(X,Y)_2$ complex showing relative disposition of para-aryl and 4-pyrazolyl groups

For instance, if donor groups are attached to para-aryl positions (Figure 4.3, right, or 4.4) they would be essentially aligned in one plane and could afford connectivity in at least two dimensions (of the next metal has only two coordination sites). It may also be

possible to attach a donor group into the 4 position of pyrazolyl ring, providing connectivity in a third dimension (Figure 4.4 right).

In this way it may be possible to construct MOF's in a single self-assembly step or by the metalloligand approach. In this latter approach, discrete metal complexes of either type of heteroditopic ligand $[ML_2]^{n+}$ would be prepared first and subsequently allowed to react with additional equivalents of the same or different metal. If one uses

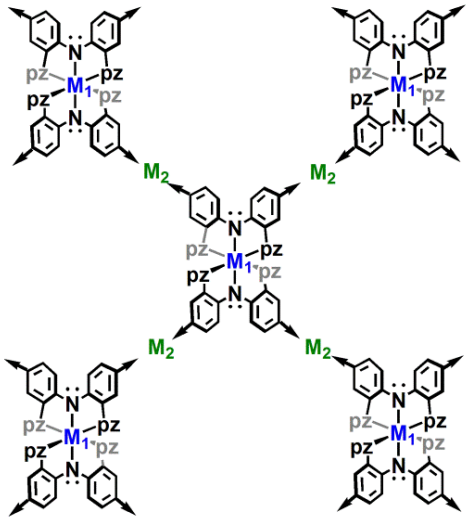

Figure 4.5. MMOFs of metal complexes of pincer-type ligands with exo-donor groups

two different metals M1 and M2 it will be then a mixed metal organic framework (MMOF) to give species similar to that in Figure 4.5. Such substitutions may provide a means to "dope" a potential semiconducting (M)MOF thereby tuning its electronic behavior.

BIBLIOGRAPHY

CHAPTER 1

(1) (a) Wanniarachchi, S.*;* Liddle, B. J.*;* Toussaint, J.*;* Lindeman, S. V.; Bennett, B.; Gardinier, J. R. *Dalton Trans.* **2011**, ***40***, 8776-8787. (b) Wanniarachchi, S.; Liddle, B. J.; Toussaint, J.; Lindeman, S. V.; Bennett, B.; Gardinier J. R. *Dalton Trans.* **2010**, ***39***, 3167–3169. (c) Wanniarachchi, S.; Hewage, J. S.; Lindeman, S. V.; Gardinier, J. R. *Organometallics*, **2013**, *32* , 2885–2888 (d) Liddle, B. J.; Wanniarachchi, S.; Hewage, J. S.; Lindeman, S. V.; Bennett, B.; Gardinier, J. R. *Inorg. Chem.* **2012**, *51* , 12720–12728.

(2) Jorgensen, C.K. *Coord. Chem. Rev*., **1966**, *1*, 164.

(3) Ward, M. D.; McCleverty, J. A. *Doton Trans*. **2002**, 275-288.

(4) Gunanathan, C.; Milsten, D. *Acc. Chem. Res*. **2011**, *44*(8), 588-602.

(5) *Rogers, M. S.; Tyler, E. M.; Akyumani, N.; Kurtis, C. R.; Apooner, R. K.; Deacon, S. E.; Tamber, S.; Firbank, S. J.; Mahmoud, K.; Knowles, P. F.; Phillips, S. E.; McPherson, M. J.; Dooly, D. M. Biochemistry*, **2007**, *46* (15), 4606–4618.

(6) Lawrence, Q. J.; Tolman, W. B. *Nature*. **2008**, 98, 333-340.

(7) Sato, O.; Cui, A.; Matsuda, R.; Tao, J.; Hayami, S. *Acc. Chem. Res*. **2007**, *40*, 361-369.

(8) Narayan, T. C.; Miyaki, T.; Seki, S.; Dinca, M. *J. Am. Chem. Soc*. **2012**, *134*, 12932-12935.

CHAPTER 2

(1) (a) Zhanga, W. –H.; Chiena, S. W.; Hor, T. S. *Coord. Chem. Rev.* **2011**, *255*, 1991–2024. (b) Braunstein, P.; Naud, F. *Angew. Chem. Int. Ed.* **2001**, *40*, 680-699. (c) Slone, C. S.; Weinberger, D. A.; Mirkin, C. A. *Progr. Inorg. Chem.* **1999**, *48*, 233-350.

(2) (a) Grützmacher, H. *Angew. Chem. Int. Ed.* **2008**, *47*, 1814-1818. (b) Angell, S. E.; Rogers C. W.; Zhang, Y.; Wolf, M. O.; Jones Jr., W. E. *Coord. Chem. Rev.* **2006**, *250*, 1829–1841.

(3) Recent examples: (a) Jiménez, M. V.; Bartolomé, M. I.; Pérez-Torrente, J. J.; Gómez, D.; Modrego, F. J.; Oro, L. A. *ChemCatChem* **2013**, *5*, 263 – 276. (b) Tornatzky, J.; Kannenberg, A.; Blechert, S. *Dalton Trans.* **2012**, *41*, 8215-8225. (c) Hounjet, L. J.; McDonald, R.; Ferguson, M. J.; Cowie, M. *Inorg. Chem.* **2011**, 50, 5361–5378.

(4) (a) Frauhiger, B. E.; White, P. S.; Templeton, J. L. *Organometallics* **2012**, *31*, 225−237. (b) Tsoureas, N.; Kuo, Y. –Y.; Haddow, M. F.; Owen, G. R. *Chem. Commun.* **2011**, *47*, 484-486. (c) Tsoureas, N.; Owen, G. R.; Hamilton, A.; Orpen, A. G. *Dalton Trans.* **2008**, 6039-6044.

(5) (a) Ruddy, A. J.; Mitton, S. J.; McDonald, R.; Turculet L. *Chem. Commun.*, **2012**, *48*, 1159–1161. (b) Fulmer, G. R.; Kaminsky, W.; Kemp, R. A.; Goldberg, K. I. *Organometallics* **2011**, *30*, 1627–1636. (c) Niu, J. –L.; Hao, X. –Q.; Gong, J. -F.; and Song, M. -P. *Dalton Trans.*, **2011**, *40*, 5135–5150. (d) van der Vlugt, J. I.; Pidko, E. A.; Vogt, D.; Lutz, M.; Spek, A. L. *Inorg. Chem.* **2009**, *48*, 7513-7515. (e) Zhang, J.; Leitus, G.; Ben-David, Y.; Milstein, D. *J. Am. Chem. Soc.* **2005**, *127*, 10840–10841.

(6) Lindner, R.; van den Bosch, B.; Lutz, M.; Reek, J. N. H.; van der Vlugt, J. I. *Organometallics* **2011**, *30*, 499-510.

(7) See for example: (a) Gloaguen, Y.; Jacobs, W.; de Bruin, B.; Lutz, M.; van der Vlugt, J. I. *Inorg. Chem.* **2013**, *52*, 1682−1684. (c) Wanniarachchi, S.*;* Liddle, B. J.*;* Toussaint, J.*;* Lindeman, S. V.; Bennett, B.; Gardinier, J. R. *Dalton Trans.* **2011**, ***40***, 8776-8787. (b) Calimano, E.; Tilley, T. D. *Dalton Trans.* **2010**, *39*, 9250-9263.

(8) Liddle, B. J.; Silva, R. M.; Morin, T. J.; Macedo, F. P.; Shukla, R.; Lindeman, S. V.; Gardinier, J. R. *J. Org. Chem.* **2007**, *72*, 5637-5646.

(9) Winter, A. M; Eichele, K.; Mack, H. –G.; Potuznik, S.; Mayer, H. A.; Kaska, W. C. *J. Organomet. Chem.* **2003**, *682*, 149-154.

(10) Wanniarachchi, S.; Liddle, B. J.; Lindeman, S. V.; Gardinier J. R. *J. Organomet. Chem.* **2011**, *696*, 3623-3636.

(11) Northcutt, T. O.; Lachicotte, R. J.; Jones, W. D. *Organometallics* **1998**, *17*, 5148-5152.

(12) Carlton, L.; Mokoena, L. V.; Fernandes, M. A. *Inorg. Chem.* **2008**, 47, 8696-703.

(13) Tejel, C.; Ciriano, M. A.; Edwards, A. J.; Lahoz, F. J.; Oro, L. A. *Organometallics* **1997**, *16*, 45-53.

(14) Jeffery, J. C.; Lebedev, V. N.; Stone, F. G. A. *Inorg. Chem.* **1996**, *35*, 2967-2976

(15) Rubio, M.; Suárez, A.; del Río, D.; Galindo, A.; Álvarez, E.; Pizzano, A. *Organometallics* **2009**, *28*, 547–560

(16) Wanniarachchi, S.; Liddle, B. J.; Kizer, B.; Hewage, J. S.; Bennett, B.; Lindeman, S. V.; Gardinier, J. R. *Inorg. Chem.* **2012**, *51*, 10572–10580.

(17) Coulson; D. R.; Satek, L. C.; Grim, S. O. *Inorg. Synth*. **1990**, *28*, 107.

(18) Hernandez-Gruel, M. A. F.; Pérez-Torrente, J. J.; Ciriano, M. A.; Oro, L. A. *Inorg.Synth.* **2004**, *34*, 128.

(19) Liddle, B.J.; Silva, R.M.; Morin, T.J.; Macedo, F.P.; Shukla, R.; Lindeman, S.V.; Gardinier, J.R *J. Org. Chem.* **2007**, *72*, 5637.

(20) (a) Goodman, M. A.; Nazarenko, A. Y.; Casavant, B. J.; Li, Z.; Brennessel, W. W.; DeMarco, M. J.; Long, G.; Goodman M. S.; *Inorg. Chem.* **2012** *51*, 1084. (b) Diez-Barra E.; de la Hoz, A.; Sanchez-Migallon A.; Tejeda, J. *J. Chem. Soc., Perkin Trans*. I **1993** 1079. (c) Katritzky, A. R.; Abdel-Rahman, A. E.; Leahyand D. E.; Schwarz, A. *Tetrahedron* **1983**, *39*, 4133.

(21) CrysAlisPro, Agilent Technologies,Version 1.171.34.46 (release 25-11-2010 CrysAlis171 .NET), (compiled Nov 25 2010,17:55:46)

(22) Dolomanov, O. V.; Bourhis, L. J.; Gildea, R. J.; Howard J. A. K.; Puschmann, H.; "OLEX2: a complete structure solution, refinement and analysis program." *J. Appl. Cryst.* **2009**, *42*, 339-341.

(23) SCALE3 ABSPACK - *An Oxford Diffraction program* (1.0.4,gui:1.0.3) (C) 2005 Oxford Diffraction Ltd.

(24) Perdew, J. P. *Phys. Rev. B*, **1986**, *33*, 8822-8824.

(25) (a) Handy, N. C.; Cohen, A. J. *Mol. Phys*, **2001**, *99*, 403-412. (b) Hoe, W.-M.; Cohen, A.; Handy, N. C. *Chem. Phys. Lett.* **2001**, *341*, 319-328.

(26) (a) Weigend, F. and Ahlrichs, R. *Phys. Chem. Chem. Phys.*, **2005**, *7*, 3297-3305. (b) Andrae, D.; Haeussermann, U.; Dolg, M.; Stoll, H.; Preuss, H.; *Theor.Chim.Acta*, **1990**, *77*, 123-141.

(27) Scalmani G., Frisch, M. J. *J. Chem. Phys.*, **2010**, *132*, 114110-114124.

(28) Gaussian 09, Revision B.01, Frisch, M. J.; Trucks, G. W.; Schlegel, H. B.; Scuseria, G. E.; Robb, M. A.; Cheeseman, J. R.; Scalmani, G.; Barone, V.; Mennucci, B.; Petersson, G. A.; Nakatsuji, H.; Caricato, M.; Li, X.; Hratchian, H. P.; Izmaylov, A. F.; Bloino, J.; Zheng, G.; Sonnenberg, J. L.; Hada, M.; Ehara, M.; Toyota, K.; Fukuda, R.; Hasegawa, J.; Ishida, M.; Nakajima, T.; Honda, Y.; Kitao, O.; Nakai, H.; Vreven, T.; Montgomery, Jr., J. A.; Peralta, J. E.; Ogliaro, F.; Bearpark, M.; Heyd, J. J.; Brothers, E.; Kudin, K. N.; Staroverov, V. N.; Kobayashi, R.; Normand, J.; Raghavachari, K.; Rendell, A.; Burant, J. C.; Iyengar, S. S.; Tomasi, J.; Cossi, M.; Rega, N.; Millam, J. M.; Klene, M.; Knox, J. E.; Cross, J. B.; Bakken, V.; Adamo, C.; Jaramillo, J.; Gomperts, R.; Stratmann, R. E.; Yazyev, O.; Austin, A. J.; Cammi, R.; Pomelli, C.; Ochterski, J. W.; Martin, R. L.; Morokuma, K.; Zakrzewski, V. G.; Voth, G. A.; Salvador, P.; Dannenberg, J. J.; Dapprich, S.; Daniels, A. D.; Farkas, Ö.; Foresman, J. B.; Ortiz, J. V.; Cioslowski, J.; Fox, D. J. Gaussian, Inc., Wallingford CT, 2009.

(29) Roscioni, O. M.; Lee, E. P. F.; Dyke, J. M. *J. Comput. Chem.* **2012**, *33*, 2049–2057.

CHAPTER 3

(1) Stephan S. Isied, Ed. *Electron Transfer Reactions: Inorganic, Organometallic, and Biological Applications;* Advances in Chemistry Series 253. American Chemical Society: Washington, DC, 1997. (b) Prassides, K., Ed. *Mixed Valency Systems: Applications in Chemistry, Physics and Biology*; Kluwer Academic Publishers: Dordrecht, 1991. (c) Robin, M. B.; Day, P. *Adv. Inorg. Chem. Radiochem.* **1967**, *10*, 247-422.

(2) (a) Kaim, W.; Lahiri, G. K. *Angew. Chem. Int. Ed*. **2007**, *46*, 1778-1796. (b) Kaim, W.; Klein, A.; Glöckle, M. *Acc. Chem. Res.* **2000**, *33*, 755-763. (c) Glover, S. D.; Goeltz, J. C.; Lear, B. J.; Kubiak, C. P. *Eur. J. Inorg. Chem.* **2009**, 585-594.

(3) (a) Creutz, C.; Taube, H. *J. Am. Chem. Soc.* **1969**, *91*, 3988-3989. (b) Creutz, C.; Taube, H. *J. Am. Chem. Soc.* **1973**, *95*, 1086-1094. (c) Crutchley, R. J. *Adv. Inorg. Chem.* **1994**, *41*, 273-325.

(4) (a) Heckmann, A.; Lambert, C. *Angew. Chem. Int. Ed.* **2012**, *51*, 326-392. (b) Hankache, J.; Wenger, O. S. *Chem. Rev.* **2011**, *111*, 5138-5178.

(5) (a) Nelsen, S. F.; Tran, H. Q.; Nagy, M. A. *J. Am. Chem. Soc.* **1998**, *120*, 298-304. (b) Szeghalmi, A. V.; Erdmann, M.; Engel, V.; Schmitt, M.; Amthor, S.; Kriegisch, V.; Nöll, G.; Stahl, R.; Lambert, C.; Leusser, D.; Stalke, D.; Zabel, M.; Popp, J. *J. Am. Chem. Soc.* **2004**, *126*, 7834-7845. (c) Lambert, C.; Nöll, G. *J. Am. Chem. Soc.* **1999**, *121*, 8434-8442. (d) Coropceanu, V.; Malagoli, M.; André, J. M.; Brédas, J. L. *J. Am. Chem. Soc.* **2002**, 124, 10519-10530. (e) Coropceanu, V.; Gruhn, N. E.; Barlow, S.; Lambert, C.; Durivage, J. C.; Bill, T. G.; Nöll, G.; Marder, S. R.; Brédas, J. L. *J. Am. Chem. Soc.* **2004**, 126, 2727-2731. (f) Lambert, C.; Risko, C.; Coropceanu, V.; Schelter, J.; Amthor, S.; Gruhn, N. E.; Durivage, J. C.; Brédas, J. L. *J. Am. Chem. Soc.* **2005**, *127*, 8508-8516. (g) Yano, M.; Ishida, Y.; Aoyama, K.; Tatsumi, M.; Sato, K.; Shiomi, D.; Ichimura, A.; Takui, T. *Synth. Metals* **2003**, 137(1-3), 1275-1276. (h) Plater, M. J.; Jackson, T. *J. Chem. Soc., Perkin Trans. 1* **2001**, *20*, 2548-2552. (i) Low, P. J.; Paterson, M. A. J.; Yufit, D. S.; Howard, J. A. K.; Cherryman, J. C.; Tackley, D. R.; Brook, R.; Brown, B. *J. Mater. Chem.* **2005**, 15, 2304-2315. (j) Bonvoisin, J.; Launay, J. –P.; Van der Auweraer, M.; De Schryver, F. C. *J. Phys. Chem.* **1994,** *98*, 5052-5057.

(6) (a) Rohde, D.; Dunsch, L.; Tabet, A.; Hartmann, H.; Fabian, J. *J. Phys. Chem. A* **2006**, *110*, 8223-8231. (b) Odom, S. A.; Lancaster, K.; Beverina, L.; Lefler, K. M.; Thompson, N. J.; Coropceanu, V.; Bredas, J. –L.; Marder, S. R.; Barlow, S. *Chem. Eur. J.* **2007**, *13*, 9637-9646. (c) Lacroix, J. C.; Chane-Ching, K. I.; Maquère, F.; Maurel, F. *J. Am. Chem. Soc.* **2006**, *128*, 7264-7276.

(7) (a) Lambert, C.; Nöll, G.; Schelter, J. *Nat. Mater.* **2002**, *1*, 69-73. (b) Lambert, C.; Nöll, G. *J. Chem. Soc., Perkin Trans. 2* **2002**, 2039-2043.

(8) Jones, S. C.; Coropceanu, V.; Barlow, S.; Kinnibrugh, T.; Timofeeva, T.; Brédas, J. –L.; Marder, S. R. *J. Am. Chem. Soc.* **2004**, *126*, 11782-11783.

(9) Nöll, G.; Avola, M. *J. Phys. Org. Chem.* **2006**, 19, 238-241.

(10) See also: (a) Sun, D.; Lindeman, S. V. ; Rathore, R.; Kochi, J. K. *J. Chem. Soc. Perkin Trans. 2* **2001**, 1585-1594. (b) Rosokha, S. V.; Sun, D. –L.; Kochi, J. K. *J. Phys. Chem. A* **2002**, *106*, 2283-2292. (c) Lindeman, S. V.; Rosokha, S. V.; Sun, D.; Kochi, J. K. *J. Am. Chem. Soc.* **2002**, *124*, 843-855.

(11) Examples with inorganic/organometallic donors and bridges are also known such as: (a) {(terpyRu)(□-terpy-$(C_2)_n$-Fc_m-$(C_2)_n$-terpy)[Ru(terpy)]$^{5+}$ (n = 0, 1; Fc = ferrocenyl, m = 1-3) Dong, T. -Y.; Lin, H. -Y.; Lin, S. –F.; Huang, C. –C.; Wen, Y. –S.; Lee, L. *Organometallics* **2008**, *27*, 555-562 and references. Polyferrocene examples: (b) Cowan, D. O.; Levanda, C.; Park, J.; Kaufman, F. *Acc. Chem. Res.* **1973**, *6*, 1-7. (c) Le Vanda, C.; Bechard, K.; Cowan, D. O.; Rausch, M.D.; *J. Am. Chem. Soc.* **1977**, *99*, 2964-2968. (d) Dong, T. –Y.; Lee, W. –Y.; Su, P. –T.; Chang, L. –S.; Lin, K. –J. *Organometallics* **1998**, *17*, 3323-3330. (e) Dong, T.-Y.; Lee, S. H.; Chang, C. K.; Lin, H. M.; Lin, K. J. *Organometallics* **1997**, *16*, 2773-2786. (f) Brown, G. M.; Meyer, T. J.; Cowan, D. O.; LeVanda, C.; Kaufman, F.; Roling, R. V.; Raush, M. D. *Inorg. Chem.* **1975**, *14*, 506-511. (g) Cowan, D. O.; Kaufman, F. *J. Am. Chem. Soc.* **1970**, *92*, 219-220. (h) Scheibitz M.; Heilmann J. B; Winter R. F; Bolte M.; Bats J. W.; Wagner M. *Dalton Trans.* **2005**, *1*, 159-170.

(12) (a) Dei, A.; Sorace, L. *Appl. Magn. Reson.* **2010**, *38*, 139-153. (b) Zanello, P.; Corsini, M. *Coord. Chem. Rev.* **2006**, *250(15+16)*, 2000-2022. (b) Pierpont, C. G. *Coord. Chem. Rev.* **2001**, *216*, 99-125. (c) Pierpont, C. G.; Lange, C. W. *Prog. Inorg. Chem.* **1994**, *41*, 331-442.

(13) Eisenberg, R.; Gray, H. B. *Inorg. Chem.*, **2011**, *50*, 9741-9751.

(14) quinone diimines: (a) Moriuchi, T.; Hirao, T. *Acc. Chem. Res.* **2012**, *45*, 347-360. (a) Uhlig, E. *Pure Appl. Chem.* **1988**, *60*, 1235-1240. (b) Vrieze, K.; Van Koten, G. *Inorg. Chim. Acta* **1985**, *100*, 79-96. (c) Balch, A. L.; Holm, R. H. *J. Am. Chem. Soc.* **1966**, *88*, 5201-5208.

(15) DAB complexes: (a) Tuononen, H. K.; Armstrong, A. F. *Dalton Trans.* **2006**, 1885-1894. Baker, R. J.; Jones, C.; Mills, D. P.; Murphy, D. M.; Hey-Hawkins, E.; Wolf, R. *Dalton Trans.* **2006**, 64-72. (c) Tuononen, H. K.; Armstrong, A. F. *Inorg. Chem.* **2005**, *44*, 8277-8284. (d) Baker, R. J.; Farley, R. D.; Jones, C.; Mills, D. P.; Kloth, M.; Murphy, D. M. *Chem. Eur. J.* **2005**, *11*, 2972-2982. (e), Baker, R. J. ;Jones, C.; Kloth, M.; Platts, J. A. *Angew. Chem. Int. Ed.* **2003**, *42*,

2660-2663. (f) Pott, T.; Jutzi, P.; Kaim, W.; Schoeller, W. W.; Neumann, B.; Stammler, H. –G.; Wanner, M. *Organometallics*, **2002**, *21*, 3169-3172. (g) Rijnberg, E.; Richter, B; Thiele, K. H.; Boersma, J.; Veldman, N.; Spek, A. L.; van Koten, G. *Inorg. Chem.* **1998**, 37, 56-63. (h) Gardiner, M. G.; Raston, C.L.; Skelton, B. W.; White, A. H. *Inorg. Chem.* **1997**, *36*, 2795-2803. (i) Gardiner, M. G.; Hanson, G. R.; Henderson, M. J.; Lee, F. C.; Raston, C. L. *Inorg. Chem.* **1994**, *33*, 2456-2461.

(16) β-diketiminatos: (a) Tsai, Y. –C. *Coord. Chem. Rev.* **2012**, *256(5-8)*, 722-758. (b) Macedo, F. P.; Gwengo, C., Lindeman, S. V.; Smith, M. D.; Gardinier, J. R. *Eur. J. Inorg. Chem.* **2008**, *20*, 3200-3211.

(17) pyridine-diimines: (a) Sieh, D.; Schlimm, M.; Andernach, L.; Angersbach, F.; Nueckel, S.; Schoeffel, J.; Susnjar, N.; Burger, P. *Eur. J. Inorg. Chem.* **2012**, *3*, 444-462. (b) Zhu, D.; Thapa, I.; Korobkov, I.; Gambarotta, S.; Budzelaar, P. H. M. *Inorg. Chem.* **2011**, 50, 9879-9887. (c) Myers, T. W.; Berben, L. A. *J. Am. Chem. Soc.* **2011**, *133*, 11865-11867. (d) Myers, T. W.; Kazem, N.; Stoll, S.; Britt, R. D.; Shanmugam, M.; Berben, L. A. *J. Am. Chem. Soc.* **2011**, *133*, 8662-8672.

(18) (a) Pierpont, C. G. *Inorg. Chem.* **2011**, *50*, 9766-9772. (b) Lange, C. W.; Conklin, B. J.; Pierpont, C. G. *Inorg. Chem.* **1994**, *33*, 1276-1283. (c) Adams, D. M.; Dei, A.; Hendrickson, D. N.; Rheingold, A. L. *Angew. Chem. Int. Ed. Engl.* **1993**, *32*, 391-392.

(19) (a) Chaudhuri, P.; Wagner, R.; Pieper, U.; Biswas, B.; Weyhermuller, T. *Dalton Trans.* **2008**, 1286-1288. (b) Verani, C. N.; Gallert, S.; Bill, E.; Weyhermüller, T. Weighardt, K.; Chaudhuri, P. *Chem. Commun.* **1999**, 1747-1748.

(20) (a) Scarborough, C. C.; Sproules, S.; Doonan, C. J.; Hagen, K. S.; Weyhermuller, T.; Weighardt, K. *Inorg. Chem.* **2012**, *51*, 6969-6982. (b) Scarborough, C. C.; Lancaster, K. M.; DeBeer, S.; Weyhermüller, T.; Sproules, S.; Wieghardt, K. *Inorg. Chem.* **2012**, *51*, 3718−3732 and references.

(21) (a) Szigethy, G.; Heyduk, A. F. *Dalton Trans.* **2012**, *41*, 8144-8152. (b) Brown, M. A.; El-Hadad, A. A.; McGarvey, B. R.; Sung, R. C. W.; Trikha, A. K.; Tuck, D. G. *Inorg. Chim. Acta*, **2000**, *300-302*, 613-621. (c) Chaudhury, P.; Hess, M.; Hildenbrand, K.; Bill, E.; Weyhermüller, T.; Wieghardt, K. *Inorg. Chem.*, **1999**, *38*, 2781-2790. (d) Camacho-Camacho, C.; Merino, G.; Martínez-Martínez, F. J.; Nöth, H.; Contreras, R. *Eur. J. Inorg. Chem.* **1999**, 1021-1027. (e) Brown, M. A.; Castro, J. A.; McGarvey, B. R.; Tuck, D. G. *Can. J. Chem.* **1999**, *77*, 502-510. (f) Bencini, A.; Ciofini, I.; Giannasi, E.; Daul, C. A.; Doclo, K. *Inorg. Chem.* **1998**, *37*, 3719-3725.

(22) Forum on Redox-Active Ligands: *Inorg. Chem.* **2011**, *50*, 9737– 9914

(23) Other recent reviews: (a) Kaim, W. *Eur. J. Inorg. Chem.* **2012**, *3*, 343-348. (b) Lyaskovskyy, V.; de Bruin, B. *ACS Catalysis* **2012**, *2*, 270-279. (c) Kaim, W. *Inorg. Chem.* **2011,** *50*, 9752-9765. (d) Kaim, W.; Schwederski, B. *Coord. Chem.Rev.* **2010**, *254(13-14)*, 1580-1588. (e) Ray, K.; Petrenko, T.; Wieghardt, K.; Neese, F. *Dalton Trans.* **2007**, 1552-1566. (f) Evangelio, E.; Ruiz-Molina, D. *Eur. J. Inorg. Chem.* **2005**, *15*, 2957-2971. (g) Hirao, T. *Coord. Chem. Rev.* **2002**, *226(1-2)*, 81-91.

(24) (a) Wanniarachchi, S.*;* Liddle, B. J.*;* Toussaint, J.*;* Lindeman, S. V.; Bennett, B.; Gardinier, J. R. *Dalton Trans.* **2011**, ***40***, 8776-8787. (b) Wanniarachchi, S.; Liddle, B. J.; Toussaint, J.; Lindeman, S. V.; Bennett, B.; Gardinier J. R. *Dalton Trans.* **2010**, ***39***, 3167 – 3169.

(25) (a) Wanniarachchi, S.; Liddle, B. J.; Kizer, B.; Hewage, J.; Bennett, B.; Lindeman, S. V.; Gardinier J. R. *Inorg. Chem.* **2012**, 50, 10572-10580. (b) Wanniarachchi, S.; Liddle, B. J.; Lindeman, S. V.; Gardinier J. R. *J. Organomet. Chem.* **2011**, ***696,*** 3623-3636.

(26) Niemeyer, M.; Goodwin, T. J.; Risbud, S. H.; Power, P. P. *Chem. Mater.* **1996**, *8*, 2745-2750.

(27) (a) Yurkerwich, K.; Parkin, G. *J. Clust. Sci.* **2010**, *21*, 225-234. (b) Reger, D. L.; Ding, Y. *Organometallics* **1993**, *12*, 4485-4492. (c) Cowley, A. H.; Carrano, C. J.; Geerts, R. L.; Jones, R.A.; Nunn, C. M. *Angew. Chem. Int. Ed. Engl.* **1988**, *27*, 277-278.

(28) (a) Zanello, P. *Inorganic Electrochemistry: theory, practice and applications,* Royal Society of Chemistry: Cambridge, 2003, pp 174-178. (b) Astruc, D. *Electron Transfer and Radical Processes in Transition-Metal Chemistry*, VCH Publishers, Inc.: New York 1995, pp 34-36.

(29) Rathore, R.; Burns, C.L.; Deselinescu, M.I.; Denmark, S.E.; Bui, T. *Org. Synth.* **2005**, *82*, 1-9.

(30) Brunschwig, B. S.; Creutz, C.; Sutin, N. *Chem. Soc. Rev.* **2002**, *31*, 168-184.

(31) (a) Hush, N. S. *Prog. Inorg. Chem.* **1967**, *8*, 391-444. (b) Hush, N. S. *Coord. Chem. Rev.* **1985**, *64*, 135-157.

(32) (a) Abbott, A. P.; Rusling, J. F. *J. Phys. Chem.* **1990**, *94*, 8910-8912. (b) Brunschwig, B. S.; Ehrenson, S.; Sutin, N. *J. Phys. Chem.* **1986**, *90*, 3657-3668.

(33) Marcus, R.A.; Sutin, N. *Biochim. Biophys. Acta* **1985**, *811*, 265-322. (b) Sutin, N. *Prog. Inorg. Chem.* **1983**, *30*, 441-499.

(34) Nishiumi, T.; Nomura, Y.; Chimoto, Y.; Higuchi, M.; Yamamoto, K. *J. Phys. Chem. B.* **2004**, *108*, 7992-8000.

(35) (a) Le Maguerès, P.; Lindeman, S. V.; Kochi, J. K. *Org. Lett.* **2000**, *2*, 3567-357. (b) Rathore, R.; Kochi, J. K. *Acta Chem. Scand.* **1998**, *52*, 114-130. (c) Bruson, H. A.; Kroeger, J. W. *J. Am. Chem. Soc.* **1940**, *62*, 36-44.

(36) (a) Weiss, E. A.; Kriebel, J. K.; Rampi, M. A.; Whitesides, G. M. *Phil. Trans. R. Soc. A*, **2007**, *365*, 1509–1537. (b) Albinsson, B.; Eng, M. P.; Pettersson, K.; Winters, M. U. *Phys. Chem. Chem. Phys.*, **2007**, *9*, 5847–5864.

(37) (a) Petrov, E. G.; May, A. *J. Phys. Chem. A*, **2001**, *105*, 10176-10186. (b) Onipko, A. *Chem. Phys. Lett.* **1998**, *292*, 267–272. (c) Lopez-Castillo, J. –M.; Jay-Gerin, J. –P. *J. Phys. Chem.* **1996**, *100*, 14289-14297. (d) Naleway, C. A.; Curtiss, L. A.; Miller, J. R. *J. Phys. Chem.* **1991**, *95*, 8434-8437. (e) McConnell, H. M. *J. Chem. Phys.* **1961**, *35*, 508–515.

(38) (a) Berlin, Y. A.; Hutchison, G. R.; Rempala, P.; Ratner, M. A.; Michl, J. *J. Phys. Chem. A* **2003**, *107*, 3970-3980. (b) Berlin, Y. A.; Burin, A. L.; Ratner, M. A. *Chem. Phys.* **2002**, *275*, 61–74. (b)

(39) (a) Gagné, R. R.; Koval, C. A., Lisensky, G. C. *Inorg. Chem.* **1980**, *19*, 2855-2857. (b) Noviandri, I.; Brown, K. N.; Fleming, D. S.; Gulyas, P. T.; Lay, P. A.; Masters, A. F.; Phillips, L. *J. Phys. Chem. B*, **1999**, *103*, 6713-6722. (c) Bond, A. M.; Oldham, K.B.; Snook, G. A. *Anal. Chem.* **2000**, *72*, 3492-3496. (d) Bao, D.; Millare, B.; Xia, W.; Steyer, B. G.; Gerasimenko, A. A.; Ferreira, A.; Contreras, A.; Vullev, V. I. *J. Phys. Chem. A* **2009**, *113*, 1259-1267.

(40) Zhao, Y.; Truhlar, D. G. *Theor. Chem. Account* **2008**, *120*, 215-241.

(41) Weigend, F. and Ahlrichs, R. *Phys. Chem. Chem. Phys.*, **2005**, *7*, 3297-3305.

(42) Scalmani G., Frisch, M. J. *J. Chem. Phys.*, **2010**, *132*, 114110-114124.

(42) Gaussian 09, Revision B.01, Frisch, M. J.; Trucks, G. W.; Schlegel, H. B.; Scuseria, G. E.; Robb, M. A.; Cheeseman, J. R.; Scalmani, G.; Barone, V.; Mennucci, B.; Petersson, G. A.; Nakatsuji, H.; Caricato, M.; Li, X.; Hratchian, H. P.; Izmaylov, A. F.; Bloino, J.; Zheng, G.; Sonnenberg, J. L.; Hada, M.; Ehara, M.; Toyota, K.; Fukuda, R.; Hasegawa, J.; Ishida, M.; Nakajima, T.; Honda, Y.; Kitao, O.; Nakai, H.; Vreven, T.; Montgomery, Jr., J. A.; Peralta, J. E.; Ogliaro, F.; Bearpark, M.; Heyd, J. J.; Brothers, E.; Kudin, K. N.; Staroverov, V. N.; Kobayashi, R.; Normand, J.; Raghavachari, K.; Rendell, A.; Burant, J. C.; Iyengar, S. S.; Tomasi, J.; Cossi, M.; Rega, N.; Millam, J. M.; Klene, M.; Knox, J. E.; Cross, J. B.; Bakken, V.; Adamo, C.; Jaramillo, J.; Gomperts, R.; Stratmann, R. E.; Yazyev, O.; Austin, A. J.; Cammi, R.; Pomelli, C.; Ochterski, J. W.; Martin, R. L.; Morokuma, K.; Zakrzewski, V. G.; Voth, G. A.; Salvador, P.; Dannenberg, J. J.; Dapprich, S.; Daniels, A. D.; Farkas, Ö.; Foresman, J. B.; Ortiz, J. V.; Cioslowski, J.; Fox, D. J. Gaussian, Inc., Wallingford CT, 2009.

(44) (a) Becke, A. D. *J. Chem. Phys.* **1993**, *98*, 5648-5652. (b) Lee, C.; Yang, W.; Parr, R. G. *Phys. Rev. B* **1988**, *37*, 785-789.

(45) (a) Hay, P. J.; Wadt, W. R. *J. Chem. Phys.*, **1985**, *82*, 270-283. (b) Wadt, W. R.; Hay, P. J. *J. Chem. Phys.*, **1985**, 82, 284-298. (c) Hay, P. J.; Wadt, W. R. *J. Chem. Phys.*, **1985**, *82*, 299-310.

(46) (a) Casida, M. E.; Jamorski, C.; Casida, K. C.; Salahub, D. R. *J. Chem. Phys.*, **1998**, *108*, 4439-4449. (b) Scalmani, G.; Frisch, M. J.; Mennucci, B.; Tomasi, J.; Cammi, R.; Barone, V. *J. Chem. Phys.*, **2006**, *124*, 094107: 1-15.

(47) SMART APEX2 Version 2.1-4, SAINT+ Version 7.23a and SADABS Version 2004/1. Bruker Analytical X-ray Systems, Inc., Madison, Wisconsin, USA, 2005.

(48) CrysAlisPro, Agilent Technologies,Version 1.171.34.46 (release 25-11-2010 CrysAlis171 .NET), (compiled Nov 25 2010,17:55:46).

(49) G. M. Sheldrick, SHELXTL Version 6.12; Bruker Analytical X-ray Systems, Inc., Madison Wisconsin, USA, 2001.